Chapter 12
Ground penetrating radar

12.1 INTRODUCTION

Since the mid-1980s, *ground penetrating radar* (GPR) has become enormously popular, particularly within the engineering and archaeological communities. However, radar has been used for geological applications since the 1960s, especially in connection with the development of *radio echosounding* of polar ice sheets. Glaciological applications of radar are now very well developed. Despite the recent upsurge in interest in the method, general experience in data processing and interpretation within the engineering community in particular has not kept pace with advances in technology or computer capabilities. There is enormous scope for the application of ground penetrating radar and it is extremely exciting to anticipate what might be achieved in the near future.

GPR applications can be divided into two virtually discrete classifications based on the main antenna frequencies. For geological applications, where depth penetration tends to be more important than very fine resolution, antennae with frequencies less than or equal to 500 MHz are used. For engineering or non-destructive testing (NDT) applications, antennae with frequencies of 500 MHz and greater are used, typically as high as 900 MHz or 1 GHz. A list of the range of applications of GPR is given in Table 12.1.

The first use of electromagnetic (EM) signals to locate remote buried objects is attributed to Hülsmeyer in a German patent in 1904, but the first published description of such investigations was by Leimbach and Löwy (1910), also in German patents. The systems used in these investigations employed continuous wave (CW) transmission. Hülsenbeck (1926) developed the first use of pulsed radar to investigate the nature of buried features.

Pulsed techniques were developed substantially over the following five decades. Its early civilian development was in radio echosounding of polar ice sheets (Cook 1960; Evans 1965; Swithinbank 1968). The first use of impulse radar for glaciological purposes was in the early 1970s (Watts *et al.* 1975). There is much pioneering research work being carried out in the glaciological field (for example, see papers by Wright *et al.* (1990), Hammond and Sprenke (1991) and Narod and Clarke (1994)). A useful review has been published by Bogorodsky *et al.* (1985). There has been wide acceptance of the radar method in certain areas of civil engineering, such as road pavement analysis and void detection behind tunnel linings. There has also been an expanding role for the method in geological applications, particularly in the rapid assessment of superficial deposits, location of swallow holes, etc. In archaeological studies, too, GPR has been used on many sites to identify potential excavation areas.

Many uses of ground penetrating radar have been described in the literature. These include the determination of permafrost thickness (Annan and Davis 1976); the detection of fractures in rock salt

Table 12.1 Range of applications of ground penetrating radar

Geological:
Detection of natural cavities and fissures
Subsidence mapping
Mapping sand body geometry
Mapping of superficial deposits
Soil stratigraphy mapping
Glacial geological investigations
Mineral exploration and resource evaluation
Peat thickness mapping and resource evaluation
Permafrost investigations
Location of ice wedges
Fracture mapping in rock salt
Location of faults, dykes, coal seams, etc.
Geological structure mapping
Lake and riverbed sediment mapping
Environmental:
Contaminant plume mapping
Mapping and monitoring pollutants within groundwater
Landfill investigations
Location of buried fuel tanks and oil drums
Location of gas leaks
Groundwater investigations
Glaciological:
Ice thickness mapping
Determination of internal glacier structures
Ice movement studies
Detection of concealed surface and basal glacier crevasses
Mapping water conduits within glaciers
Determination of thickness and type of sea and lake ice
Sub-glacial mass balance determination
Snow stratigraphy mapping
Engineering and construction:
Road pavement analysis
Void detection
Location of reinforcement (rebars) in concrete
Location of public utilities (pipes, cables, etc.)
Testing integrity of building materials
Concrete testing
Archaeology:
Location of buried structures
Detection and mapping of Roman Roads, etc.
Location of post-holes, etc.
Pre-excavation mapping
Detection of voids (crypts, etc.)
Location of graves
Forensic science:
Location of buried targets (e.g. bodies and bullion)

(Thierbach 1974; Unterberger 1978; Nickel *et al.* 1983; Olsson *et al.* 1983); and archaeological investigations (Bevan and Kenyon 1975; Imai *et al.* 1987; Bevan 1991). Examples of civil engineering and of other geological applications have been described by Darracott and Lake (1981), Leggo (1982), Ulriksen (1982), Leggo and Leech (1983), Davis and Annan (1989), Moorman *et al.* (1991), Doolittle (1993), and Huggenberger *et al.* (1994), among others. Cross-hole radar systems for use in crystalline rock have been described by Nilsson (1983), Wright and Watts (1982) and Olsson *et al.* (1990). GPR has also been used in police investigations to help locate buried bodies, such as in a double murder inquiry on Jersey, Channel Islands, in the 1980s, and in a gruesome search for human remains at two houses in Gloucester in 1994. In the latter, radar was instrumental in detecting where the corpses of 10 murdered women had been hidden within thick concrete inside the buildings, and in locating the remains of two other victims buried in a nearby field.

For regional and large-scale investigations, radar measurements have been made increasingly from aircraft and satellites. Such *remote sensing techniques* are beyond the scope of this chapter. Nevertheless, for sub-surface mapping in arid regions for hydrogeological purposes, for example, satellite radar imagery has been used to locate important features that would otherwise be extremely difficult to locate using ground-based surveys. An example of this is the identification of an ancient river drainage system now buried beneath desert sands in Africa and which was later proven to be an important source of potable water.

Ground radar was developed further by the US Army during the Vietnam War. Systems were constructed in order to locate labyrinths of tunnels excavated and used by the Viet Cong. At the end of the Vietnam War, the potential of GPR for civilian purposes was identified by Geophysical Survey Systems Inc. (GSSI), who are still the largest ground radar manufacturer internationally. In recent years other manufacturers have developed GPR systems, such as the PulseEKKO (Sensors & Software Ltd, Canada) and a range of systems produced by ERA Technologies Ltd, UK. Other companies are developing antennae to add on to existing radar systems, such as Radarteam AB (Sweden). Following the Falklands conflict in 1982, a radar system was developed with the aim of locating plastic mines that had been sown indiscriminately from the air.

12.2 PRINCIPLES OF OPERATION

A radar system comprises a signal generator, transmitting and receiving antennae, and a receiver that may or may not have recording facilities or hardcopy graphical output. Some advanced systems have an onboard computer that facilitates data processing both while acquiring data in the field, and post-recording.

The basic constituents of a radar system are shown in Figure 12.1. The radar system causes the transmitter antenna (Tx) to generate a wavetrain of radiowaves which propagates away in a broad beam. As radiowaves travel at high speeds (in air 300 000 km/s or 0.3 m/ns),

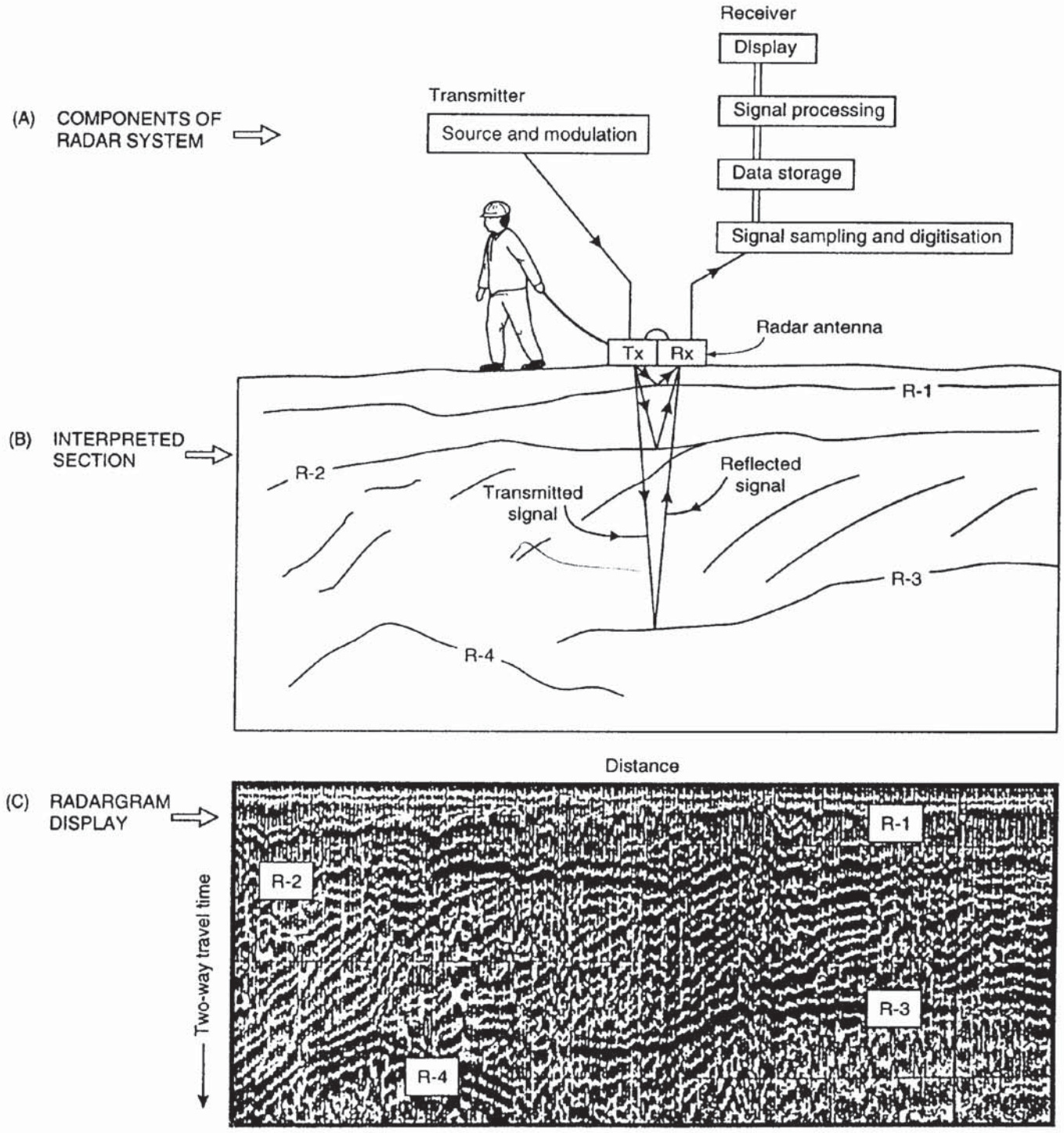

Figure 12.1 Simplified diagram of (A) the constituents of a radar system with (B) the interpreted section of (C) the radargram display. Adapted from Butler *et al.* (1991) and Daniels *et al.* (1988)

the travel time of a radiowave from instant of transmission through to its subsequent return to the receiving antenna (Rx) is of the order of a few tens to several thousand nanoseconds (ns; 10^{-9} seconds). This requires very accurate instrumentation to measure the transmit instant precisely enough for the final accuracy of the system to be reasonable with respect to the travel times in question. The antennae are used in either a monostatic or bistatic mode. *Monostatic mode* is when one antenna device is used as both transmitter and receiver, whereas *bistatic mode* is when two separate antennae are used with one serving as a transmitter and the other as a receiver. There are specific cases (such as in *wide-angle reflection and refraction* (WARR) measurements) when the bistatic mode is advantageous over the monostatic mode. The PulseEKKO system uses only bistatic antennae. For the majority of this chapter it can be assumed that any antennae are deployed in monostatic mode unless indicated otherwise.

The transmitter generates a pulse of radiowaves at a frequency determined by the characteristics of the antenna being used at a repetition rate of typically 50 000 times per second. The receiver is set to scan at a fixed rate, normally up to 32 scans per second, depending upon the system being used. Each scan lasts as long as the total two-way travel time range, which can be set from a few tens to several thousand nanoseconds. Each scan is displayed on either a video screen or a graphic recorder or both. As the antenna is moved over the ground, the received signals are displayed as a function of their two-way travel time, i.e. the time taken from instant of transmission to time of detection by the receiver, in the form of a *radargram*. This display is analogous to a seismic section (seismogram).

The pulse length of the transmitted radiowave should be short enough (typically < 20 ns, depending upon antenna frequency and type) to provide resolvable reflections. It is important, therefore, that the shape and characteristics of the transmitted radiowave are both determinable and highly repeatable. The significance of this point will be discussed below (see Section 12.5). The manner in which the recorded signals are displayed on a graphic recorder, for example, are determined by the operator; a simplified output is illustrated in Figure 12.2. Signals with amplitudes greater than the set threshold are printed dark on the radar section as illustrated. In some cases, it may be most suitable to print both positive and negative, or when just positive or just negative. Displays can also be output in terms of *variable area wiggle* or wiggle trace only (just as in seismic data displays). Commonly, the more sophisticated digital recording systems display the amplitudes of the signals according to a grey scale or colour menu; for example, the strongest reflections can be picked out by the brightest colours.

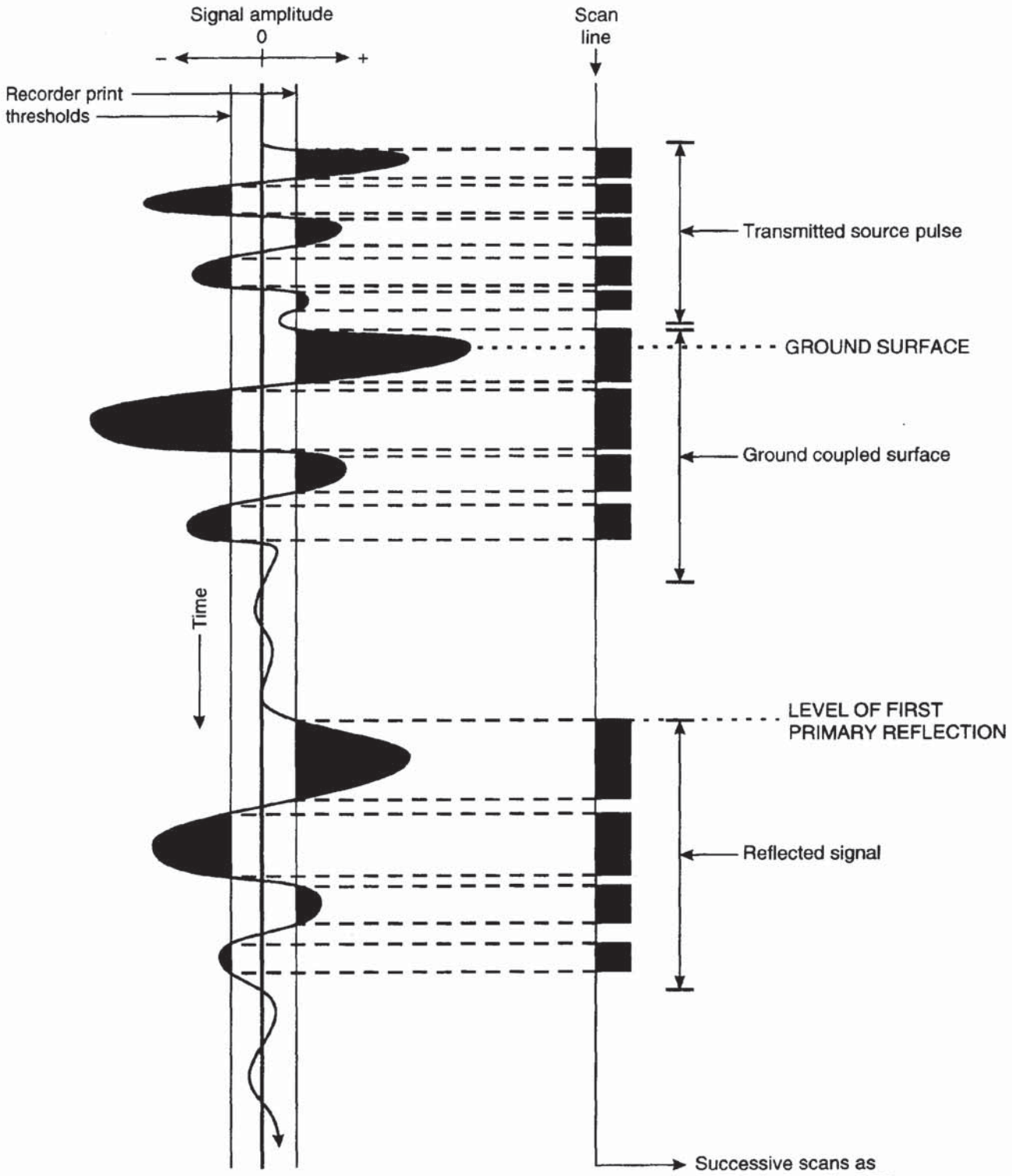

Sketch of a single radar pulse and reflections as seen by the receiver

Note that the source pulse consists of more than one wavelength and that it may have a complex waveshape. Ground coupling affects the shape and duration of the downgoing wavelet and thus the waveshape of any reflection is equally complex, but with a pulse-broadened duration due to attenuation of the higher frequency components of the signal. The reflection event consists of several wavelets, not just one, and it is imperative that this be borne in mind during the interpretation of radar data.

The measurement system should have sufficient dynamic range and sensitivity to be able to detect the low signal strengths associated with the returning radar pulses. It should also be able to produce printouts with adequate clarity for interpretation.

While the manufacturer's specifications may indicate the measurement accuracy of the timing within the instrument (e.g. to ± 1 ns), this should not be interpreted as being equivalent to the resolution capability of interpretation. Vertical and horizontal resolution are discussed in Section 12.5.

Figure 12.2 (*opposite*) Schematic example of the translation of the received waveform (one scan) on to a graphic recorder output

12.3 PROPAGATION OF RADIOWAVES

12.3.1 Theory

The electromagnetic properties of materials are related to their composition and water content, both of which exert the main control over the speed of radiowave propagation and the attenuation of electromagnetic waves in materials.

The speed of radiowaves in any medium is dependent upon the speed of light in free space ($c = 0.3$ m/ns), the relative dielectric constant (ε_r) and the relative magnetic permeability ($\mu_r = 1$ for non-magnetic materials) (see Box 12.1). The success of the ground radar method relies on the variability of the ground to allow the transmission of radiowaves. Some materials, such as polar ice, are virtually transparent to radiowaves. Other materials, such as water-saturated clay and seawater, either absorb or reflect the radiowaves to such an extent that they are virtually opaque to radiowaves. It is the contrast in relative dielectric constant between adjacent layers that gives rise to reflection of incident electromagnetic radiation. The greater the contrast, the greater will be the amount of radiowave energy reflected. The proportion of energy reflected, given by the *reflection coefficient* (R), is determined by the contrast in radiowave velocities, and, more fundamentally, by the contrast in the relative dielectric constants of adjacent media (see Box 12.2). In all cases the magnitude of R lies in the range ± 1. The proportion of energy transmitted is equal to $1 - R$. The equations given in Box 12.2 apply for normal incidence on a planar surface assuming no other signal losses and refer to the amplitude of a signal. The power reflection coefficient is equal to R^2.

Box 12.1 Speed of radiowaves

The speed of radiowaves in a material (V_m) is given by:

$$V_m = c/\{(\varepsilon_r\mu_r/2)[(1+P^2)+1]\}^{1/2}$$

where c is the speed of light in free space, ε_r is the relative dielectric constant, and μ_r is the relative magnetic permeability ($=1$ for non-magnetic materials). P is the *loss factor*, such that $P=\sigma/\omega\varepsilon$, and σ is the conductivity, $\omega=2\pi f$ where f is the frequency, ε is the permittivity $=\varepsilon_r\varepsilon_0$, and ε_0 is the permittivity of free space (8.854×10^{-12} F/m).

In low-loss materials, $P\approx0$, and the speed of radiowaves, $V_m = c/\sqrt{e_r} = 0.3/\sqrt{\varepsilon_r}$.

It should always be remembered when dealing with ground radar that the radiation is electromagnetic and its propagation is described by Maxwell's equations with the electric (E) component orthogonal to the magnetic (H) component (Figure 12.3). The specific shape and size of the directivity pattern lobes are functions of the dielectric constant(s) of the host media. There is a danger in making the comparison of radargrams to seismograms that the vector nature of radar may be overlooked, so that incorrect assumptions are made about the way the radiowaves behave in geologic media. While seismic data processing can be used effectively in most cases, the electromagnetic polarisable characteristics of the radiowaves are more analogous to seismic S-waves than to P-waves.

Box 12.2 Amplitude reflection coefficient

The amplitude reflection coefficient is:

$$R = \frac{(V_1 - V_2)}{(V_1 + V_2)}$$

where V_1 and V_2 are the radiowave velocities in layers 1 and 2 respectively, and $V_1 < V_2$. Also:

$$R = \frac{\sqrt{\varepsilon_2} - \sqrt{\varepsilon_1}}{\sqrt{\varepsilon_2} + \sqrt{\varepsilon_1}}$$

where ε_1 and ε_2 are the respective relative dielectric constants (ε_r) of layers 1 and 2, applicable for incidence at right-angles to a plane reflector. Typically, ε_r increases with depth.

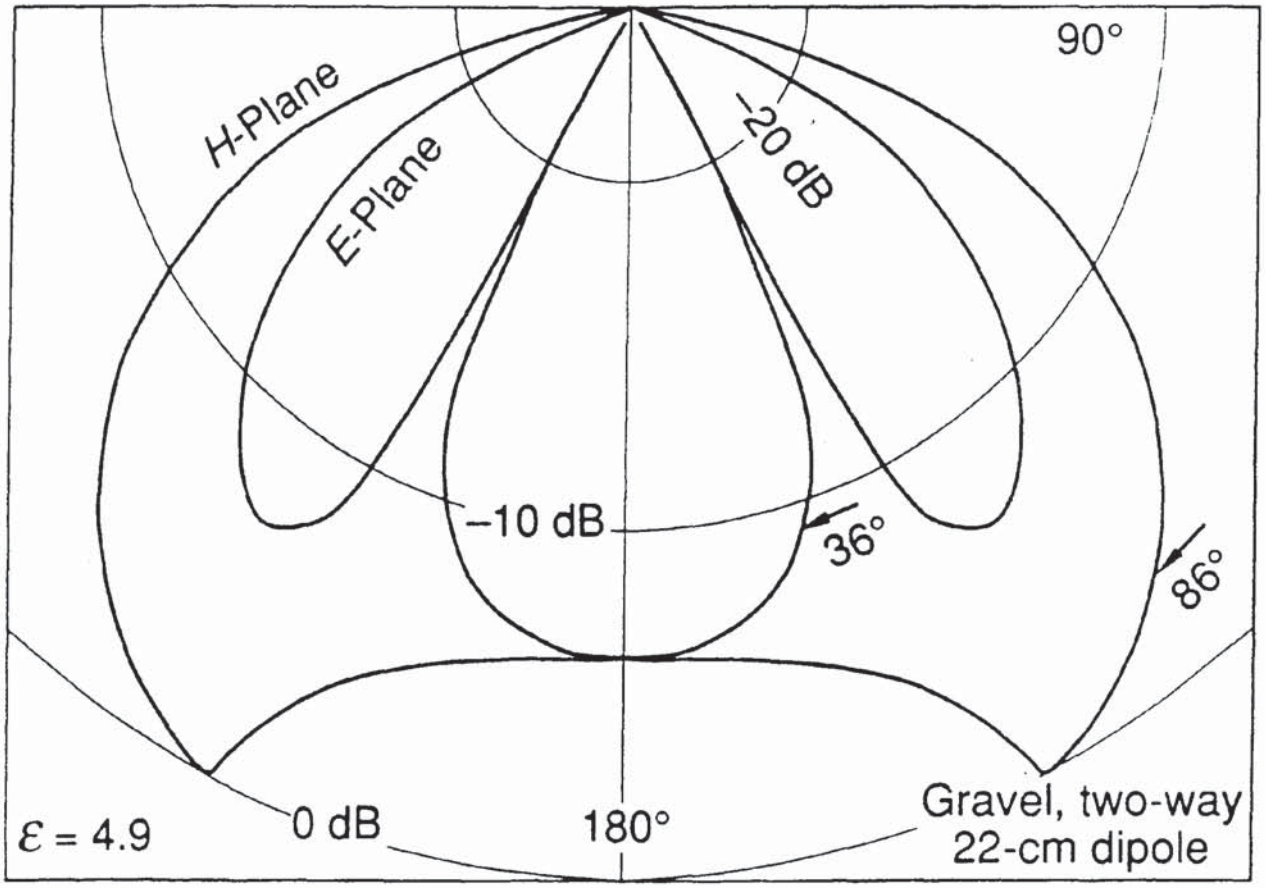

Figure 12.3 Theoretical *E*- and *H*-plane radar directivity patterns for a 22 cm resistively-loaded dipole situated over a medium with $\varepsilon = 4.9$. From Acrone *et al.* (1993), by permission

12.3.2 Energy loss and attenuation

Factors that result in a decrease in signal strength as radiowaves propagate through sub-surface media are illustrated schematically in Figure 12.4. Energy loss occurs as a consequence of reflection/ transmission losses about each interface and occur each time the radiowaves pass through a boundary. Furthermore, if there are objects with dimensions of the same order as the wavelength of the radar signal, these objects will cause scattering of energy in a random manner. This is known as *Mie scattering* and causes 'clutter' noise on the radar section. It is analogous to the noise seen on marine radar screens caused by the backscatter from seawaves in rough weather.

In addition to reflection/transmission losses at interfaces, energy is lost by *absorption* (turning the electromagnetic energy into heat). This is best pictured by analogy with a microwave oven which uses high-power radiowaves to cook food. A further loss of energy is caused by the geometrical spreading of the energy. The radar signal is transmitted in a beam with a cone angle of 90°. As the radio signals travel away from the transmitter, they spread out causing a reduction in energy per unit area at a rate of $1/r^2$, where r is the distance travelled.

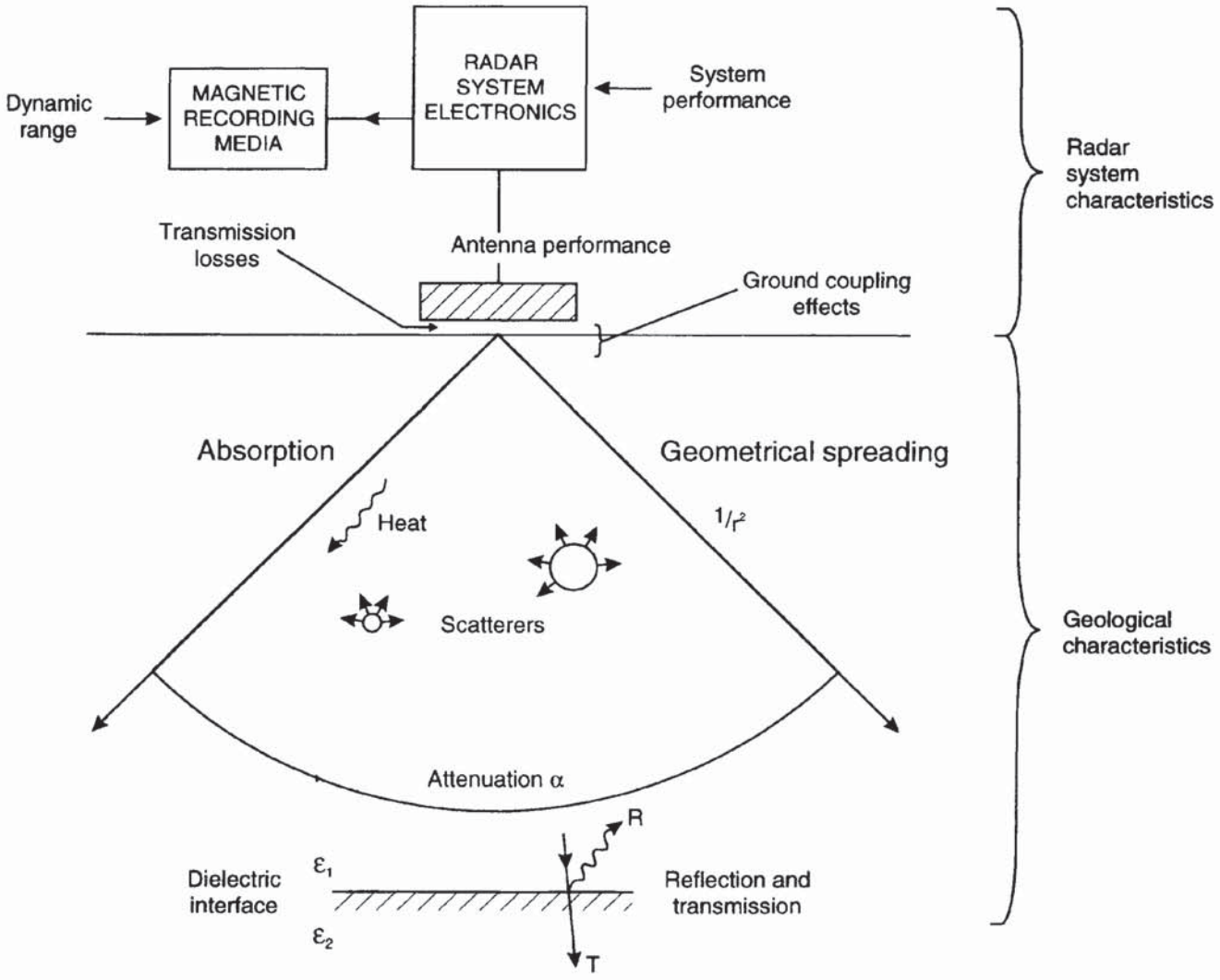

Figure 12.4 Processes that lead to reduction in signal strength

A fundamental cause of the loss of energy is *attenuation* which is a complex function of the dielectric and electrical properties of the media through which the radar signal is travelling. The attenuation factor (α) is dependent upon the electric (σ), magnetic (μ) and dielectric (ε) properties of the media through which the signal is propagating as well as the frequency of the signal itself ($2\pi f$). The bulk behaviour of a material is determined by the corresponding physical properties of the various constituents present and their respective proportional abundances.

As with other electromagnetic waves, the depth by which the signal has decreased in amplitude to $1/e$ (that is, to 37%) of the initial value is known as the skin depth (δ) and is inversely proportional to the attenuation factor (i.e. $\delta = 1/\alpha$). Mathematical definitions of the attenuation factor and skin depth are given in Box 12.3. Using the final term for the skin depth, and substituting typical values for seawater, it can be seen that the skin depth in seawater is only 1 cm, and for wet

clay it is only 0.3 m. Where fresh dry rock is encountered, the conductivity term decreases substantially and hence the skin depth increases, and much greater depth penetration is likely. The variation in skin depth is shown in Figure 12.5 as a function of ground resistivity at the extremes of expected *in situ* relative dielectric constants (McCann *et al.* 1988).

Box 12.3

If the peak electric field strength on transmission is E_0, and at a distance x away it has reduced to E_x, the ratio of the two amplitudes is given by:

$$E_0/E_x = \exp(-\alpha x)$$

where α is the attenuation coefficient;

$$\alpha = \omega\left\{\left(\frac{\mu\varepsilon}{2}\right)\left[\left(1+\frac{\sigma^2}{\omega^2\varepsilon^2}\right)^{1/2}-1\right]\right\}^{1/2}$$

where $\omega = 2\pi f$ where f is the frequency (Hz), μ is the magnetic permeability ($4\pi \times 10^{-7}$ H/m), σ is the bulk conductivity at the given frequency (S/m), and ε is the dielectric permittivity where $\varepsilon = \varepsilon_r \times 8.85 \times 10^{-12}$ F/m and ε_r is the bulk relative dielectric constant. The formula is valid for non-magnetic materials only.

The term $(\sigma/\omega\varepsilon)$ above is equivalent to the *loss factor* (P), such that:

$$P = \sigma/\omega\varepsilon = \tan D.$$

Also, skin depth $(\delta) = 1/\alpha$. When $\tan D \ll 1$, $\delta = (2/\sigma)(\varepsilon/\mu)^{1/2}$. Numerically:

$$\delta = (5.31\sqrt{\varepsilon_r})/\sigma, \text{ where } \sigma \text{ is in mS/m.}$$

It is important to remember that the simplified version of skin depth is valid only when the loss factor is considerably less than one. In order to determine when such conditions are valid, the graph shown in Figure 12.6 should be used. The figure shows the theoretical conductivity values (in mS/m) when the loss factor is equal to one. Thus the observed conductivity for the condition of being much less than unity to apply should be of the order of 0.05 of the theoretical conductivity. For example, if the observed true conductivity is 15 mS/m, then the loss factor needs to be considered in its full form in all cases other than when a 900 MHz antenna is being used, as long as the relative dielectric constant is greater than or equal to 6. If the full form of the attenuation factor is not used under these circumstances, the derived value of skin depth will be overestimated.

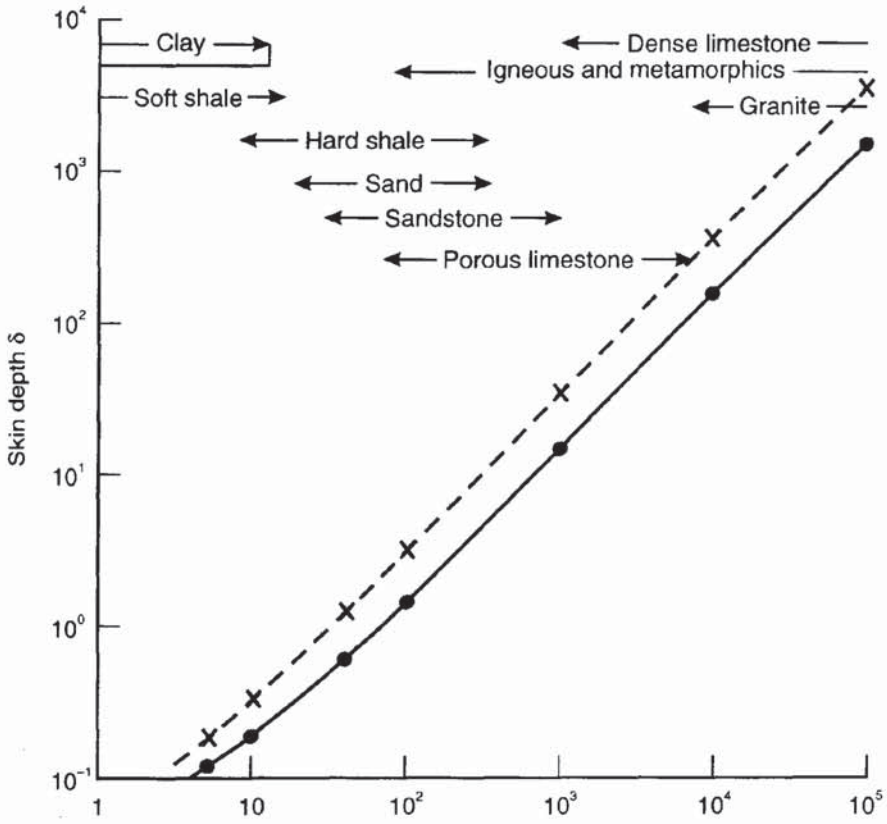

Figure 12.5 Variation of skin depth (δ) as a function of resistivity for $\varepsilon_r = 8$ and 40. After McCann *et al.* (1988), by permission

It should be noted that the skin depth does not equate to the depth of penetration of the ground radar. To determine radar range, instrumental factors also need to be taken into consideration in addition to those related to the sub-surface target and to the media through which the radiowaves travel. The total path loss for a given distance is made up of five terms: antenna losses; transmission losses between the air and the ground; losses caused by the geometrical spreading of the radar beam; attenuation within the ground as a function of the material properties; and losses due to scattering of the radar signal from the target itself. The radar range equation and definition of a radar system performance (Q) are given in Box 12.4 and the components affecting radiated and return power are illustrated schematically in Figure 12.7.

The system performance of modern radar equipment is between 120 and 160 dB, enabling a three-fold improvement in depth penetration under the same ambient conditions over that of a radar system with $Q = 80$ dB. The variation of radar signal range is shown in Figure 12.8 as a function of both attenuation and radar system performance (Q).

Within Box 12.4 are listed three types of target: smooth and rough plane reflectors and a point target. Of particular importance is the gF

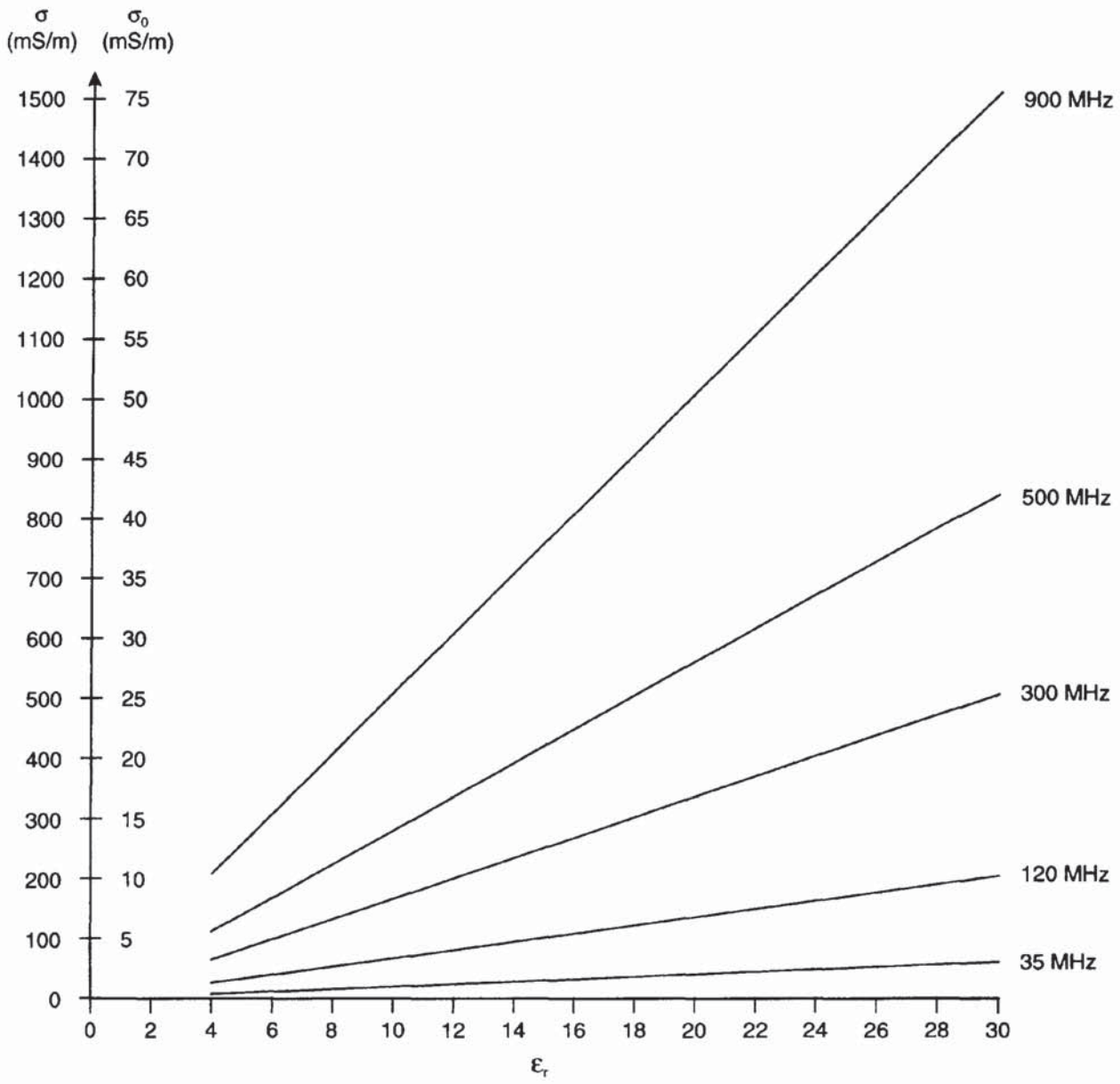

Figure 12.6 Conditions under which the loss factor (tan D) $\ll 1$

term in the first equation in Box 12.4. This product defines the power scattered by the target and also directed back to the receiver. The term g is the backscatter gain of the target and F is the target scattering cross-sectional area.

For a smooth plane reflector, the incident signal returned appears to be an image of the source, albeit reduced in power by the power reflection coefficient R ($=r^2$, where r is the amplitude reflection coefficient) of the interface, radiating upwards from a distance twice as far away as the boundary. The theory behind this is the same as in simple optics for a plane reflector.

Box 12.4 Radar range equation, and definition of Q
(Annan and Davis 1977)

Radar range equation (Ridenour 1947)
Q is the system performance (in decibels):

$$Q = 10\log\left\{\frac{E_{Tx}E_{Rx}G_{Tx}G_{Rx}V^2(gF)\exp(-4\alpha z)}{64\pi^3 f^2 z^4}\right\}.$$

The various terms are defined in Figure 12.7. Also:

$$Q = 10\log(P_{min}/P_s)$$

where P_{min} is the minimum detectable signal power, and P_s is the source power.

In low-loss materials the range of z is approximately $10D_2$. In high-loss materials the range is approximately D_2/D_1, where:

$$D_1 = 2A/(40-10B_2)$$

$$D_2 = \frac{\{-Q+10\log(S)+10\log V^2+10[B_1+(B_3-2)\log f]\}}{40-10B_2}$$

$$S = E_{Tx}E_{Rx}G_{Tx}G_{Rx}/64\pi^3$$

where B_1, B_2 and B_3 are as listed in the table below.

Type of target	gF	B_1	B_2	B_3
Smooth, plane reflector	$\pi z^2 R$	$\log(\pi R)$	2	0
Rough, plane reflector	$\pi(V^2/16f^2+Vz/2f)R$	$\log(\pi VR/2)$	1	−1
Rayleigh point target	$(64\pi^5 a^6 f^4/V^4)R$	$\log(64\pi^5 a^6 f^4/V^4)$	0	4

For a rough, specular reflector, there is difficulty in defining the cross-sectional area of the target. Cook (1975) suggested that it equates to the area of the first Fresnel zone (see Figure 12.9). Consequently, where the wavelength of the roughness of the surface is greater than the diameter of the first Fresnel zone, the cross-sectional area, and hence the gF product, can be estimated. Where the wavelength of the surface roughness is less than the diameter of the first Fresnel zone, and especially when the amplitude of the roughness is greater than one-quarter wavelength, the actual cross-sectional target area is difficult to calculate. The power reflection coefficient would be reduced as a consequence of the greater scatter arising from such a surface roughness. The significance of the first Fresnel zone in terms of interpretation and resolution is discussed further in Section 12.5.

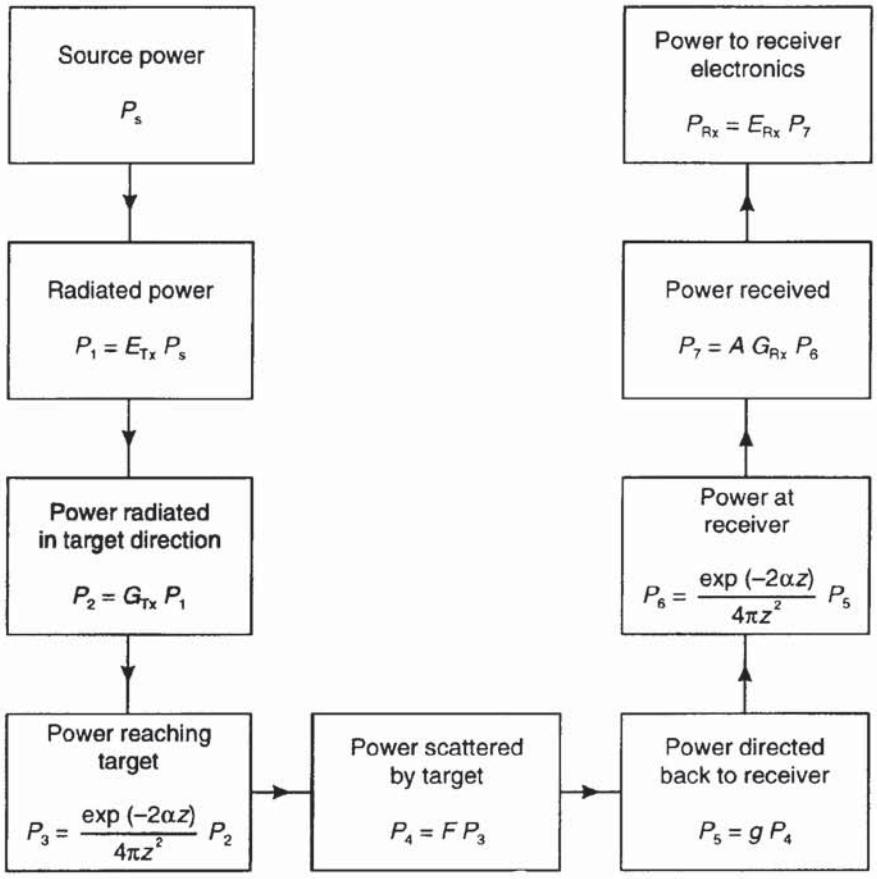

Figure 12.7 Block diagram illustrating radiated and return power for a radar system. After Annan and Davis (1977), by permission

$E_{Tx,\,Rx}$	=	efficiency of transmitter/receiver antenna
$G_{Tx,\,Rx}$	=	transmitter/receiver gain
g	=	backscatter gain of target
F	=	target scattering cross-sectional area
z	=	distance of target from antenna
α	=	attenuation coefficient of medium
V	=	radiowave velocity of medium
A	=	effective area of receiver antenna $(= V^2/4\pi f^2)$
f	=	frequency of signal
R	=	power reflection coefficient at a boundary

For a point target, the characteristics of the returned energy is described by the Rayleigh Law of scattering in which the gF product is very strongly dependent upon frequency (to the fourth power). It is assumed for the expression in Box 12.4 for a point source, that the radius of the target (a) is much smaller than the wavelength of the incident radiation. In materials that consist of cobbles and gravel, for example, or where the geological units are severely distorted over distances shorter than the wavelength of the incident energy, then the

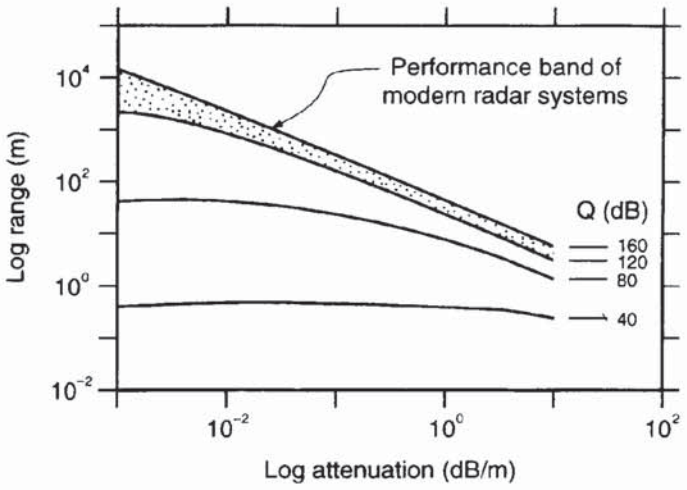

Figure 12.8 Radar range for radars with different system performances (Q) over a range of attenuation. From Davis and Annan (1989), by permission

amount of energy scattered is likely to be large and the resulting radargram is likely to show very few, if any, coherent reflection events associated with such materials. This characteristic can in itself be used indirectly during interpretation as being diagnostic of such material.

It has been shown (see Box 12.3) that attenuation is directly proportional to frequency. The higher the frequency, the greater will be the amount of attenuation. It is also evident that the bulk relative dielectric constant (ε_r) and bulk conductivity at the given frequency (σ) also affect attenuation significantly. Each of these properties is affected by the composition of the material and the electrical behaviour and relative abundance of each constituent. The loss factor ($\tan D$ in Box 12.3) is directly proportional to conductivity and inversely proportional to the relative dielectric constant and frequency. For saturated granular media, the conductivity and the relative dielectric constant of the saturating fluid will dominate over the respective matrix values. The bulk relative dielectric constant (ε_r) is roughly equal to the product of porosity (ϕ) and relative dielectric constant for the fluid (ε_f). The effect of this is that the more conductive the saturating fluid, and the greater the proportion of fluid present with a correspondingly high relative dielectric constant (remember: ε_r for water = 81), the greater will be the attenuation. Similarly, the greater the clay content, the greater will be the loss factor and hence attenuation. The importance of clay is that it possesses bound water within its lattice structure. Clay minerals also exhibit particular electrical properties as a result of their physicochemical structure, the details of which are beyond the scope of this section.

For both geological and engineering materials the electrical and dielectric properties, especially as functions of frequency, are still poorly understood. Furthermore, the petrophysical characteristics of such materials are largely unknown. The electrical and dielectric properties of materials are discussed in Section 12.4.

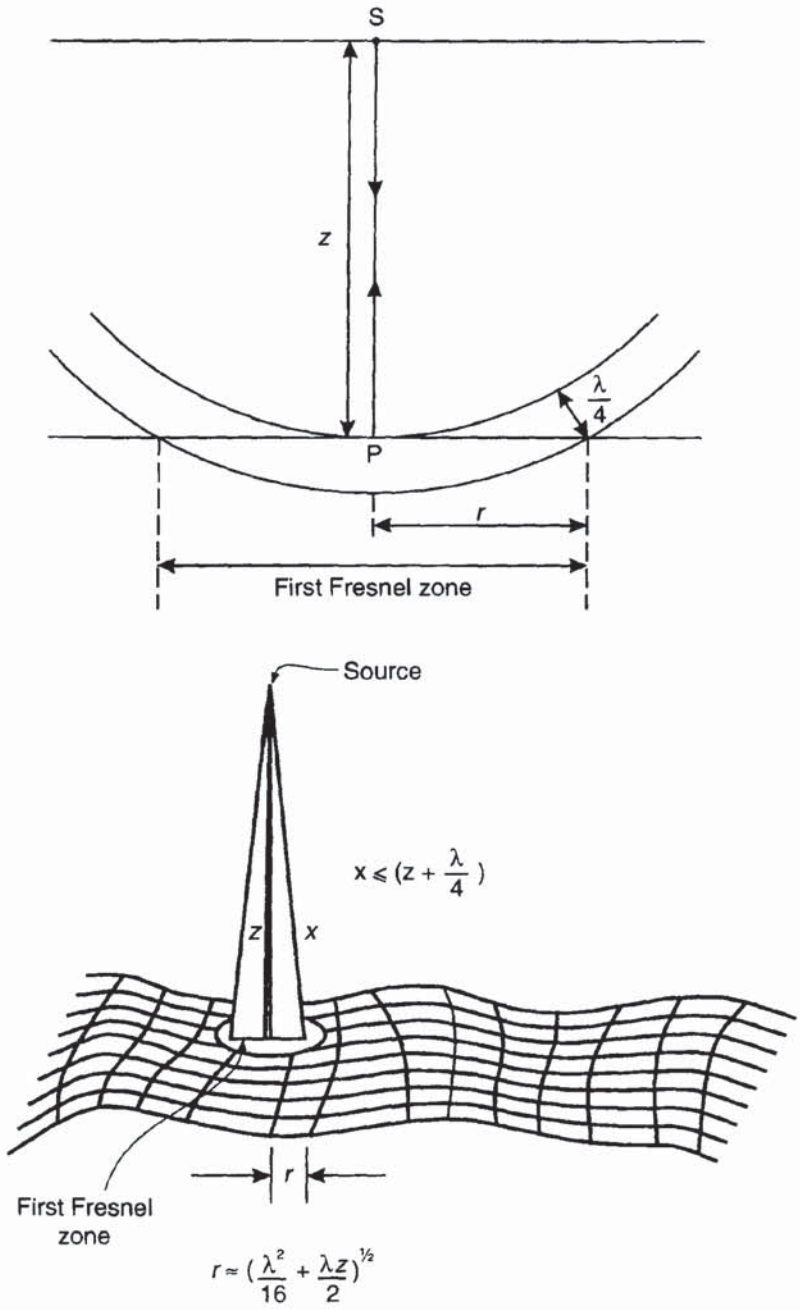

Figure 12.9 Reflection from a rough, specular interface; the target cross-sectional area is equivalent to the area of the first Fresnel Zone. After Annan and Davis (1977), by permission

12.3.3 Horizontal and vertical resolution

Vertical resolution is a measure of the ability to differentiate between two signals adjacent to each other in time. Simplistically, vertical resolution is a function of frequency. Each radar antenna is designed to operate over a range of frequencies (bandwidth) where the peak power occurs at the centre frequency of the antenna. It is the centre frequency that labels individual antenna; hence a 500 MHz antenna has a centre frequency of 500 MHz, for instance. The centre frequency is also inversely proportional to the pulse period (in nanoseconds). The

Table 12.2 Theoretical vertical resolution for two geological materials at three frequencies

	Antenna frequency (MHz)		
	120	500	900
Soil			
Wavelength (cm)	62.5	15	8
Resolution (cm)	15.6	3.75	2
Bedrock			
Wavelength (cm)	92	22	12
Resolution (cm)	23	5.5	3

500 MHz antenna, therefore, has a pulse period of 1/500 MHz = 2 ns, and for 35 MHz the pulse period is $1/35 \times 10^6$ or 28.6 ns. The equivalent length (in metres) of the pulse is the product of the pulse period and the radiowave velocity for the appropriate material. In a wet soil ($V = 0.06$ m/ns) and with a 100 MHz antenna (pulse period = 10 ns), the pulse (wave) length is 0.06×10 m or 0.6 m. Resolution can be taken as one-quarter of the wavelength (h) of incident radiation; $h = V/f$, where V is the radiowave velocity, and f is its frequency. In the last case, if the wavelength is 60 cm, the *theoretical* vertical resolution is 15 cm.

Examples of theoretical minimum resolutions for two different materials at three separate frequencies are listed in Table 12.2. The first example in the table is for a typical soil with $V = 0.075$ m/ns, and the second, a massive rock such as limestone with $V = 0.110$ m/ns. The vertical resolutions given are the very best that could be achieved theoretically. In reality, the resolution is less than these figures owing to the complex nature of the source waveform and the ground responses.

An antenna placed directly on the ground will produce a 'ground coupled' signal. That is, the transmitted waveform in air will not be reproduced when being transmitted into the ground. The material affects the shape, form and amplitude (power) of the downgoing source wavetrain and effectively filters it. The source pulse length decreases with increasing frequency, but describes the main pulse lobe only. With ground coupling, and depending upon the transmitter efficiency, the downgoing wavetrain is usually several times longer than the pulse length described in the manufacturer's literature for a given antenna. This complexity of source waveshape has serious consequences for interpretation.

If the downgoing radar wave has, for instance, three cycles with a total period of 25 ns, this means that a reflection from any interface will have equal if not greater complexity of shape and longer period. The lengthening is due to the loss of higher frequency components within the signal as higher frequencies are attenuated preferentially with respect to lower frequencies.

If two interfaces are separated by only a few tens of centimetres, for example, and the radiowave velocity of the material in between is such that the time interval between a reflection from the first (uppermost) interface and one from the second is shorter than the period of the source wavetrain, the onset of the second reflection will be masked by the tail of the first, and thus may not be resolved.

Another complexity is that the downgoing signal travels from the transmitter in a cone of radiation with a finite-sized footprint. The first Fresnel zone describes the minimum area in which features with smaller dimensions will not be imaged. The radius of the first Fresnel zone is indicated in Figure 12.9. The finite size of this footprint affects both the vertical resolution (when interfaces are steeply dipping or have high-amplitude surface roughness relative to the wavelength of the incident radiowaves), and the horizontal resolution. The larger the first Fresnel zone, the lower will be the horizontal resolution in discriminating between adjacent targets. Furthermore, spatial resolution is also affected by the conical beam width of the downgoing radiowaves (see Figure 12.10); the narrower the beam width, the greater will be the spatial resolution. Horizontal resolution is inversely proportional to $\sqrt{\alpha}$, where α is the attenuation coefficient (Daniels *et al.* 1988). Consequently, the horizontal resolution is actually better over a high-loss material than over a low-loss medium. Where radar systems permit horizontal stacking of adjacent scans to improve the signal-to-noise ratio, horizontal resolution is reduced as the amount of horizontal stacking is increased. There is a practical compromise to

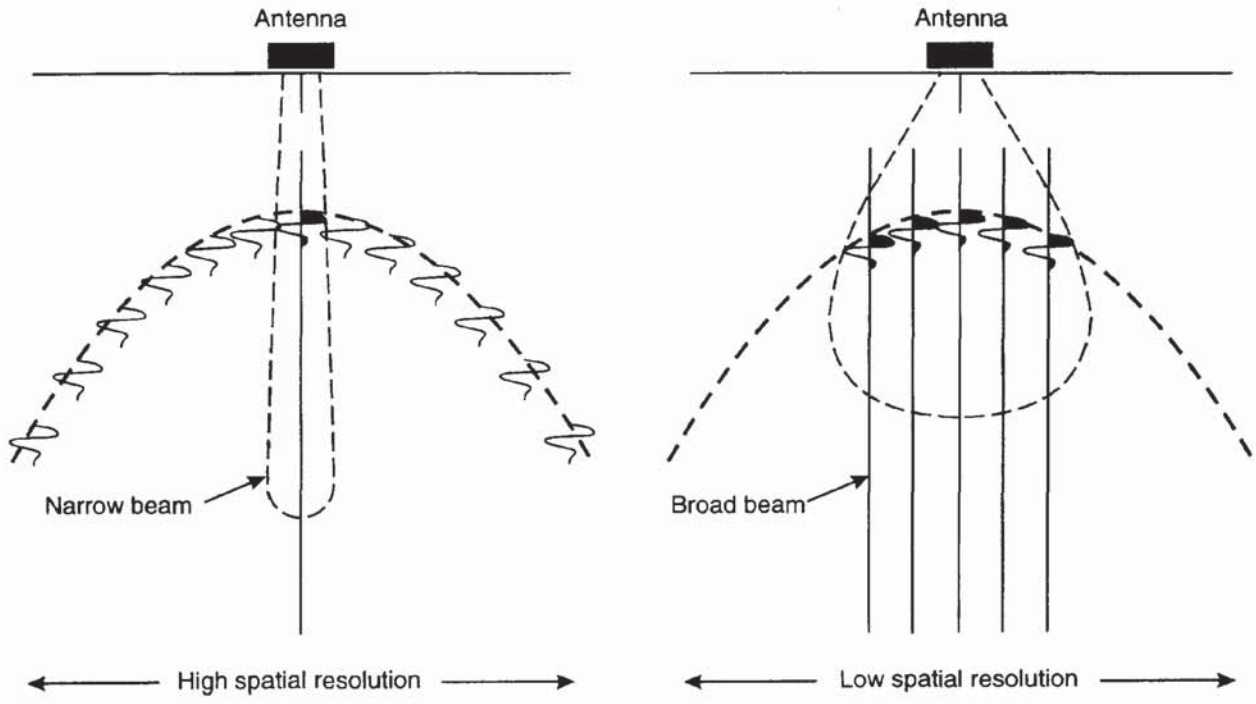

Figure 12.10 Horizontal resolution due to beam width

be reached between optimising return signal strengths by horizontal stacking and reducing horizontal resolution.

When *synthetic aperture radar* (SAR) is used, measurements are made by a single antenna at a number of different positions and the results combined to simulate a narrower beam than would have been achieved by using just an isolated antenna at one location. Details of the SAR or holographic radar are beyond the scope of this chapter.

12.4 DIELECTRIC PROPERTIES OF EARTH MATERIALS

The dielectric behaviour of a material is described in terms of its complex permittivity (ε^*) and complex conductivity (σ^*) which are interrelated (see Box 12.5). The high-frequency permittivity (ε_∞) is taken as the lowest real permittivity when the imaginary permittivity (ε'') is zero (see Figure 12.11). The real permittivity (ε') increases as frequency decreases. When the material is a non-conductor, the frequency–permittivity behaviour is described by a semicircle, the centre of which is located on the real permittivity axis half-way between the high-frequency and static permittivities (ε_∞ and ε_s respectively). The imaginary permittivity (ε'') indicates the absorption or energy loss within the dielectric material, and this in turn contributes to the absorption of radiowaves within the ground.

Box 12.5 Complex permittivity and conductivity

Complex permittivity ε^* of a non-conductive material is given by:

$$\varepsilon^* = \varepsilon' + i\varepsilon''.$$

When ε'' is plotted as a function of ε', the resultant graph is a semicircle. The plot is known as a Cole–Cole plot after its originators, Cole and Cole (1947).

If the material has a conductivity σ, then:

$$\varepsilon^* = \varepsilon' + i(\varepsilon'' + \sigma_s/\omega\varepsilon_0)$$

where σ_s is the static or DC conductivity, and ε_0 is the permittivity of free space. At low frequencies, the DC term dominates and produces a characteristic low-frequency tail (see Figure 12.11). The ε'' term is the frequency-dependent loss related to the relaxation response phenomena associated with water molecules (King and Smith 1981).

The complex conductivity σ^* is given by:

$$\sigma^* = \sigma' + i\sigma'' = j\omega\varepsilon_0\varepsilon^*.$$

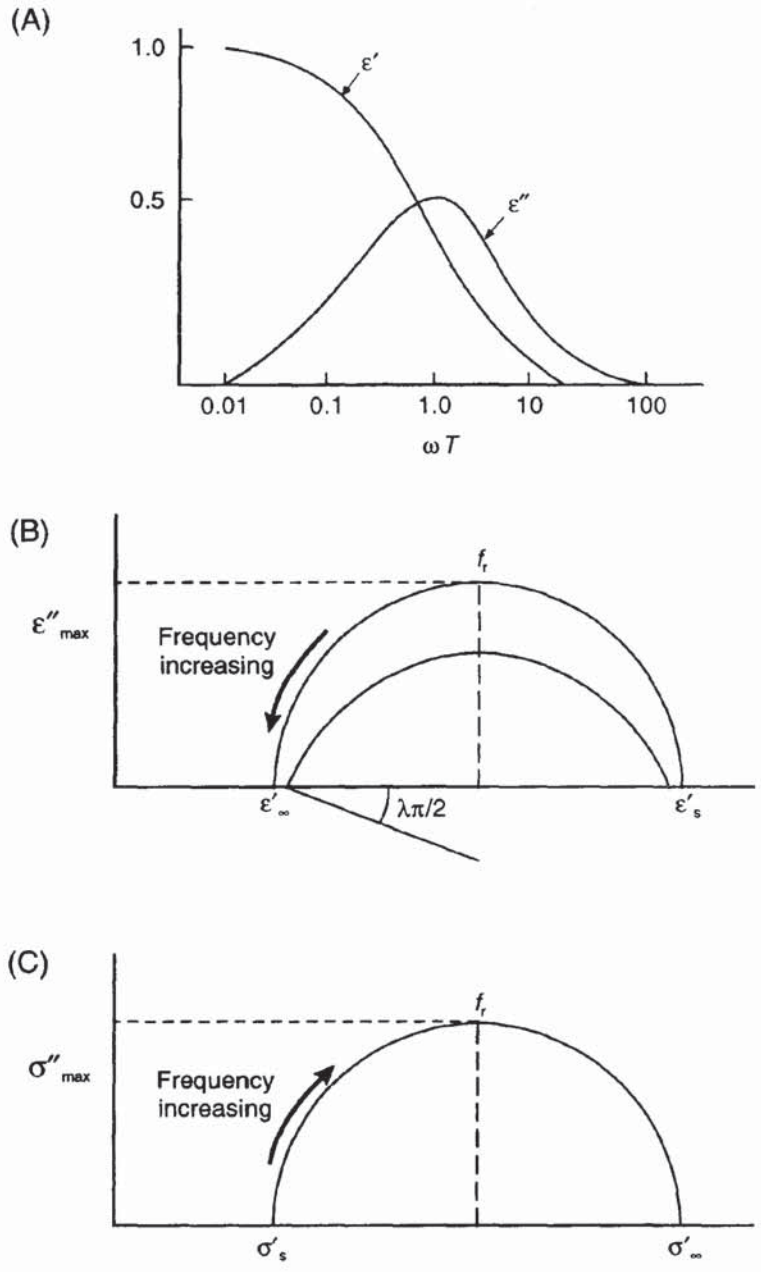

Figure 12.11 Cole–Cole plot of complex permitivity

If the material is conductive, then an appropriate additional term has to be included within the definition of the complex permittivity (Box 12.5). Conductivity also contributes to the loss within the material.

The relative dielectric constant (ε_r) varies from 1 in air through to 81 in water. For most geological materials, ε_r lies in the range 3–30. Consequently, the range of radiowave velocities is large (see Box 12.1), from around 0.06 to 0.175 m/ns (Figure 12.12). The speed of radiowaves in air is 299.8 mm/ns. In trying to estimate depths to any given target it is *essential* to have a detailed knowledge of the

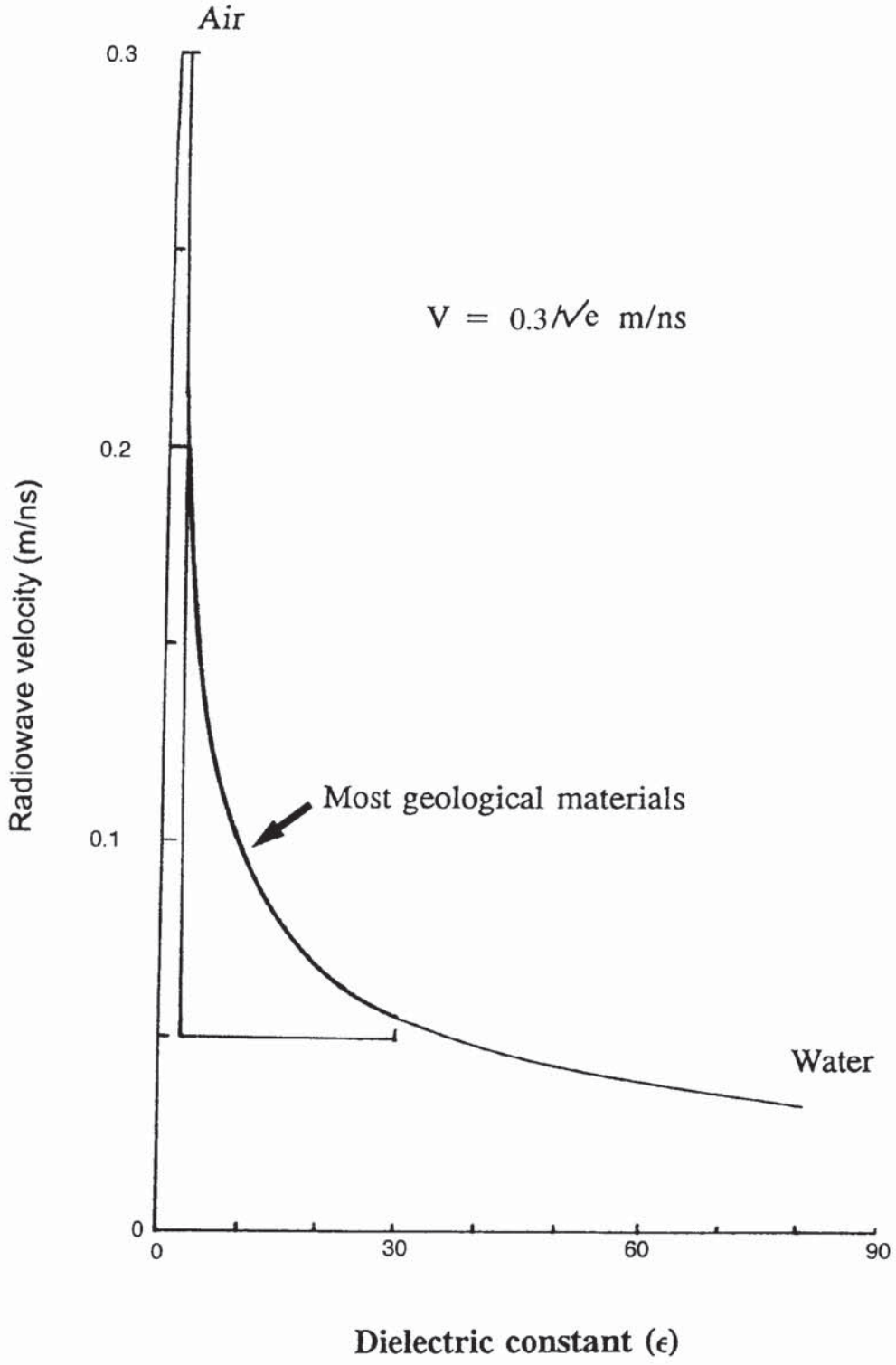

radiowave velocities through the sub-surface materials present. This aspect of radar interpretation will be dealt with in Section 12.6.

A list of the relative dielectric constants and associated radiowave velocities for a variety of geological and man-made materials is given

Figure 12.12 Radiowave velocities as a function of relative dielectric constant

Table 12.3 Table of relative dielectric constants and radiowave velocities for a range of geological and man-made materials

Material	ε_r	V(mm/ns)
Air	1	300
Water (fresh)	81	33
Water (sea)	81	33
Polar snow	1.4–3	194–252
Polar ice	3–3.15	168
Temperate ice	3.2	167
Pure ice	3.2	167
Freshwater lake ice	4	150
Sea ice	2.5–8	78–157
Permafrost	1–8	106–300
Coastal sand (dry)	10	95
Sand (dry)	3–6	120–170
Sand (wet)	25–30	55–60
Silt (wet)	10	95
Clay (wet)	8–15	86–110
Clay soil (dry)	3	173
Marsh	12	86
Agricultural land	15	77
Pastoral land	13	83
Average 'soil'	16	75
Granite	5–8	106–120
Limestone	7–9	100–113
Dolomite	6.8–8	106–115
Basalt (wet)	8	106
Shale (wet)	7	113
Sandstone (wet)	6	112
Coal	4–5	134–150
Quartz	4.3	145
Concrete	6–30	55–112
Asphalt	3–5	134–173
PVC, Epoxy, Polyesters	3	173

Data from Johnson *et al.* (1979), McCann *et al.* (1988), Morey (1974), Reynolds (1990b, 1991b)

in Table 12.3. It should be emphasised that the values of both relative dielectric constants and radiowave velocities should be taken only as guide figures. The lack of ranges for some materials is due to the paucity of measurements made and is not meant to imply that there is no variation within these materials. The ranges given are also not meant to be extremes. As more results are published the ranges listed may need to be extended as the true variability of both parameters becomes more widely realised.

Cook (1975) has produced a schematic illustration (Figure 12.13) to show the likely probing distances achievable for different geological

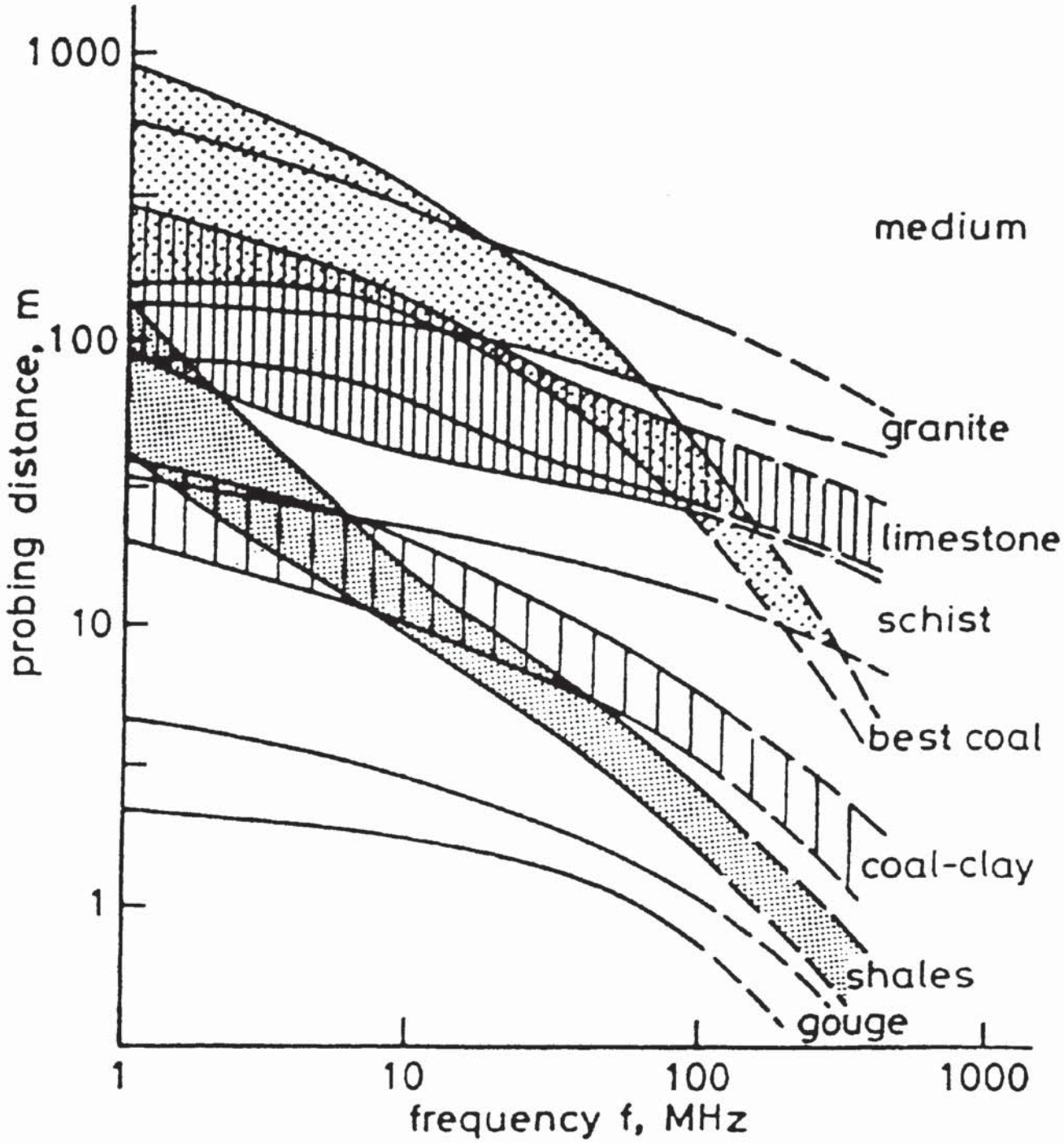

materials over the frequency range from 1 to 500 MHz. Clay-rich materials have much shorter probing distances than more massive rocks such as granite and limestone.

Most materials, whether geological or man-made, are a complex mixture of components each of which is likely to have different electrical and dielectric properties. Grain size and even grain shape

Figure 12.13 Probing distances as a function of frequency for different geological materials. From Cook (1975), by permission

can affect bulk electrical and dielectric behaviour. Most rocks contain a degree of moisture, either as 'free' liquid contained within pore spaces, or 'bound' within the mineral lattice as with many types of clay minerals. Since the relative dielectric constant of water is high (81) relative to that of dry rock, even a small amount of water may increase the bulk permittivity of the rock. An example of the effect of soil moisture content of a variety of rocks on the relative dielectric constant is shown in Figure 12.13. Furthermore, the amount of water present within a rock will also affect the speed of propagation of radiowaves. The radar velocity through freshwater is 3.3×10^7 m/s (0.033 m/ns) whereas it is 1.2×10^8 m/s (0.12 m/ns) through a low-porosity sandstone (McCann *et al.* 1988).

The relative dielectric constant of a layered material has been demonstrated to be related to porosity (ϕ) by considering the proportion of constituents present and their respective relative dielectric constants. The relationships between constituent and bulk relative dielectric constants and porosity are given in Box 12.6; the variations of radiowave velocity with porosity for water-saturated and air-saturated porous media are illustrated in Figure 12.14. If the relative dielectric constant for each constituent of the material is known and that of the bulk material is measured or derived from the radiowave velocity, then the total porosity can be calculated.

Box 12.6 Relative dielectric constants and porosity
(Parkomenko 1967)

The relationship between bulk relative dielectric constant (ε_r) and porosity (ϕ) is:

$$\varepsilon_r = (1 - \phi)\,\varepsilon_m + \phi\varepsilon_w \qquad (1)$$

where ϕ is the porosity, ε_m and ε_w are the relative dielectric constants for the rock matrix and pore fluid water, respectively. This is valid when the external field is applied parallel to the bedding.

When the external field is applied perpendicular to the bedding, then:

$$\varepsilon_r = \varepsilon_m\varepsilon_w/[(1 - \phi)\varepsilon_m + \phi\varepsilon_w].$$

Using the simplified relationship that $V = c/\sqrt{\varepsilon_r}$, for low-loss materials, where c is the radiowave velocity in air, and substituting in equation (1) for ε_r, then:

$$V = c/[(1 - \phi)\varepsilon_m + \phi\varepsilon_w]^{1/2}.$$

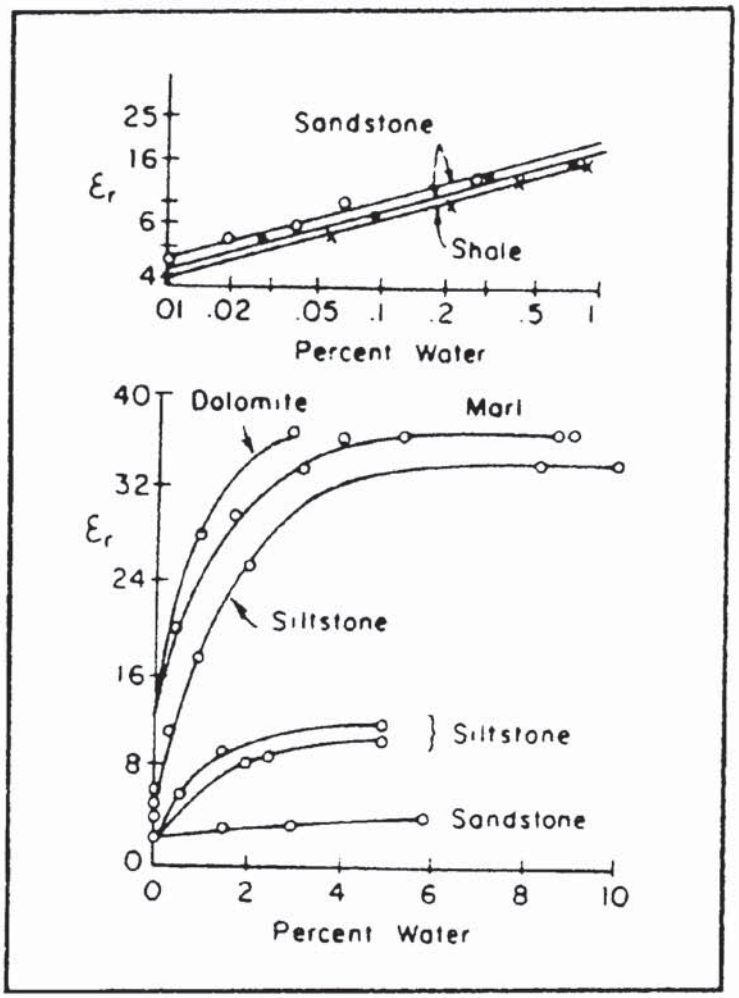

Figure 12.14 Effect of soil moisture content of rock on ε_r. From King and Smith (1981), by permission

From Figure 12.15 it can be seen that the radiowave velocity decreases with increasing soil moisture content. Consequently, wetter materials have a better vertical resolution than dry materials, although the attenuation in wetter materials is greater than for dry so depth penetration is likely to be smaller.

The determination of porosity assumes only a two-component system, i.e. made up of a matrix and pore spaces that are saturated with either air or another fluid of known relative dielectric constant. It also assumes that all the pore spaces are saturated with one fluid. This situation may not be achieved in many cases in nature.

Total porosity is the proportion of volume not filled by the solid constituents within a material and includes isolated pore/fracture space. The *effective porosity* is the porosity available to free fluids and excludes the isolated unconnected pores/fractures and space occupied by bound water in clays (Sheriff 1991). The isolated pore/fracture space (*residual porosity*) is thus the difference between the total and effective porosities. The permeability of a material is a measure of the

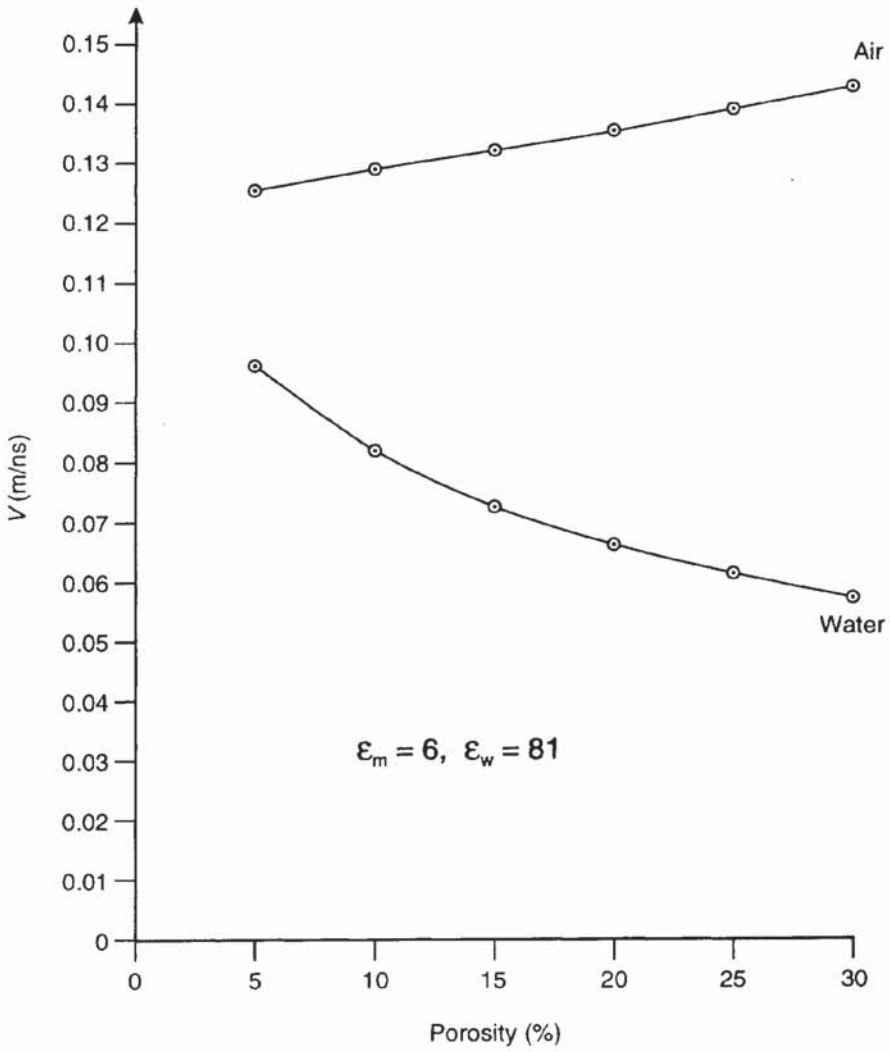

Figure 12.15 Radar velocities as a function of porosity for air- and water-saturated granular materials

ease with which a fluid can flow through the pore spaces within a given medium and thus is a function of the connectivity of the pore space, i.e. the effective porosity. Permeability is also a function of the viscosity of the fluid, the rate of fluid flow and the hydraulic pressure gradient causing the flow.

When electrical resistivity is used to derive porosity of clean granular rocks, such as by using Archie's Formula, it is the effective porosity which is being determined. Electrical continuity is provided by the electrolytes within the connected interstitial spaces. Dielectric measurements, however, are not dependent upon the connectivity and thus can be used to determine the total porosity. Conversely, values of porosity derived from the use of radiowave velocities are always likely to be overestimates of the effective porosity.

Microporosity – i.e. porosity at a scale of the order of microns but still large relative to the sensitivity of the electrical measuring system –

becomes especially significant in dielectric analysis. Electrical conductivity is affected by pore geometry and pore surface area. Clay not only affects the physical communication between pores and pore throats (affecting permeability as well as porosity), but the type of clay provides differing surface areas for double-ionic polarisation (Reynolds and Taylor 1992). For example, authigenic kaolinite occurs as disc-like 'booklets' whereas illite forms ribbons (Klimentos and McCann 1990; Klimentos 1991). The form of the clay, therefore, can affect the surface area within the pore space and it is probable that, at the scale of the order of microns, the microporosity has a measurable effect on the electrical properties. In contrast, ultrasonic acoustic methods appear to be less sensitive to this. This is not to say, however, that the microporosity does not influence the physical properties measured using acoustic methods, but that as yet the acoustic methods are not able to resolve the effects of microporosity. Indeed, electrical properties are being modelled by reference to the fractal nature of porosity (Ruffet *et al.* 1991). As it is the *effective* porosity that is directly related to permeability, the latter will only be determinable once the former can be derived accurately.

The significance of porosity, permeability and the dielectric properties of fluids is of particular importance in dielectric logging of hydrocarbon wells and in contamination mapping, for example.

Dielectric properties of concretes have also been demonstrated to exhibit a surprisingly large degree of variation (Reynolds 1991b; Reynolds and Taylor 1992). The relative dielectric constant can vary by more than 50% over a distance of less than 0.1 m within the same mix of concrete; the resulting change in radiowave velocity is of the order of 35%, with velocity decreasing with depth into the concrete. The effect is thought to be related to the amount of micro-cracking present within the concrete, with a greater amount of cracking present nearer the surface (hence more air present, thus the higher radiowave velocity). While this is but one isolated example, it does serve to demonstrate that even within a relatively controlled material like concrete, there is still a high degree of variability in the electrical properties.

12.5 MODES OF DATA ACQUISITION

There are three modes of deployment of radar systems; reflection profiling (using either monostatic or bistatic antennae); wide-angle reflection and refraction (WARR) or common-midpoint (CMP) sounding; and transillumination or radar tomography.

12.5.1 Radar reflection profiling

Figure 12.1 provides an example of radar being used to obtain a reflection profile. One or more radar antennae are moved over the

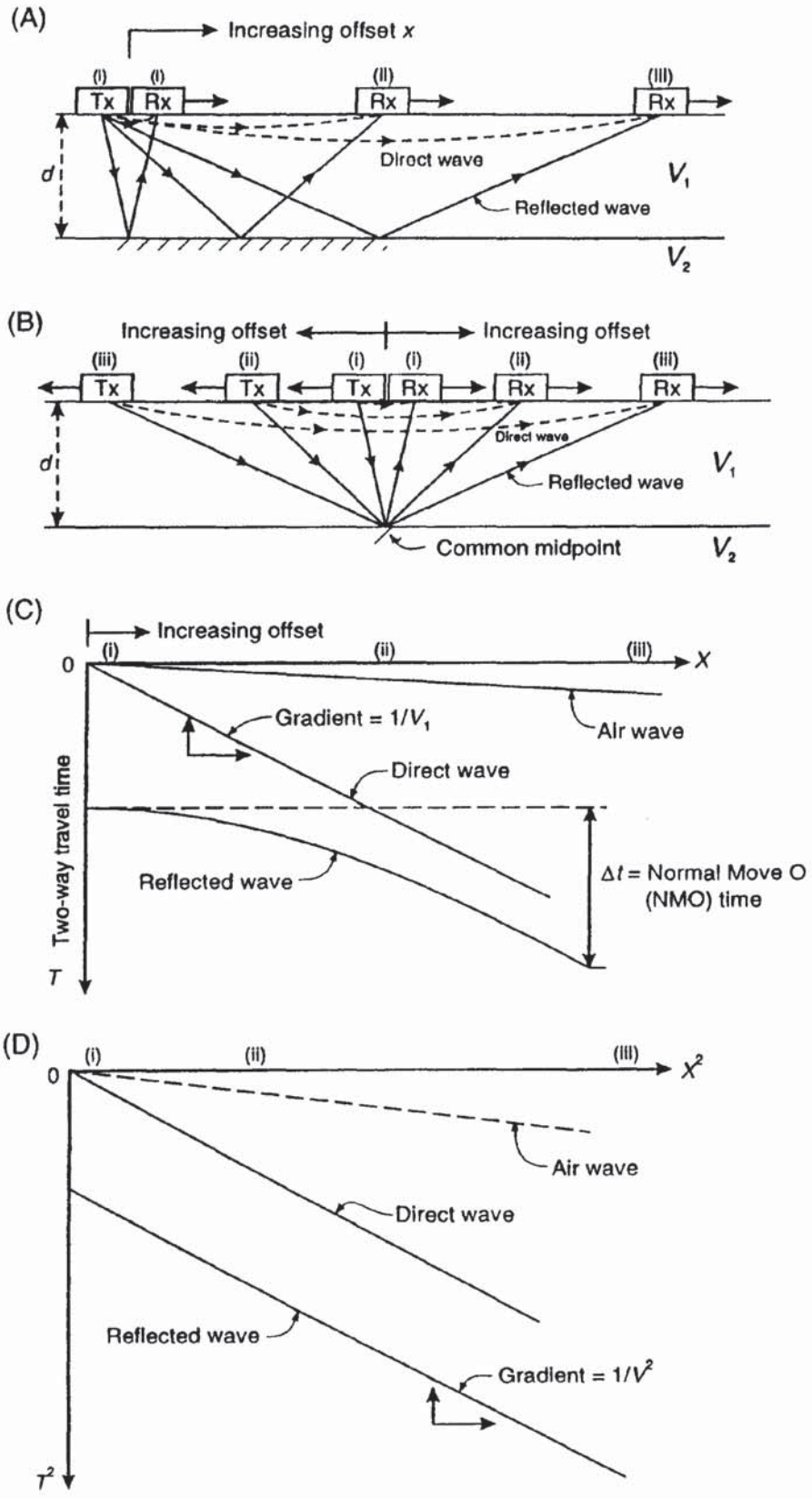

Figure 12.16 (A) WARR sounding and (B) CMP sounding with (C) a time-distance ($T-X$) graph with normal moveout, and (D) the corresponding T^2-X^2 graph

ground surface simultaneously, with the measured travel times to radar reflectors being displayed on the vertical axis while the distance the antenna has travelled is shown on the horizontal axis. This mode of surveying is analogous to continuous seismic reflection profiling (see Chapter 6).

If the radiowave velocities have been measured independently (see next section) or reflections correlated with changes in ground characteristics observed from borehole data, then depths to the reflectors can be determined. See Section 12.7 for more details of interpretation techniques.

12.5.2 Wide-angle reflection and refraction (WARR) sounding

The WARR antenna configuration is shown in Figure 12.16A. The transmitter is kept at a fixed location and the receiver is towed away at increasing offsets. The location of a WARR sounding should be over an area where the principal reflectors are planar and either horizontal or dipping only at very shallow angles. It is also assumed that the material properties are uniform and that the reflector characteristics are the same over the sub-surface area over which the WARR sounding is undertaken. This assumption may not be true in all cases.

To avoid having to make this last assumption, an alternative and preferable deployment for the same analysis is the common midpoint (CMP) sounding. In this case, both the transmitter and receiver are moved away from each other so that the midpoint between them stays at a fixed location (see Figure 12.16B). In the CMP case, the point of reflection on each sub-surface reflector is used at each offset, and thus areal consistency at depth is not a requirement. The equivalent positions between the WARR and CMP soundings are given as (i), (ii) and (iii) in Figure 12.16.

12.5.3 Transillumination or radar tomography

The transillumination mode of deployment is where the transmitter and receiver are on opposite sides of the medium under investigation (Figure 12.17). The method is used underground within mines, for example, where the transmitter is located in one gallery and the receiver is either in a gallery to one side of the transmitter, or in a gallery above or below. Alternatively, the radar antennae can be located down boreholes and the radar signals are then propagated from one, through the medium in between, to the other.

The transillumination mode is also common in non-destructive testing (NDT) investigations of man-made structures, particularly using very high frequency and hence small antennae (e.g. 900 MHz centre frequency). Examples include testing concrete columns and masonry pillars.

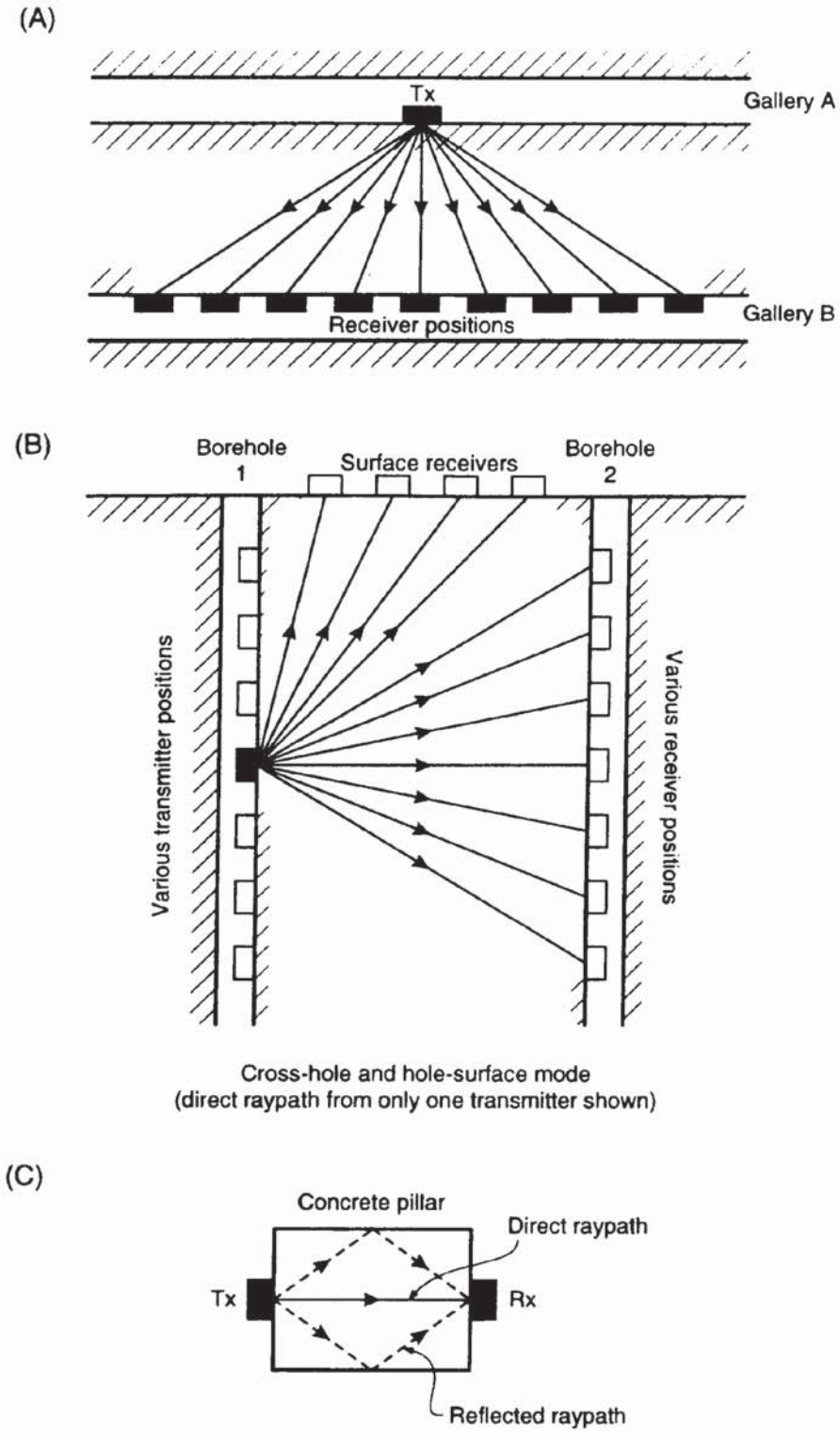

Figure 12.17 Transillumination and cross-hole radar modes of data acquisition: (A) between galleries in a mine, (B) between boreholes or hole-surface, and (C) through a concrete pillar. In all cases the direct distance between transmitter (Tx) and receiver (Rx) antennae is known. Modes shown in (A) and (B) are also known as *radar tomography*

As the relative positions of the antennae are known at all times, and hence the distances between them, it is a simple matter to calculate the mean radiowave velocity of the appropriate raypath. If the signal amplitude is also measured, in addition to travel times, then attenuation can be determined. More details of this method have been given by Annan and Davis (1977). Sophisticated data-processing routines exist in order to produce tomograms that are analogous to seismic equivalents (see Chapter 6).

12.6 DATA PROCESSING

12.6.1 During data acquisition

All ground radar systems provide a means of filtering the data during acquisition. It is usually possible to set both highpass and lowpass filters to sharpen the signal waveform at the time of the survey. As with seismic filtering during acquisition, there is a significant element of qualitative feel to choosing appropriate filter settings. More sophisticated digital systems allow vertical and horizontal filtering as well as more powerful gain-setting options with which to optimise the data quality. As a rule of thumb, it is advisable to keep the filter settings as broadband as possible so that potentially valuable data are not excluded during the acquisition phase. It is far cheaper to filter broadband data after the field work has been completed than to realise that the data quality has been compromised by the use of filter settings which are too harsh, thereby necessitating a repeat of the fieldwork!

Digital systems have the function of stacking a limited number of adjacent traces in order to improve the signal-to-noise ratio. This works well in areas where the structure is largely parallel or subparallel to the ground surface. When steeper structures are present, horizontal stacking over too many adjacent scans can produce lateral smearing and a defocusing of the radar image.

12.6.2 Wide-angle reflection and refraction (WARR) sounding

If two separate antennae are used, one as a transmitter and the other as a receiver, in bistatic mode, it is possible to determine the vertical variation in radiowave velocity (and hence relative dielectric constant). If only one antenna is available in monostatic mode, it is not possible to undertake WARR sounding and hence velocity determination can only be by either direct correlation with adjacent borehole logs, targets at known depths of burial or by guesswork; the latter is the most commonly employed and may give depth estimates accurate to $\pm 20\%$.

In each of the WARR or CMP configurations three types of waves may be identified:

- the airwave, travelling from the transmitter to the receiver through the air at the speed of radiowaves in air (0.3 m/ns);
- the direct wave, travelling directly from the transmitter through the near-surface ground to the receiver at the speed of radiowaves in the near-surface medium (V_1);
- the reflected wave, travelling from the transmitter to the interface from which it is reflected to the receiver, also at the speed of radiowaves in the first layer (V_1).

The travel times for both the airwave and the direct wave plot as straight-line segments on the T–X graph, but those for the reflected wave plot on a curved (hyperbolic) line. The difference in travel time between zero offset and at finite offset is the *normal moveout* (NMO) time (Figure 12.16C). However, when these travel-time data are plotted on a T^2–X^2 graph, all the segments appear as straight lines (Figure 12.16D). The inverse gradients of each line are equal to the respective radiowave velocity squared. Further details of the velocity sounding techniques have been given by Arcone (1984).

The radiowave velocity determined for layer 1 is a time-averaged value over the interval from zero time to t_0, and is hence a root-mean-squared velocity (V_{RMS}). Where travel-time data are obtained for deeper reflections, the velocities determined from the above analysis for each layer are also RMS values. To determine a geologically more meaningful velocity for a particular layer, it is then necessary to use the Dix Formula to derive the 'interval velocity'. This analysis is exactly the same as for seismic reflection data and more complete details are given in Chapter 6.

12.6.3 Post-recording data processing

Only digital data can be processed post-recording. The degree of processing is often determined by (a) the budget available; (b) the time available; (c) data quality; (d) the available processing capability (software and hardware); (e) the requirement that the final interpretation justifies further analysis; and (f) the structural detail on the raw record meriting detailed quantitative data processing.

The first step is to filter the data in order to focus the image. For many applications this is sufficient in order to locate sub-surface features. For more detailed analysis, a wide range of processes are available, up to and including the same as for multifold seismic reflection data, including attribute analysis, details of which are given in Chapter 6.

The radar system produced by Geophysical Survey Systems Inc. has a suite of data-processing packages available called RADAN™

(Radar Data Analyser). The format of data recorded on to magnetic media, typically 2.5 Gbyte magnetic tape or magneto-optical disk, can be converted from SEG 2 to SEG Y format in order to be compatible with seismic industry-standard workstations. A program to convert from SEG 2 to SEG Y has been published by Bennett (1990). Datafile formats for radar data have been specified by the SEG Engineering and Groundwater Geophysics Committee (Pullan 1990). Similarly, Sensors & Software Ltd have a range of computer software designed for use with their PulseEKKO system, which produces data in a format compatible with seismic data-processing software.

Of particular significance is the ability to restore correct sub-surface geometrical relationships through the process of migration. Diffraction hyperbolae can be migrated back to the apex from which the diffraction originated. Dipping planar surfaces can be corrected to their correct position relative to ground locations. Otherwise, significant errors can be made by believing that the location of a particular sub-surface feature on a raw radargram is exact, whereas it is only a virtual image and may be displaced from its actual position by significant horizontal and vertical distances. The principles of migration are discussed more fully in Chapter 6.

Other methods of quantitative analysis are available through *image analysis*. Rather than operate on the waveforms of the data, the radargram is scanned for analysis of trends. For example, trends such as reflections dipping in a particular direction can be picked out. Statistically significant trends can be identified from the entire radargram and displayed automatically as line interpretations for subsequent manual analysis.

12.7 INTERPRETATION TECHNIQUES

12.7.1 Graphic interpretation

From both analogue and digital radar data, hardcopy radargrams can be analysed in terms of identifying reflections and diffractions and measuring the two-way travel times to such identifiable events. By assuming, or having measured, a value for the appropriate relative dielectric constant – and hence obtained a realistic radiowave velocity – the two-way travel times to specific events can be translated into depths. Where radar data have been acquired over a regular grid, and reflections identified over significant areas, it is then possible to produce posted two-way travel time maps, or *isopachyte maps*, indicating the depth to, or thickness of, a particular layer, given a realistic measure of the radiowave velocity.

This approach is particularly prevalent in road pavement analysis, where the number of discrete layers is usually well constrained with

up to four parallel to sub-parallel layers (bound layer of bitumen or concrete, granular layer, upper and lower sub-grades). The travel times to interpreted interfaces can be digitised off paper radargram records and, using an appropriate radiowave velocity for each of the discrete layers, the depths to each interface can be determined. There would need to be careful consideration of the accuracy of picking the onset of the various reflections on the radargrams as well as the likely reliability of the radiowave velocities used to derive depths. Local variability in radiowave velocities can occur within concretes (see Section 12.4; different mixes, even though all within specification), or due to changes in moisture content (see Section 12.4). Individual horizons, such as the sub-base, may have been prepared in layers, and these may be detected. In some cases the boundary between layers may be fuzzy – so where does the radar reflection come from? Is it always from the same relative position between layers? These are questions that need to be answered in road pavement work prior to the production of final drawings. In all cases, a statement as to the errors and limits of measurement should be made. There is no such thing as an absolute measure of depth using remote methods, particularly radar.

The interpreted data can be displayed in a wide range of ways using modern computer-aided design (CAD) systems and 3-D graphics software packages. While the final output may be extremely colourful and fancy, it should be remembered that the basic data analysis may be just that – basic! While the final drawings may indicate millimetre accuracy, is this justified? At present, the uncertainties and local variability in the dielectric properties of materials and the subjective nature of defining the onset position of reflections tend to make claims of such accuracy unjustified. As the electrical and dielectric properties of materials used in road pavements become better known, accuracies and reliabilities will improve.

In addition to interface mapping, it is possible to use the variations in character displayed on the radargram as an indication of sub-surface conditions. For example, areas of high attenuation may reveal zones with elevated conductivities which may be associated with pollution, or clay pockets. Sub-surface cavities may be evident by the resonance within the void space, indicated on the radargram as a series of large-amplitude pulses which are laterally very restricted. Zones of cobbles or severely distorted strata may be evident by the loss of coherency of primary reflection events. Delamination of road pavements may also be indicated by diagnostic character changes on radargrams (delamination is also evident when imaged using infrared thermography under appropriate conditions).

12.7.2 Quantitative analysis

Basic depth determination depends upon an adequate knowledge of the radiowave velocity and its vertical and lateral variation within

a given survey area. Where WARR/CMP data have been acquired, then a detailed picture of the velocity field can be obtained. Consequently, geologically diagnostic values of the radiowave velocity, or more particularly of the relative dielectric constant, can be used to aid interpretation.

Where detailed quantitative attribute analysis has been undertaken of the recorded radiowave data – such as amplitude analysis, reflection coefficient determination, as well as variations in ε_r – then a much more comprehensive understanding of a site can be gained. Indeed, given adequate data quality, careful processing may yield more valuable information about the petrophysics of a given geological or engineering regime than would otherwise have been possible. High-level processing and analysis are becoming much more important where detailed discrimination is required, such as in hydrocarbon exploration and reservoir engineering, and in contaminated land investigations. The use of ground radar in both cases is likely to develop considerably over the next few years.

12.7.3 Interpretational pitfalls

The two commonest pitfalls in the interpretation of radar data are (a) not being able to identify the ground surface, and (b) misidentifying each black band on a black and white radargram as being caused by a discrete horizon. The easiest way to identify ground level, especially with antennae with centre frequencies $\geqslant 500$ MHz, is to raise and lower the antenna above the ground surface. A distinctive cusp appears on the radargram and clearly indicates where the ground level is represented.

The over-identification of the number of layers highlights a real difficulty, especially with analogue radar data: how are the primary reflections to be identified from multiples, secondary events, and the tail of other primary reflections? Furthermore, when waveforms intersect each other, they cause interference which may give the appearance of a 'termination' of one dark band with respect to another. Geologically, this may be misinterpreted as one horizon abutting against another. If the geological conditions are such that the radargram is ambiguous in this regard, then there is justification for detailed quantitative analysis if the data have been recorded digitally. If the data have been produced as an analogue record, there is little that can be done to resolve the dilemma. The quantitative analysis can pick out likely multiple events (these are purely time repeats of earlier primary events), and by deconvolution, the shape of the downgoing wavetrain can be determined and hence primary reflection events identified. Subsequent migration can help to reduce diffraction hyperbolae and, by restoring some of the sub-surface geometry of primary reflections, can help to resolve geologically significant detail that otherwise would have been obscured.

The difficulties in distinguishing between geologically significant reflections and extraneous reverberations, multiples, noise, diffractions, off-section ghosts, etc., make the determination of soil and rock stratigraphy difficult in some cases. In others, the stratigraphy can be determined quite readily; one such example (from Best and Spies, 1990) is shown in Figure 12.18. An analogue record obtained in 1976

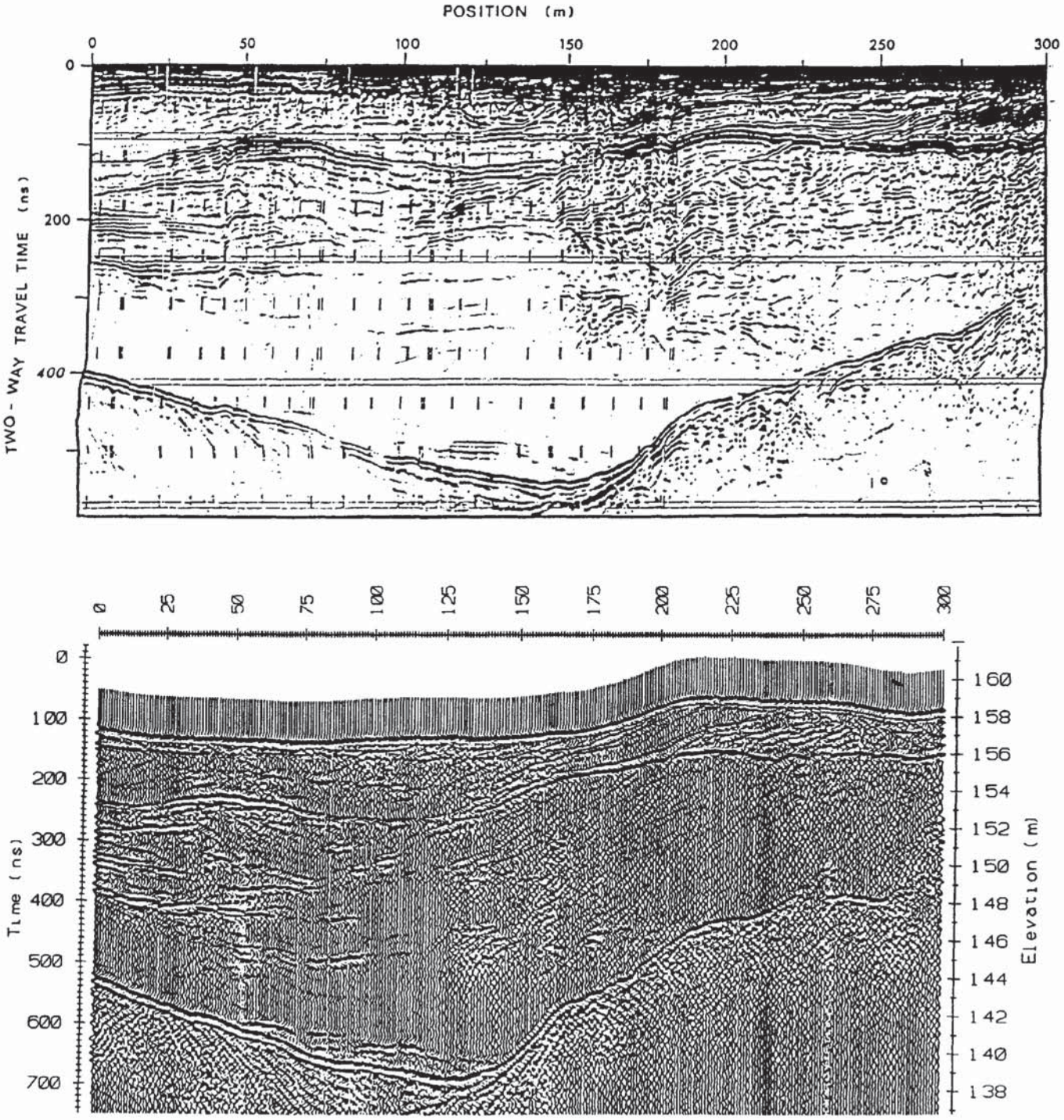

Figure 12.18 Radargram obtained in 1976 compared with one in 1991. From Best and Spies (1990), by permission

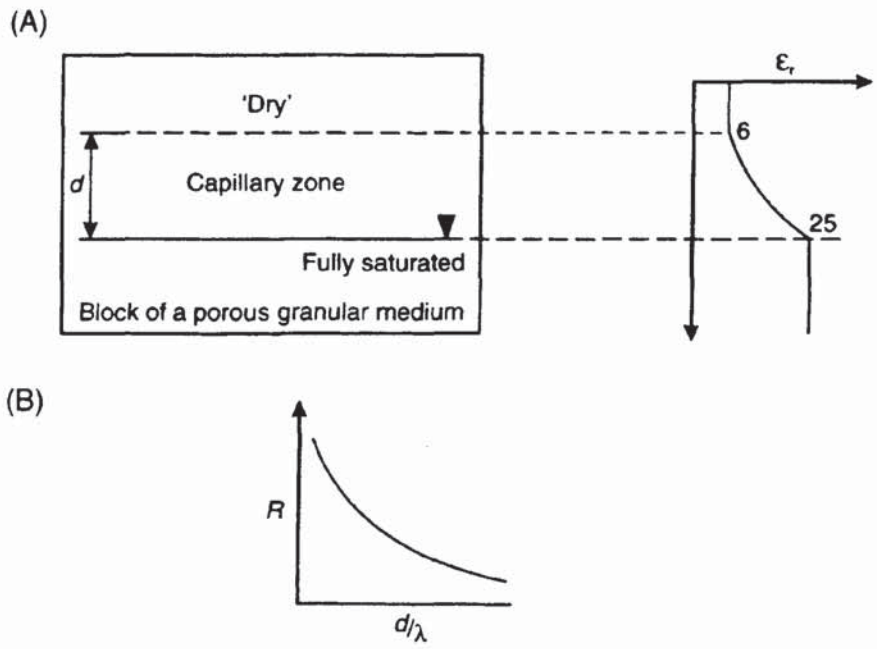

Figure 12.19 Effect of thickness of a capillary zone on the observed reflection strength arising from the water table. (A) A capillary zone of thickness d over the water table has a relative dielectric constant (ε_r) which increases to a maximum when fully saturated. (B). The amplitude reflection coefficient (R) decreases as the ratio of the thickness of the capillary zone to wavelength of incident radiowaves increases

is compared with a digital radargram produced over the same area more recently. While the gross structure is evident in the 1976 analogue record, the detail is much crisper in the digital record.

There are situations when the water table is detectable on a radargram and others where it is not. The reason for this is that the ratio of the thickness of the capillary zone to the wavelength of the incident radiowaves needs to be small (i.e. $d <$ wavelength) in order to provide sufficient contrast in relative dielectric constant between the unsaturated and saturated material to reflect a significant proportion of the energy (Figure 12.19). If the capillary zone is thick with respect to the wavelength, then the rate of change of relative dielectric constant with depth through this zone is small. The effect of this is that, for each incremental increase in the relative dielectric constant, a proportion of the incident energy is reflected so that the total reflected energy is smeared from the capillary zone, and hence the resulting reflection amplitude is too low to be detected with any clarity. In contrast, if the transition from dry to saturated is virtually instantaneous (e.g. the change in relative dielectric constant is from 6 to 25), then the amplitude reflection coefficient $|R|$ is 0.34 (using the expression in Box 12.2), which is a very strong return.

12.8 APPLICATIONS AND CASE HISTORIES

12.8.1 Sedimentary sequences

Ground penetrating radar has been demonstrated to be a valuable tool in mapping sediment sequences with a high degree of spatial

resolution on both land and through freshwater. An example of the improvement in data quality in mapping soil stratigraphy was given in Figure 12.18. Other examples are given in Section 12.8.7. A common failing of the analysis of radargrams acquired in stratigraphic investigations is over-interpretation of the data. Too often apparently coherent events are taken as indicating individual sedimentary interfaces without due regard for the physics of thin-bed interference, vertical and horizontal resolution limits, the finite size of the first Fresnel zone, migration effects, the complex form of the incident wavetrain, etc. It is in these applications that seismic data processing is likely to play an important role; for example, see the paper by Huggenberger *et al.* (1994).

Ground radar can be deployed over frozen lakes and has been used to investigate sub-lake sediments through freshwater up to 27 m deep; an example of a through-ice survey is shown in Figure 12.20. The lake ice provides a stable platform over which the radar was towed. The freshwater within the lake is virtually transparent to radiowaves and the lake sediments are clearly evident through 4.8 m of freshwater. The resolution of the system (100 MHz antenna) is such that individual horizons within the sediment can be picked out. Note that the reflection returns associated with the lake bed comprise at least four bands owing to a ringy source. Furthermore, the period of the initial wavetrain (around 70 ns) might be misinterpreted by some as indicating the presence of up to 6 m of ice (radiowave velocity through ice is

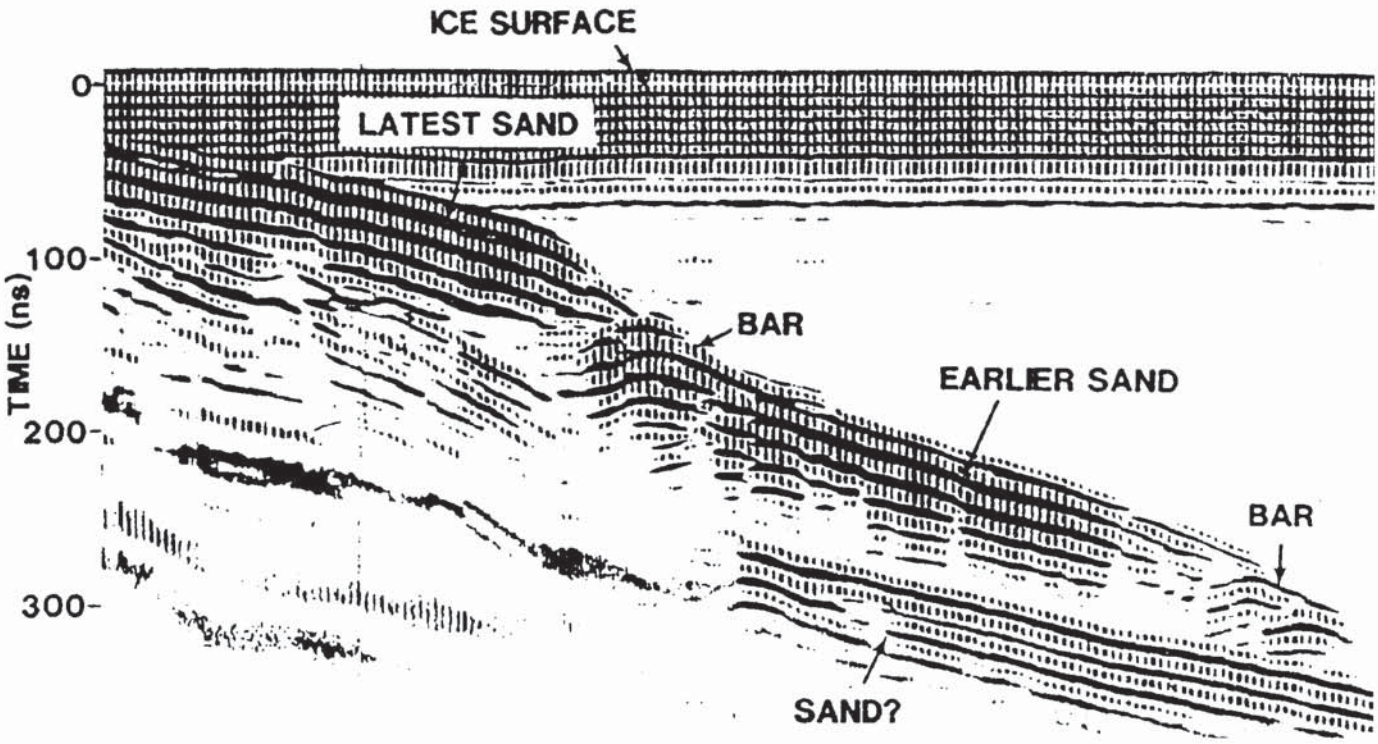

Figure 12.20 Radargram over an icecovered lake obtained using a 100 MHz antenna. Maximum water depth is 4.8 m; width of profile is 25 m; 500 ns two-way travel time range. From Mellett (1993), by permission

0.167 m/ns). The actual thickness was only 0.15 m. The two-way travel time through the ice layer would only have been around 2 ns. This shows effectively that, using a low-frequency antenna (100 MHz), near-surface features cannot be resolved at all as they are totally masked within the initial ground-coupled wavetrain. The radiowave velocity through the freshwater can be calculated knowing the depth of water (about 4.8 m) and the total travel time (around 300 ns). These values would give a radiowave velocity of 0.032 m/ns (from $2 \times 4.8/300$), ignoring the ice layer and assuming low-loss media. As a double check, the relative dielectric constant of water is 81, which thus gives a radiowave velocity of $0.3/\sqrt{81}$, or 0.033 m/ns (refer to Box 12.1 for the equation).

12.8.2 Hydrogeology and groundwater contamination

As environmental protection measures become more stringent, and the pressure on preserving the quality of groundwater sources increases, so the need to identify groundwater pollution grows. Davis and Annan (1989) have demonstrated how ground radar was used to locate and map out a plume of contaminated water leaking out from a landfill site; a schematic plan of the site area is shown in Figure 12.21A. Along the line of the radar transect shown in this figure, the soil consists of fine sand and overlies bedrock which occurs at a depth of about 20 m. A radar survey was undertaken using a PulseEKKO III radar system and the resulting radargram is shown in Figure 12.21B.

Where penetration of the radiowaves into the superficial sediments occurs, reflections are seen and are thought to be due to horizons with different grain size and density, and hence different soil moisture contents. It is also very clear on this section that there are areas where either only very weak reflections occur, such as at 150 m along the profile at around 400 ns two-way travel time, or the signals are completely attenuated. The presence of contamination, which has an associated high electrical conductivity, attenuates the radar signals severely.

Several boreholes had been constructed along the survey line and the conductivity of the groundwater was measured. The solid line joining a series of black dots on Figure 12.21B indicates the position below which the porewater conductivity is greater than 10 mS/m. As it was known that the superficial deposits were reasonably consistent in their properties over the area of the site, it is evident, therefore, that the pollution plume approaches the surface between 40 and 60 m (as proven by the borehole data) and that it also extends between 110 and 150 m along the profile line at a depth of about 6 m below ground level. The second part of the plume had not been expected, and thus the results from the radar survey were extremely useful in providing this additional information. A ground conductivity survey to

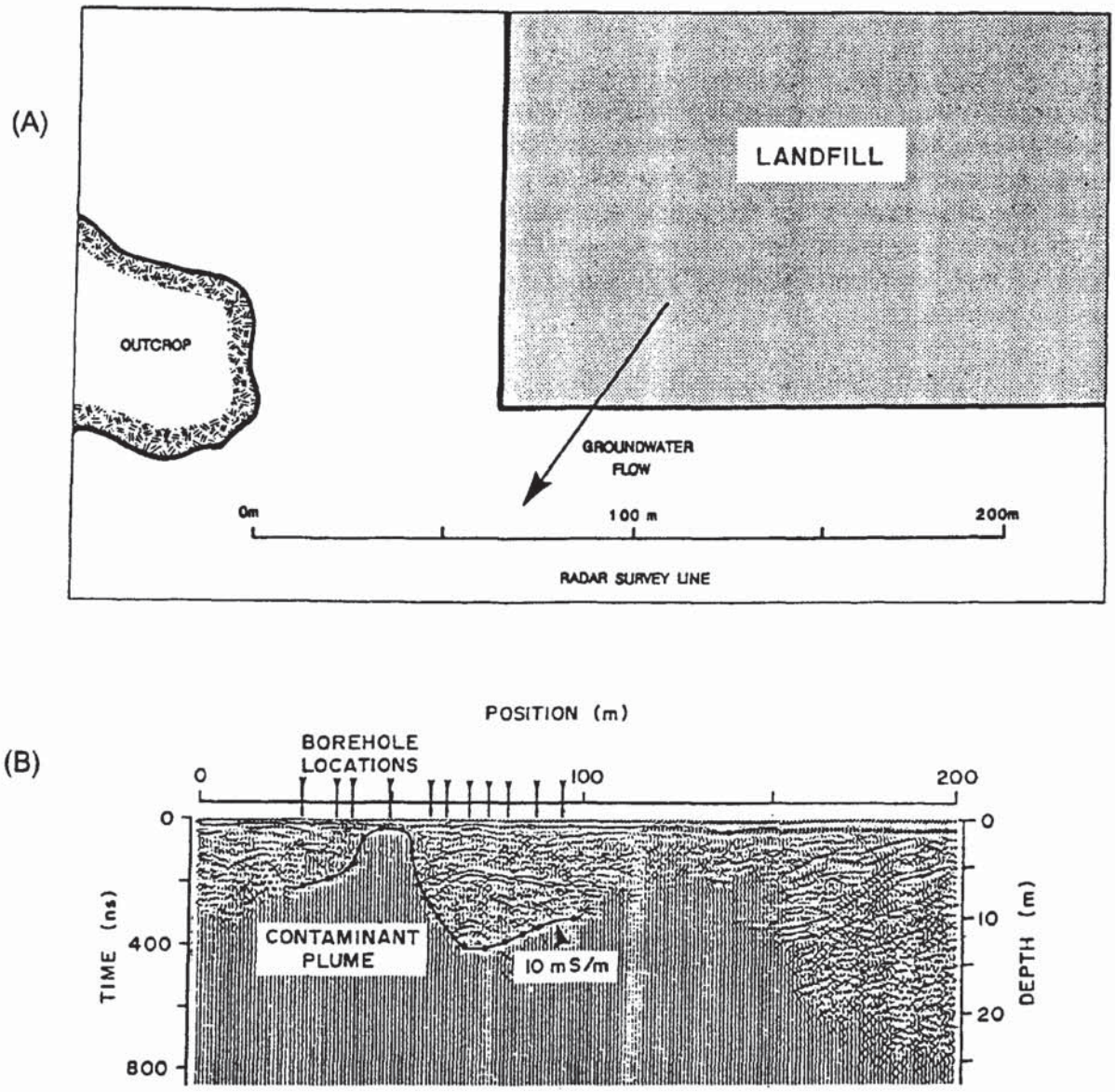

Figure 12.21 Radar section showing the effect of a conductive pollution plume caused by leachate migrating from a landfill. From Davis and Annan (1989), by permission

complement the radar work would have provided a non-invasive method of determining the spatial variation in sub-surface conductivity without having to drill extra boreholes, which in themselves may make the spread of the pollution worse.

Where it can be demonstrated that radar surveys would be useful under the ambient geological and ground conditions, and that the pollution can be detected by radar, then changes in the pollution plume can be mapped. By undertaking repeat surveys along the same ground transects, it is possible to detect changes as a function of time. Furthermore, where remediation measures are undertaken, the success of such treatment can be monitored using radar.

In certain cases, the actual pollution itself may not be detectable using radar, but the containers from which the pollution originated

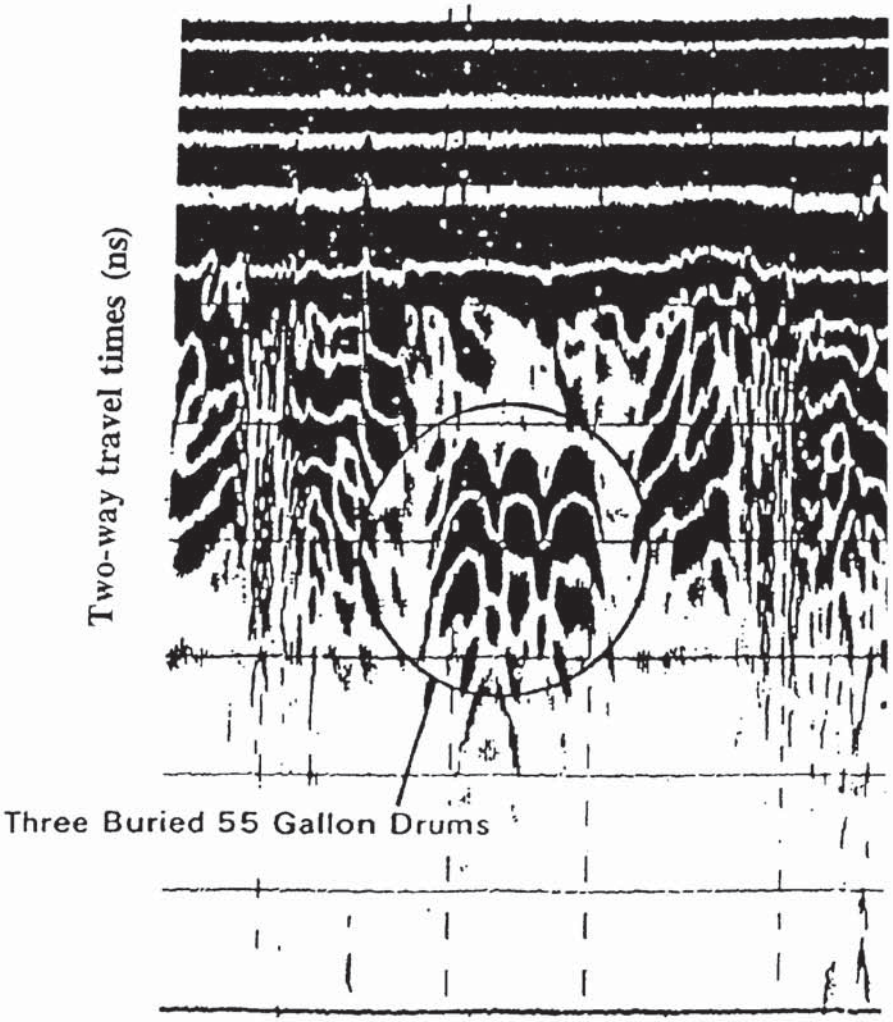

Figure 12.22 Radar record over three buried drums laid side by side

may be. Consider the case of buried 55-gallon steel drums which may have leaked their contents. Figure 12.22 shows a radar record over three buried drums. Note the characteristic diffractions arising from the drums which are located side-by-side. Also note that the incident radar waveform consists of more than one band, and hence the diffractions from the drums give the appearance of lower diffractions; these are the tails of the primary diffractions.

Ground penetrating radar is being used extensively in the Netherlands for hydrogeological assessment in groundwater management. Falling water tables and deteriorating water quality seriously affect agriculture and nature conservation and potable water supplies. Van Overmeeren (1994) has provided examples of types of hydrogeological applications current in the Netherlands where there are four main radar targets: (a) tectonic and sedimentary structures; (b) water tables within sandy deposits in push moraines, river terraces and sand dunes; (c) perched water tables as distinct from regional water tables; and (d) spatial extent and continuity of buried clay and peat layers within the superficial deposits.

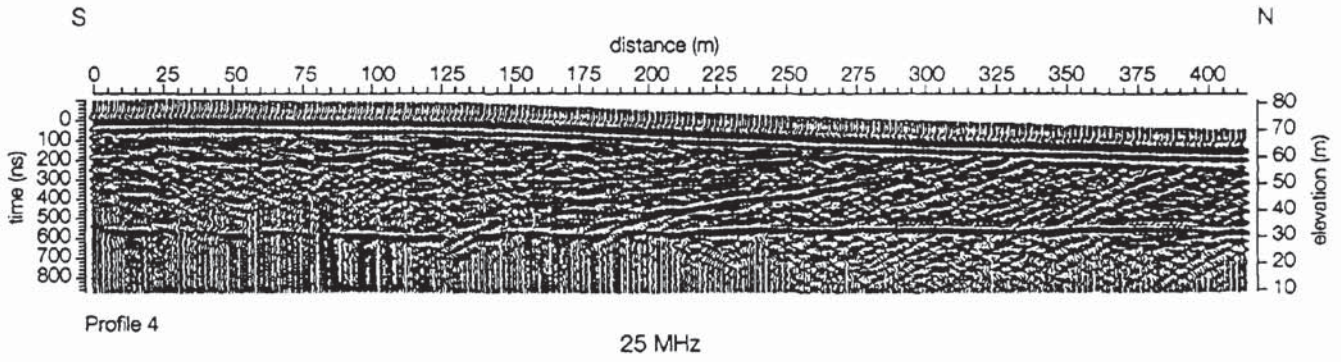

Figure 12.23 Radargram acquired with 25 MHz antennae over a sandy ice-push moraine. The water-table reflection is evident at an elevation of 30 m. Note the slight vertical displacement in this reflection where an inclined reflection due to a clay layer intersects the water table at 185 m. From van Overmeeren (1994), by permission

A radargram acquired using a PulseEKKO IV with 25 MHz antennae and station interval of 1 m is shown in Figure 12.23. The profile was obtained over push moraine comprising mainly sand. The section has been corrected for topography and has identical horizontal and vertical scales. The water table is evident as a horizontal reflection with a large amplitude. In the northern part of the section, the reflection is largely continuous whereas it is less so in the southern, most elevated, part. This suggests that the depth of penetration of the radar is at its limits here and that the greater depth below ground level to the water table in the southern part results in the poorer data quality. Using a radiowave velocity of 0.145 m/ns (derived from CMP measurements), the water table is still evident at 42 m below ground level. The radargram also reveals reflections from interfaces above the water table. The oblique reflections are associated with interfaces between sandy layers of different grain size or between sandy and clayey sediments. In both cases, the interface marks a change in moisture content and hence a contrast in relative dielectric constant.

A conspicuous reflector with a large amplitude and dipping southwards is evident in the middle of the section. There is a small vertical offset (around 2 m) in the water-table reflection where it is intersected by the inclined event. The step in the water table is thought to be caused by an inclined clay layer which gives rise to the strong oblique reflection.

Van Overmeeren (1994) has described another example of the hydrogeological usefulness of GPR, where a radargram (Figure 12.24A) was acquired using a PulseEKKO IV with 50 MHz antennae and a station interval of 0.5 m. The survey transect was over a valley with marine interglacial deposits passing into an uplifted ridge of ice-pushed sediments. A clay layer forms part of the marine formation. The objective of the radar survey was to map the lateral continuity of the clay layer and to locate its western limit (see Figure 12.24B which is a schematic interpretation of part of Figure 12.24A). The clay layer, which occurs at a depth of 15 m below ground level, sustains an artesian aquifer which is recharged by infiltration in the

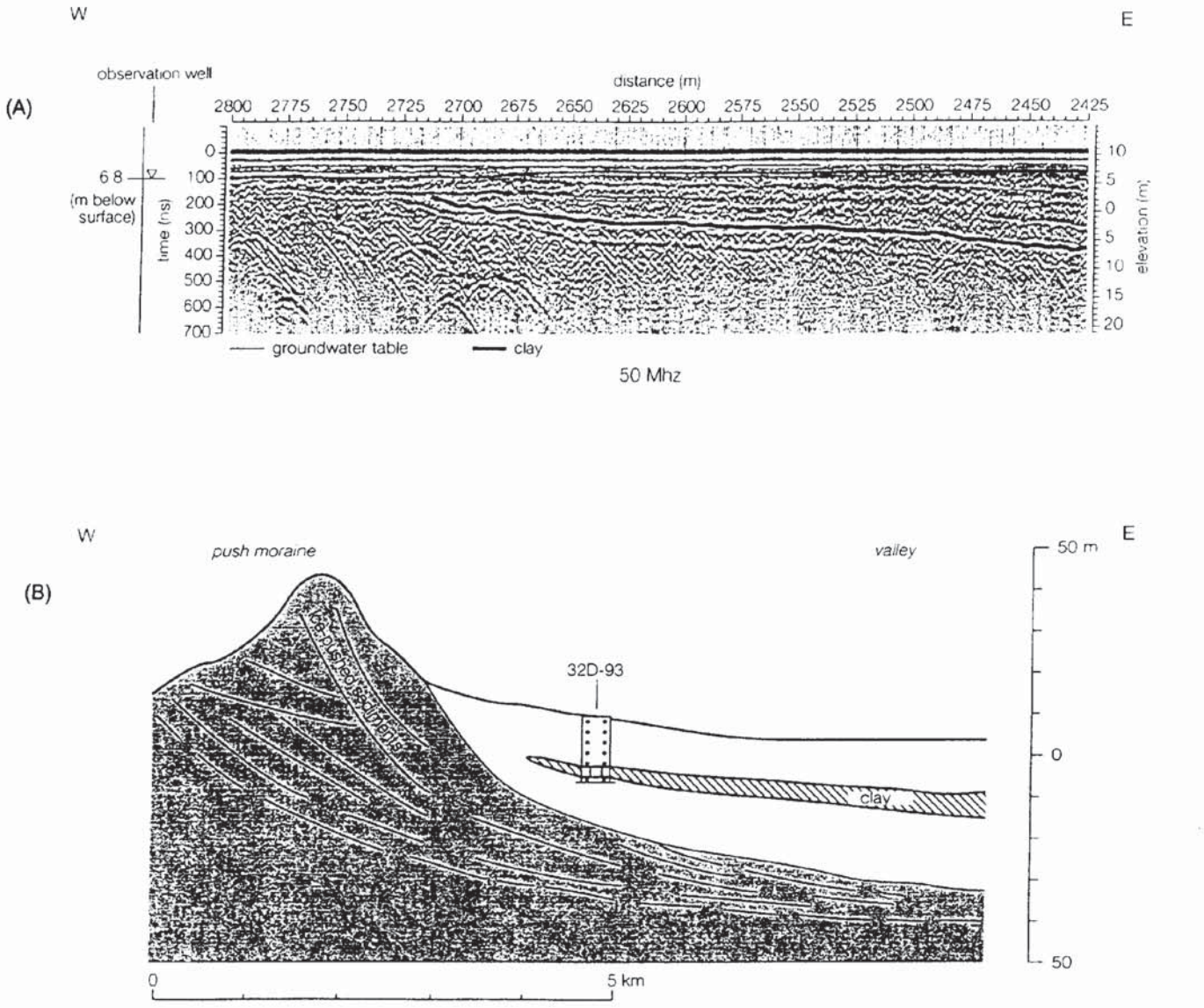

higher ice-pushed ridge. The precise boundaries of the clay layer were required for groundwater flow modelling.

In the radargram (Figure 12.24A), the vertical exaggeration is 2.5 times the horizontal scale. The regional groundwater level is at a depth of about 7 m, as determined from a nearby observation well. A radar CMP test near the well produced a value of the radiowave velocity of 0.115 m/ns for the sediments above the water table. In the area of the survey, the average radiowave velocity was found to be 0.075 m/ns for sediments above the clay band, which is in close agreement with a known value of 0.06 m/ns for sand saturated with freshwater. In contrast, dry sand has a radiowave velocity of 0.15 m/ns. The field-derived radiowave velocity is strongly indicative of freshwater-saturated sands above the clay layer, which can be

Figure 12.24 (A) Radargram acquired with 50 MHz antennae over a sandy ice-push ridge on to which interglacial marine sediments, including a clay layer, onlap. The clay layer is indicated by a solid black line. The water table occurs at a depth of about 7 m. (B) General interpretation of the part of the radargram shown in (A). The clay layer has been verified by a borehole (32D-93). From van Overmeeren (1994), by permission

identified on the radargram as a coherent reflection with large amplitude. The reflection from the clay layer persists clearly until station 2715 where it is cross-cut by an onlapping horizon.

The radargram shows that sensible reflection events arising from the sub-surface geology can be identified to an interpreted depth of 12 m, with the exception of several diffraction-like events in the western part of the radargram which occur at interpreted depths of about 16 m. Note in Figure 12.24A that the reflections are largely coherent across the section, but become increasingly incoherent or disturbed west of station 2675 where the ice-pushed ridge is encountered. The more chaotic nature of reflection events here, due to diffraction hyperbolae, is typical of ice-pushed moraine in this area.

Although the water table occurs at shallow depth below ground level (around 3–5 m), reflection events at significant depth are still evident on the radargram. Elsewhere in the Netherlands, the detection of buried clay layers below the water table has proved impossible, yet at this location it is obvious that the radar survey has provided extremely valuable information about the clay layer. This is attributed to the high electrical resistivity of the surface layers resulting in very little attenuation of the radar energy.

The transparency of freshwater saturated sediments to radiowaves has also been demonstrated in North America using a PulseEKKO IV with 100 MHz antennae (Figure 12.25). The reflection arising from the water table is clearly seen as a coherent reflection with a large amplitude between stations 375 and 625 at an elevation of around 500 ft (about 152 m). Diffraction hyperbolae arising from two cables/pipes above the water table are also obvious (arrowed). Note that there are many reflections evident from the sub-surface geology present to depths of around 33 ft (10 m). The data are published

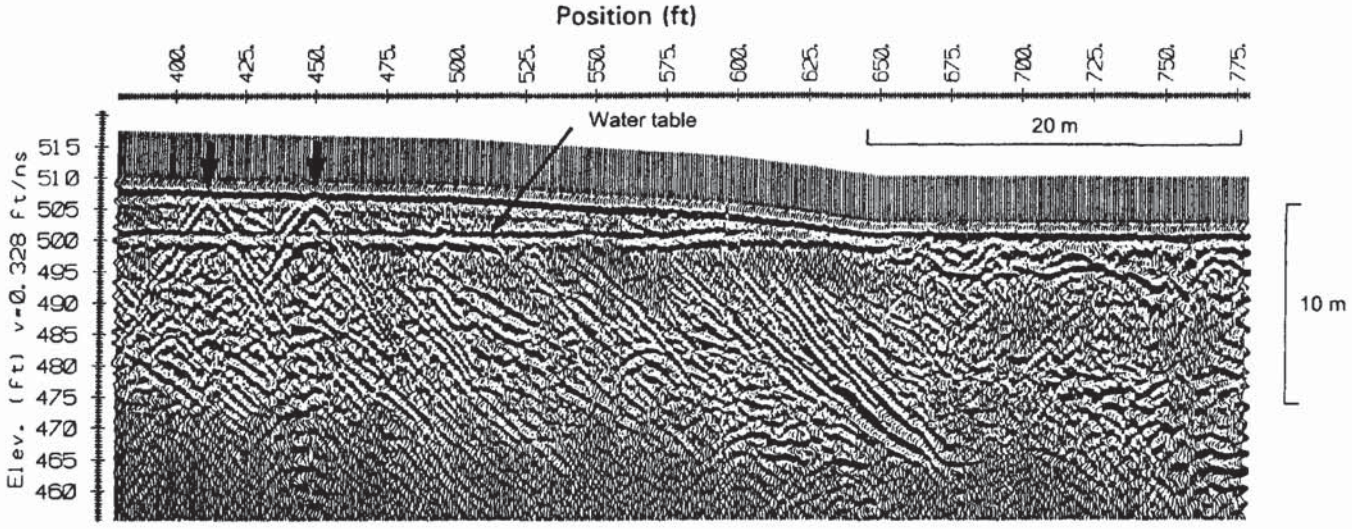

Figure 12.25 Radargram acquired using 100 MHz antennae with a PulseEKKO IV system showing the water table (flat-lying reflection arrowed) and two diffraction hyperbolae from near-surface cables/pipes. Data courtesy of Michigan Department of Natural Resources, Environmental Response Division and Sensors & Software Inc.

courtesy of the Michigan Department of Natural Resources, Environmental Response Division, and of Sensors & Software Inc.

In addition to investigations into natural groundwater resources, there is a growing need to map groundwater contamination (Greenhouse *et al.* 1993). Such pollution can arise from leachate migrating from a landfill, from saline water ingressing inland due to over-exploitation of freshwater sources, natural hydrocarbon contamination (from oil shales, etc.), through to chemical spillages (deliberate or otherwise) over timescales that can range from a few hours to many years. For example, could a chemical spill from an overturned railway tanker be monitored using geophysical methods? Or can petroleum products that have leaked from pipes at a refinery and which have ponded below ground at the water table be mapped?

Some chemicals can migrate from the source of contamination extremely quickly and would be difficult to detect by any means. However, an increasing amount of research is being undertaken to examine the protracted contamination of groundwater. The reason is that there are enormous quantities of carcinogenic organic groundwater contaminants, such as DNAPLs (colloquially pronounced as 'dee-napples') – DNAPLs are dense, non-aqueous phase liquids. The main chemical concerned is perchloroethylene (PCE) which is one of the main constituents of the dry-cleaning and metal-cleaning industries. PCE is but one of a type of liquids known as 'chlorinated organic solvents'. Other well-known chemicals are trichloroethylene (TCE) and dichloromethane (DCM) which are paint-strippers and metal-degreasers. In 1986, it is reported that in the USA alone, 120 million litres of PCE and 200 million litres of TCE were manufactured. Once used, a small but significant proportion of these volumes is disposed of underground, around dry-cleaning establishments, car-service garages, in landfills and waste lagoons, and as residues on old industrial sites.

As their name suggests, DNAPLs are dense (with a density of 1.623 Mg/m^3) and sink rapidly through the local groundwater leaving a residual trail of 5–20% of the pore volume, and eventually ponding for a time on a low-permeability layer such as a clay aquitard. DNAPLs also have low viscosity and low surface tension which allow the chemicals to migrate rapidly through porous media. They can even pass through very fine fractures in clay given adequate time. It is estimated that in the USA, the cost of cleaning up the existing DNAPL contamination to acceptable standards is in excess of one thousand billion dollars.

An excellent overview of a controlled experiment to examine the detectability of DNAPLs has been presented by Greenhouse *et al.* (1993). A schematic of the experimental site is shown in Figure 12.26. A 9 × 9 m cell was constructed by driving corrugated steel sheet piles, sealable at their joints, through the 3.3 m thick surficial aquifer into the underlying clay aquitard. Two concentric walls contained a 0.5 m

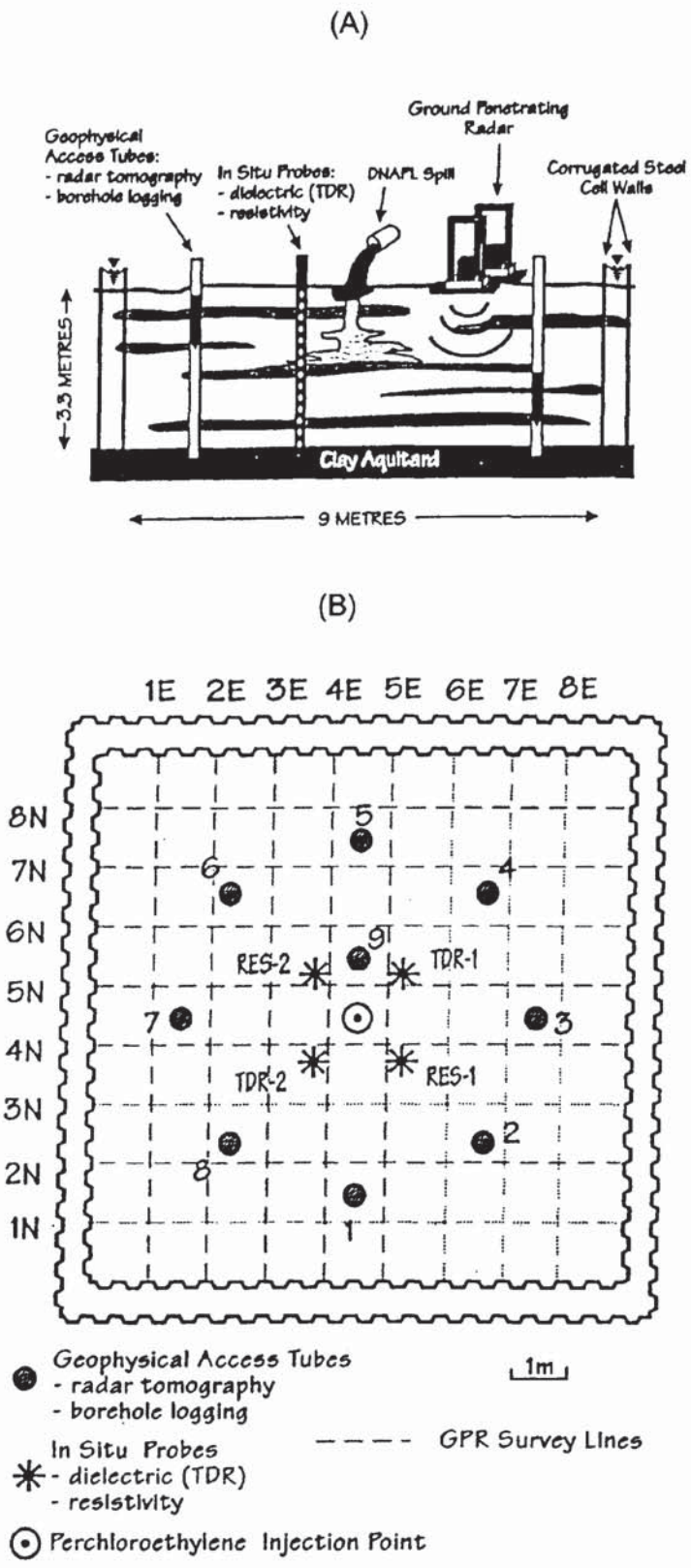

Figure 12.26 (A) Schematic cross-section of the 9×9m test cell at Borden. (B) Plan view of the Borden test cell showing access tubes AT1-9, resistivity probe locations RES-1 and RES-2, TDR locations TDR-1 and TDR-2, the 1 m radar grid and the point of PCE injection. From Greenhouse *et al.* (1993), by permission

wide moat which effectively isolated the inner section hydraulically from its surroundings and allowed the interior water table to be maintained at a depth of 0.15 m below the ground surface. A tarpaulin covered the ground to restrict evaporation. The test cell was instrumented via nine vertical access tubes for radar tomography and borehole logging, and had four further vertical *in situ* probes to measure resistivity and relative dielectric constants (using time domain reflectometry; TDR). Surface ground radar traverses were undertaken repeatedly over two sets of orthogonal profiles with a 1 m line interval using a PulseEKKO IV radar system with 200, 300, 500 and 900 MHz antennae. Over a period of 70 hours, 770 litres of PCE were injected under a constant head of 2 m of water at the centre of the test cell at a point 0.6 m below the ground surface. Geophysical imaging of the test cell began several days before the contaminant injection and continued over 912 hours after the injection had been completed. Measurements were made throughout the period of the experiment so as to obtain time-dependent datasets. Geophysical measurements continued for several weeks after the main experiment had been completed in order to monitor the removal of the PCE from the test cell, which was undertaken by flushing the cell with surfactants.

Of the substantial body of data obtained from this experiment, a time series of radargrams obtained along transect 5N (Figure 12.26) using 200 MHz antennae is shown in Figure 12.27. Three radargrams are shown ranging from one obtained before any injection of PCE had occurred, and two acquired at 16 and 920 hours after injection. What is clear from comparing the two radargrams after injection is that PCE appears to pond at a depth of 1 m (iv on Figure 12.27B) and then drains downwards leaving a residual ((v) on Figure 12.27C) at 1 m depth with ponding above the clay aquitard evident at (vi).

These experiments demonstrated that PCEs can be imaged successfully using a variety of geophysical methods, and that GPR can be used to monitor both the migration and the subsequent remediation of the contaminated ground. Further aspects of the radar surveys have been reported by Brewster *et al.* (1992a, b), for example. A GPR survey at a site where DNAPL contamination was known to have occurred has been described by Carpenter *et al.* (1994), although no DNAPLs were imaged directly using radar.

12.8.3 Glaciological applications

Radar mapping of the polar ice sheets has been one of the most widely used geophysical methods in both Greenland and Antarctica. Radio echosounding has been developed substantially since its early use in the 1960s. Determination of ice thicknesses is now accurate to around 1% and has provided excellent agreement with values derived from both seismic and gravity surveys, as well as with borehole control.

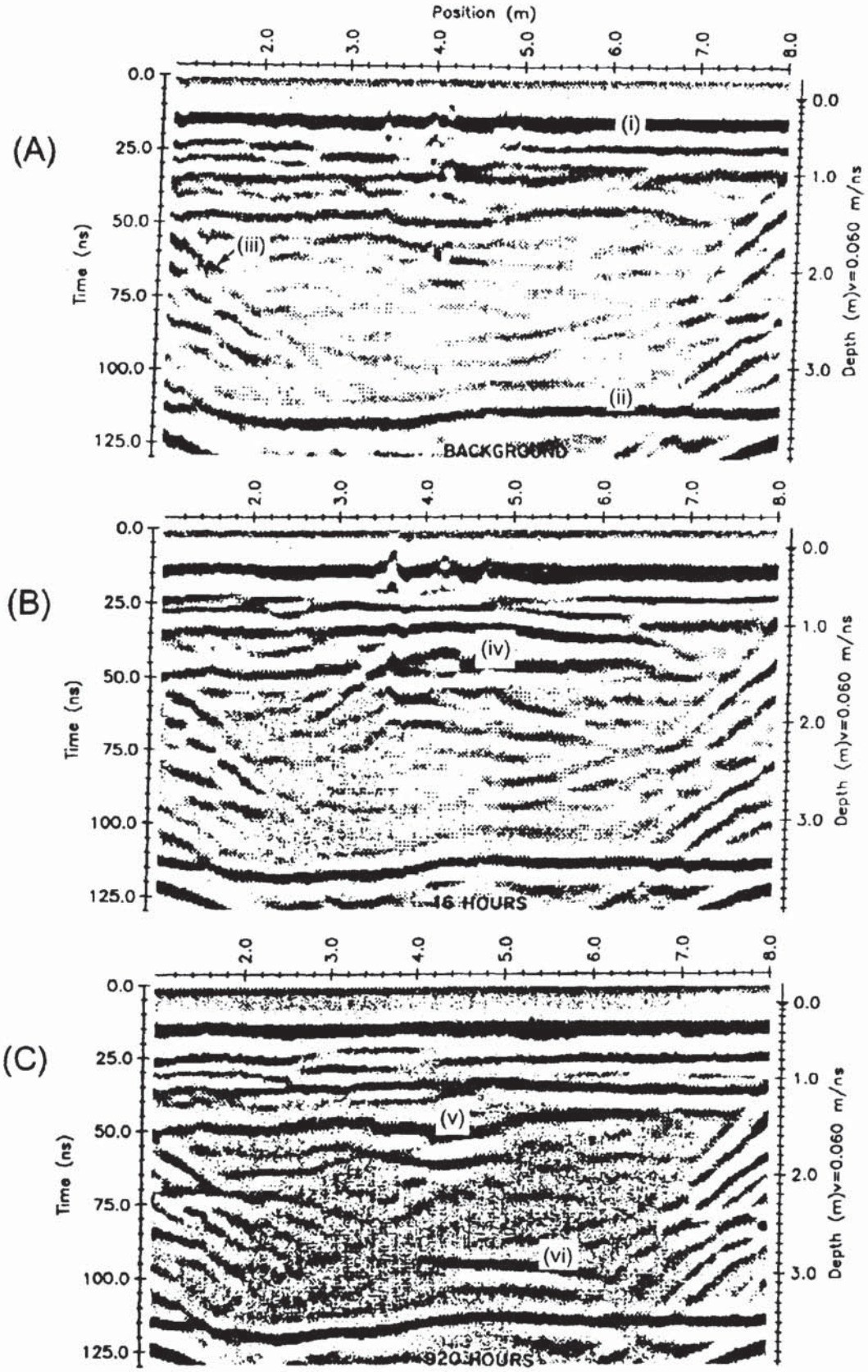
Position (m)
2.0
3.0
4.0
5.0
6.0
7.0
8.0
(A)
(i)
(ii)
(iii)
BACKGROUND
(B)
(iv)
16 HOURS
(C)
(v)
(vi)
920 HOURS
Time (ns)
0.0
25.0
50.0
75.0
100.0
125.0
Depth (m) v=0.060 m/ns
1.0
2.0
3.0

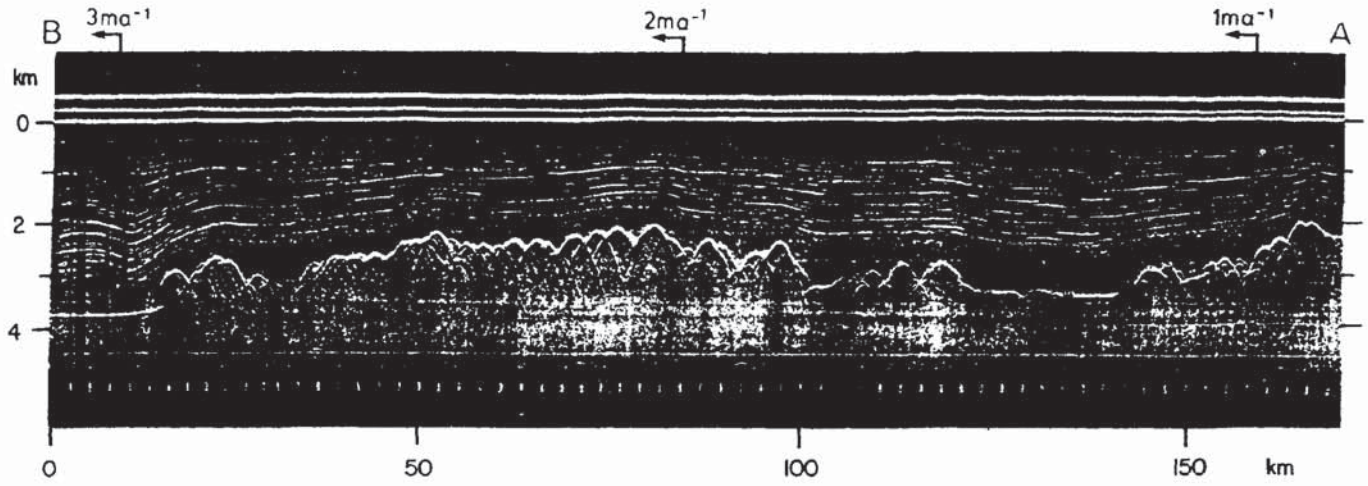

Figure 12.28 Radio echosounding record from along an ice flow line near Vostok, Antarctica. From Robin and Swithinbank (1987), by permission

An example of a radargram obtained using a 60 MHz antenna system over an ice flowline near the Russian research station Vostok, in Central Antarctica, is shown in Figure 12.28 (Robin and Swithinbank 1987). The total depth of penetration is around 3800 m. Three principal features are evident on this profile. The first is that there are a series of sub-parallel reflections within the ice itself. These horizons are thought to be due to elevated concentrations of sulphate (H_2SO_4) arising from large eruptions from volcanoes located outside Antarctica and transported in atmospheric aerosols to become incorporated within the polar snow, or from horizons which have undergone melting during the summer months (when the ice was at the surface) and subsequent refreezing. Ice has a thermal memory and the dielectric properties of the ice can be used to identify layers that have undergone melting and refreezing (Reynolds 1985). Some of the most prominent internal reflections can be traced over thousands of square kilometres and appear to be interfaces formed at the same time, and thus can be used as isochrons. These can then be used in the analysis of the dynamics of the flow of the ice sheet.

The second feature is that the bedrock surface can be seen very clearly and exhibits a range in elevation of about 1500 m. The bedrock topography is thus a hidden range of mountains. The third feature is located at the left-hand end of this profile at the base of the ice sheet. Note the flat, bright reflection at 3800 m depth. This is produced from what has been interpreted to be the surface of a large sub-glacial freshwater lake. The contrast in relative dielectric constants between the basal ice and the freshwater has given rise to this characteristic style of reflection. This type of feature can also be seen in another radio echosounding record shown in Figure 12.29 (Drewry 1986). Also note in both Figures 12.28 and 29 that there is a zone about 500 m wide immediately above the bedrock in which internal reflections are absent. This is possibly due to the basal deformation of the ice being such that the scale of deformation distorts the layering to such an extent that coherency is lost.

Figure 12.27 (*opposite*) Borden test cell imaged along profile line 5 N (see Figure 12.26) using 200 MHz antennae. Radargram (A) was acquired prior to PCE injection, and radargrams in (B) and (C) were obtained 16 and 920 hours after injection. (i) = cell surface; (ii) = top of clay aquitard; (iii) = reflections off the vertical cell walls; (iv) = pooled PCE at 1 m depth; (v) = a zone of residual PCE; and (vi) = PCE pooled on the clay aquitard. After Greenhouse *et al.* (1993), by permission

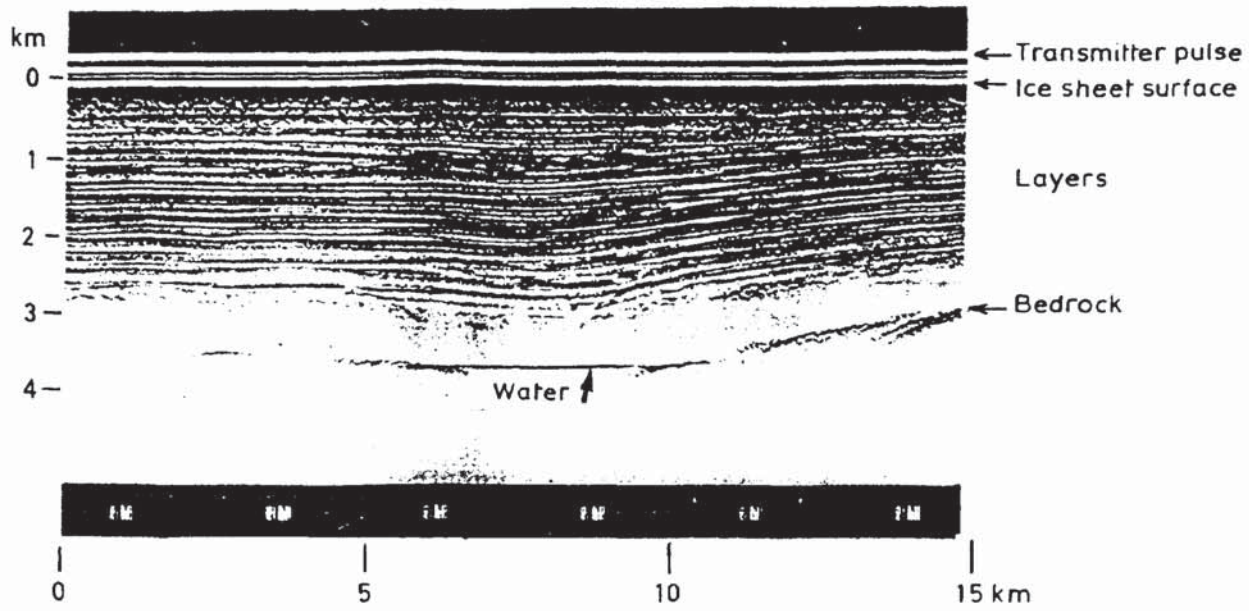

Figure 12.29 Radio echosounding record from a site in East Antarctica. From Drewry (1986), by permission

A radar system developed for radio echosounding (Wright *et al.* 1990) utilises antennae with much lower centre frequencies (1, 2, 4, 8 and 12.5 MHz) than those used previously ($\geqslant$60 MHz). Records using this new system are shown in Figure 12.30. A 4 MHz centre-frequency antenna was used in this example which was obtained on Ice Stream B, near the Transantarctic Mountains. In Figure 12.30A, diffractions arising from near-surface crevasses and internal reflections are evident. The latter are also evident in Figure 12.30B, which shows the radar record for the lowermost 400 m of ice. In addition, a 'bright spot' is observed within the basal ice and is thought to be due to entrained basal rock debris or trapped water. Strong diffractions also occur at the base of the ice, just below the 400 m mark. These are thought to emanate from either bottom crevasses within the base of the ice or from within a saturated till layer sandwiched between the ice and the bedrock.

At the other extreme of range, Forster *et al.* (1991) have developed a very-high-frequency radar which transmits 200 mW at 11 GHz with a 2 GHz bandwidth to measure detailed snow stratigraphy (Figure 12.31A). This radar has an effective resolution in snow of around 5 cm. The normalised power return is plotted as a function of depth (Figure 12.31B), assuming a uniform radiowave velocity through the snow—which leads to an inaccuracy of about 2% in depth determination over the shallow range of depth penetration ($<$3 m). The importance of a device like this is that it can be used to determine the effect of shallow sub-surface strata on measurements made by satellite remote sensors, such as synthetic aperture radar imagers, radar altimeters and passive microwave radiometers (Forster *et al.* 1991).

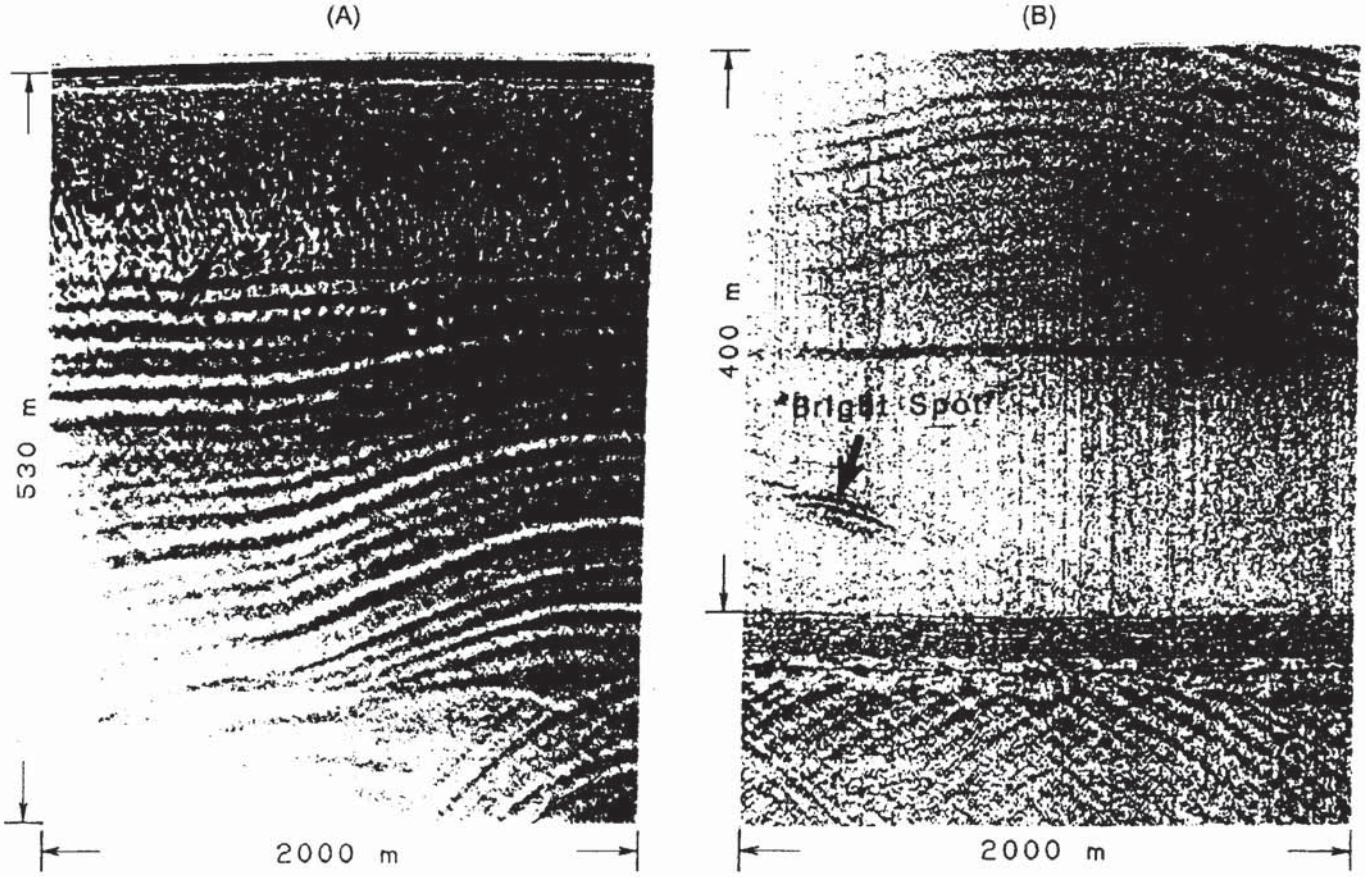

Figure 12.30 Low-frequency (4 MHz) records of sub-ice sheet environs: (A) diffractions from surface crevasses, and internal reflections; and (B) internal reflections and diffractions from basal crevasses and from a deformed sub-glacial sediment zone. From Wright *et al.* (1990), by permission

12.8.4 Engineering applications on man-made structures

Radar has enormous potential for use on engineered constructions. In these cases, the geometry and materials of each structure should be known. However, what can be at odds is whether the structure has been constructed according to the required specifications. Indeed, the construction methods may have left a legacy of subtle differences in physical properties within the structure. Radar can be used to ensure that, for example, reinforcement mesh has been placed at the correct level within concrete slabs. In some cases, the act of pouring the concrete can displace the mesh, so that instead of being located within the middle of a slab it is pushed to the bottom, and therefore cannot perform the function for which it was intended. Similarly, the location of reinforcement bars ('rebars') can be checked using higher-frequency radar (e.g. 500 MHz, 900 MHz or higher centre frequency) as shown in Figure 12.32.

An embankment made of fill material, which consisted largely of crushed dolerite, was thought to be uniform in its properties throughout. A radar survey using a 120 MHz antenna revealed sub-horizontal layering within the fill which were interpreted to be associated with compacted horizons. These layers had been produced by the

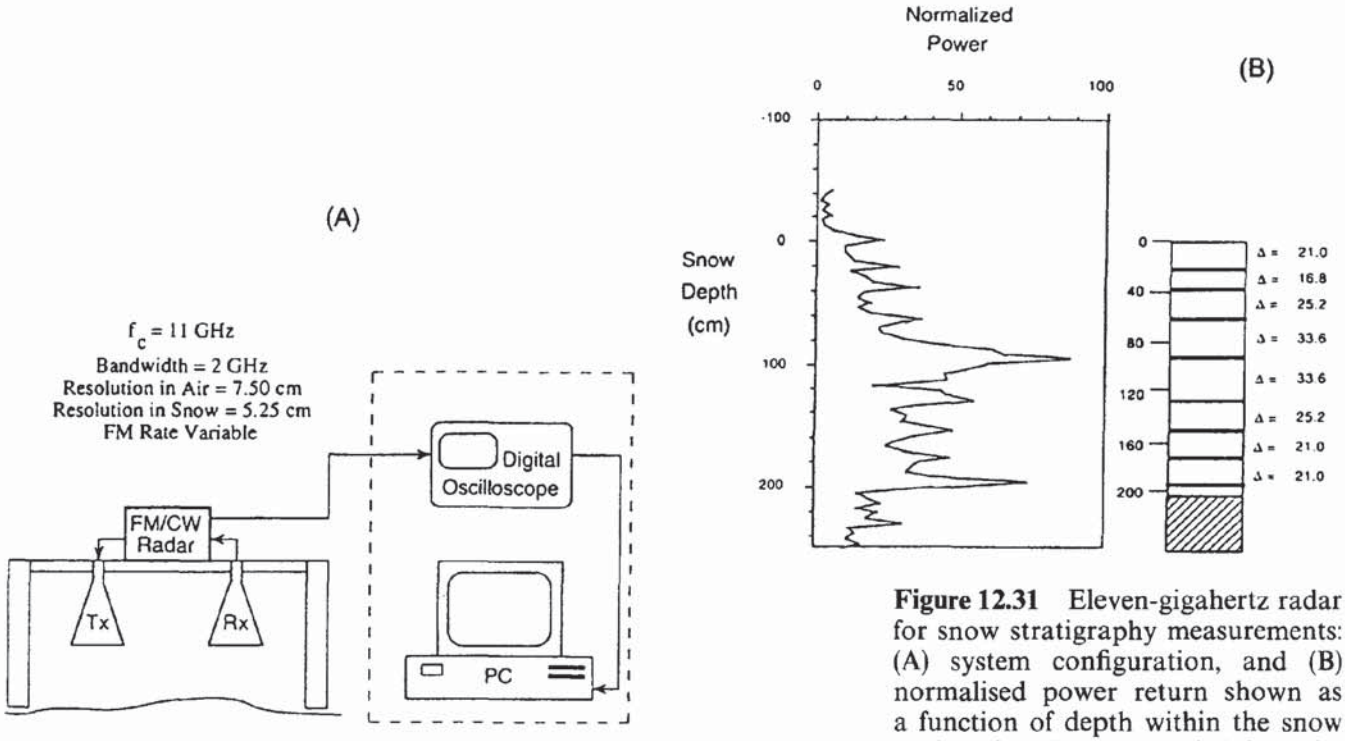

Figure 12.31 Eleven-gigahertz radar for snow stratigraphy measurements: (A) system configuration, and (B) normalised power return shown as a function of depth within the snow pack. After Forster *et al.* (1991), by permission

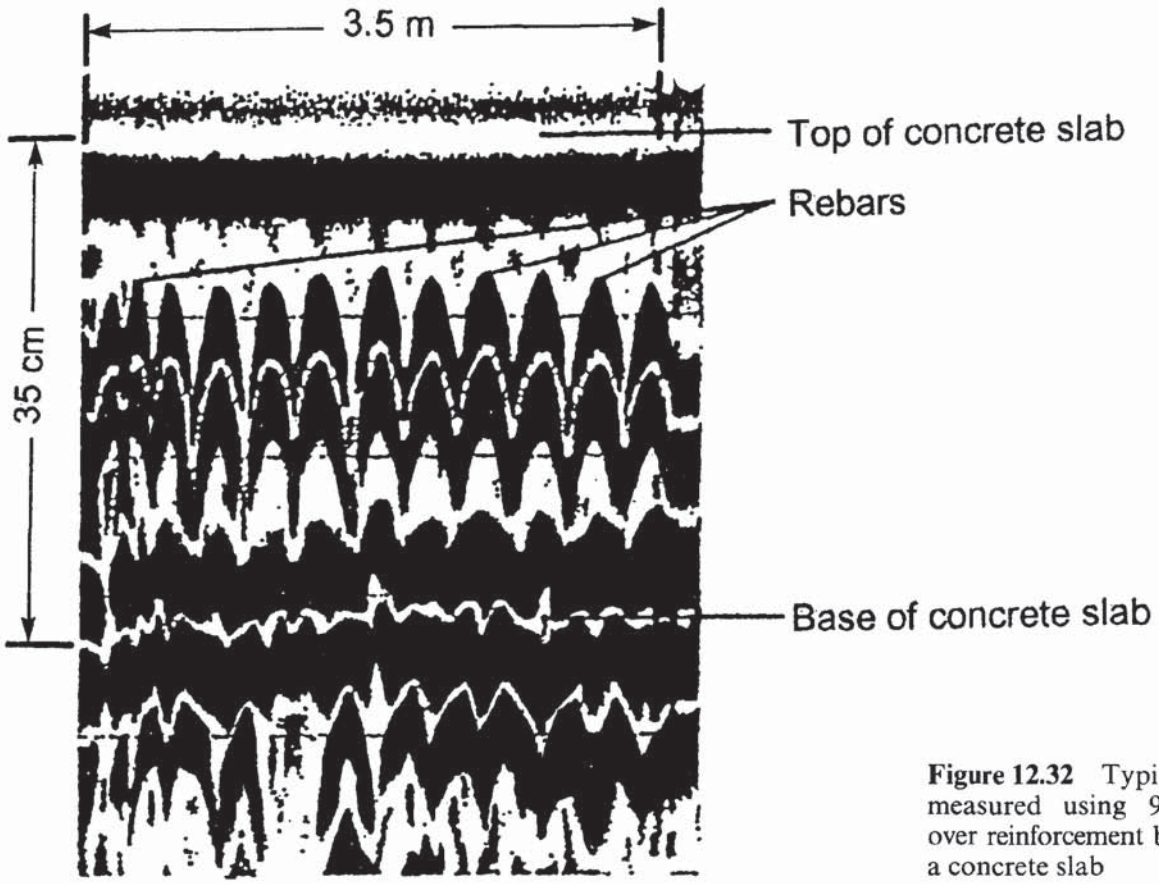

Figure 12.32 Typical radar record measured using 900 MHz antenna over reinforcement bars (rebars) within a concrete slab

contractor's vehicles driving over the fill along roadways. Distinct reflections were evident from these horizons and occurred as a result of the reduction in soil moisture content (and hence altered dielectric constant) of the compacted horizons (Reynolds and Taylor 1992).

Water-retaining dykes along Dutch rivers have been provided at various locations with granular filters. The purpose of these filters is to reduce the groundwater potential inside and below the dyke in order to increase the stability and prevent bursting of a clay layer at the lee side of the dyke (Figure 12.33A). The gravel-filled filter must be in hydraulic contact with the underlying sandy layers. The filters have a working life of several decades but suffer with becoming clogged by finer particles. Consequently, it is necessary to monitor the filters periodically, preferably using non-destructive methods. Ground penetrating radar has been used successfully in such investigations, as reported by de Feijter and van Deen (1990).

Radar surveys were carried out when the groundwater level was at its maximum and also at its minimum, over a time interval of several years. A sample radargram is shown in Figure 12.33B, which was obtained using a 300 MHz antenna with a GSSI radar system. The horizontal reflection arises from the water table (with its multiple). Reflection III is caused evidentally by the filter–dyke interface. Note, however, that none of the horizontal layers within the dyke itself is imaged. Indeed, the zone to the right of the filter–dyke interface shows significant attenuation of the radar energy, most probably because of the presence of water-saturated sandy clay and clay.

The ground radar method lends itself very well to the investigation of road pavements and bridge decks as they are made up of discrete layers. Radar can be used to measure layer thicknesses and to detect areas of delamination, where one horizon separates from another causing weakness in the road. This can lead to rapid deterioration of the road surface. As the depth of investigation is small (usually < 1 m) and as fine vertical resolution is required, high-frequency antennae are used, typically 900 MHz centre frequency. One or more antennae are fixed to a frame on a vehicle so as to maintain a fixed and known geometry. The vehicle drives along the road being surveyed at speeds up to several tens of kilometres per hour. The graphical output is viewed for evidence of anomalous zones which might indicate potential problems within the road base. Radar can also be used to check that the specified thickness of sub-base material has been put down during construction or if there are areas where the sub-base is defective.

The radar method has considerable applications within stone and brick masonry. The method has also been used to investigate the internal composition of statues and of masonry façades of historic buildings.

In most of these applications, the radar method complements other non-destructive testing methods, such as acoustics (e.g. in bridge deck

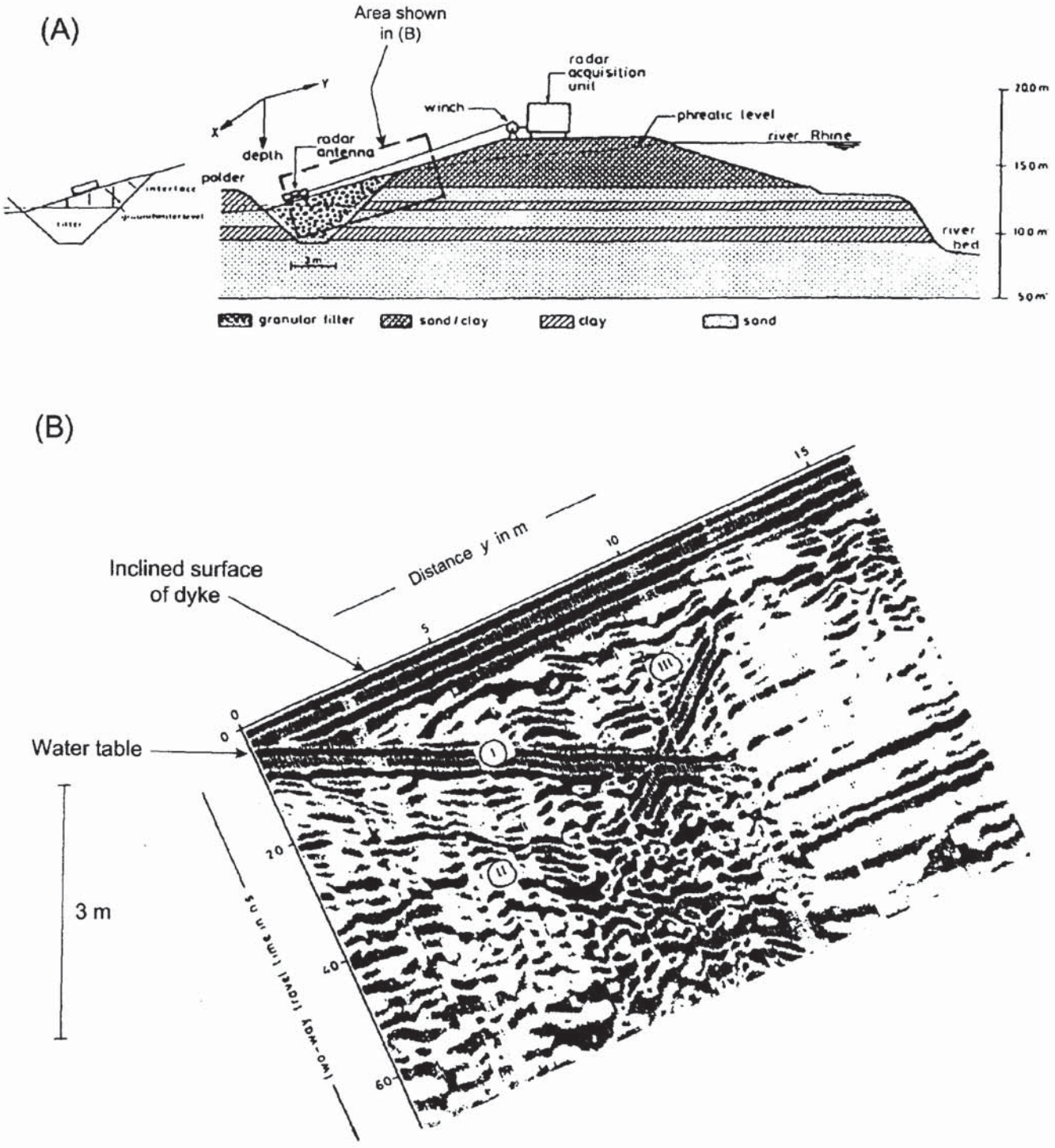

surveys), nuclear density measurements and thermal imaging (e.g. road studies). As with all geophysical methods, some ground-truth data are invaluable for correlation purposes. In road pavement studies, cores are used to provide point-to-point correlation with radargrams. The major advantage of the radar method is that it is entirely non-destructive.

Figure 12.33 (A) Cross-section of a dyke adjacent to the River Rhine, illustrating the engineered sub-structure, and the disposition of a radar transect shown in (B): 300 MHz radargram taken at highwater level. After de Feijter and van Deen (1990), by permission

12.8.5 Voids within man-made structures

One of the commonest applications of ground penetrating radar in the investigation of man-made structures is the detection and location of voids. Radar has been used extensively to inspect the condition of brick-lined tunnels and sewers. In the latter case, radar is often used in conjunction with closed-circuit TV (CCTV).

Two particular aspects of radar make the method particularly suited to such investigations. One is that the speed of radiowaves in air is around three times faster than in solid materials and thus produces a pronounced velocity 'pull-up' effect in association with a significant void. The second is the occurrence of resonance which happens when the wavelength of the incident radiowave energy is the same as, or shorter than, the dimensions of the void.

An example of a radargram acquired in a sewer survey is given in Figure 12.34A. This shows an extract of a radargram obtained where an air void was found above the crown of a sewer. Two features are evident on the radar section: one is the obvious difference in position of the crown of the sewer each side of the void (Figure 12.34B); the second is the obvious lozenge-shaped anomaly associated with the air void (picked out with white dashed lines in Figure 12.34A). The data were acquired using a vertical-looking 500 MHz antenna with a GSSI SIR-3 radar system.

Not all air voids occur as failures in construction. There are examples where radar has been used to locate hidden crypts in churches and in other historic buildings, or old Second World War air-raid shelters whose locations have been lost.

An excellent example of a radargram showing the location of a crypt has been provided by Stratascan from a survey at Worcester Cathedral (Figure 12.35). This particular survey profile was carried out at right-angles to the long axis of the Charnel House which has an arched roof. The stone–air interface of the roof of the Charnel House is obvious by the bright strong amplitude reflections, the apex of which is at 7.5 m along the profile. Note that at about 6 ns above the top of the Charnel House roof reflection, there is a much weaker reflection which has the same shape as the reflection from the crypt. This is interpreted to be from the top surface of a line of stones used to construct the ceiling arch of the Charnel House.

The bright domed reflection at the bottom of the radargram is not due to a heap of rubble on the floor of the Charnel House, but is the reflection arising from the floor itself. That it is domed is purely due to the velocity pull-up effect from the air-filled crypt. Given an air-filled void 2 m deep, the reflection from the floor would occur at a two-way travel time some 26 ns ahead of a reflection from a comparable depth within the adjacent soil. Note also that the reflection from the stone–air interface at the ceiling of the Charnel House has the form of a leading white then positive, etc., whereas the reflection from the

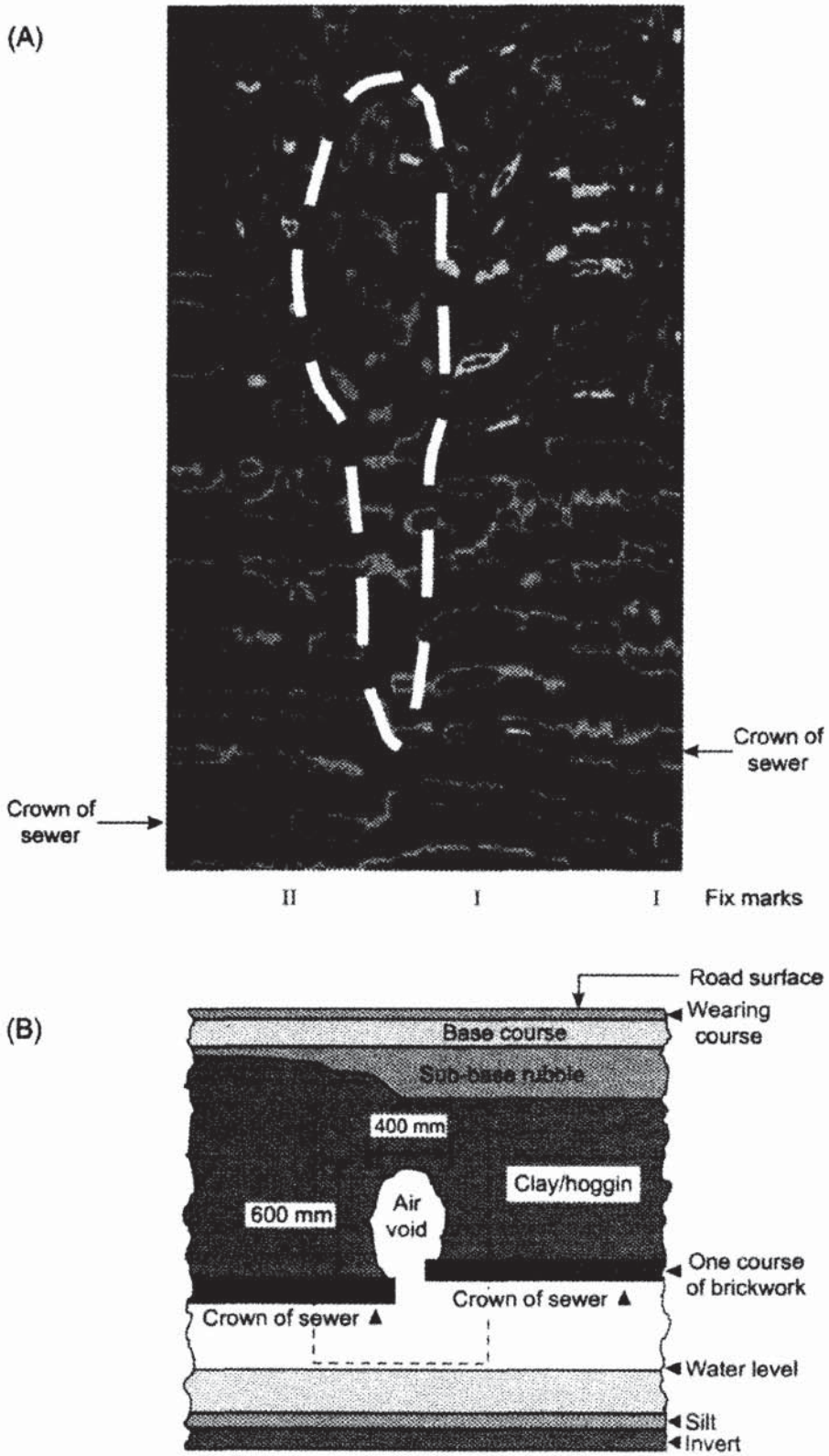

Figure 12.34 (A) Radargram through clay/hoggin material above a damaged sewer; a void is evident on the section and is delineated by dashed lines. The actual situation is shown in (B). Courtesy of Stratascan Ltd

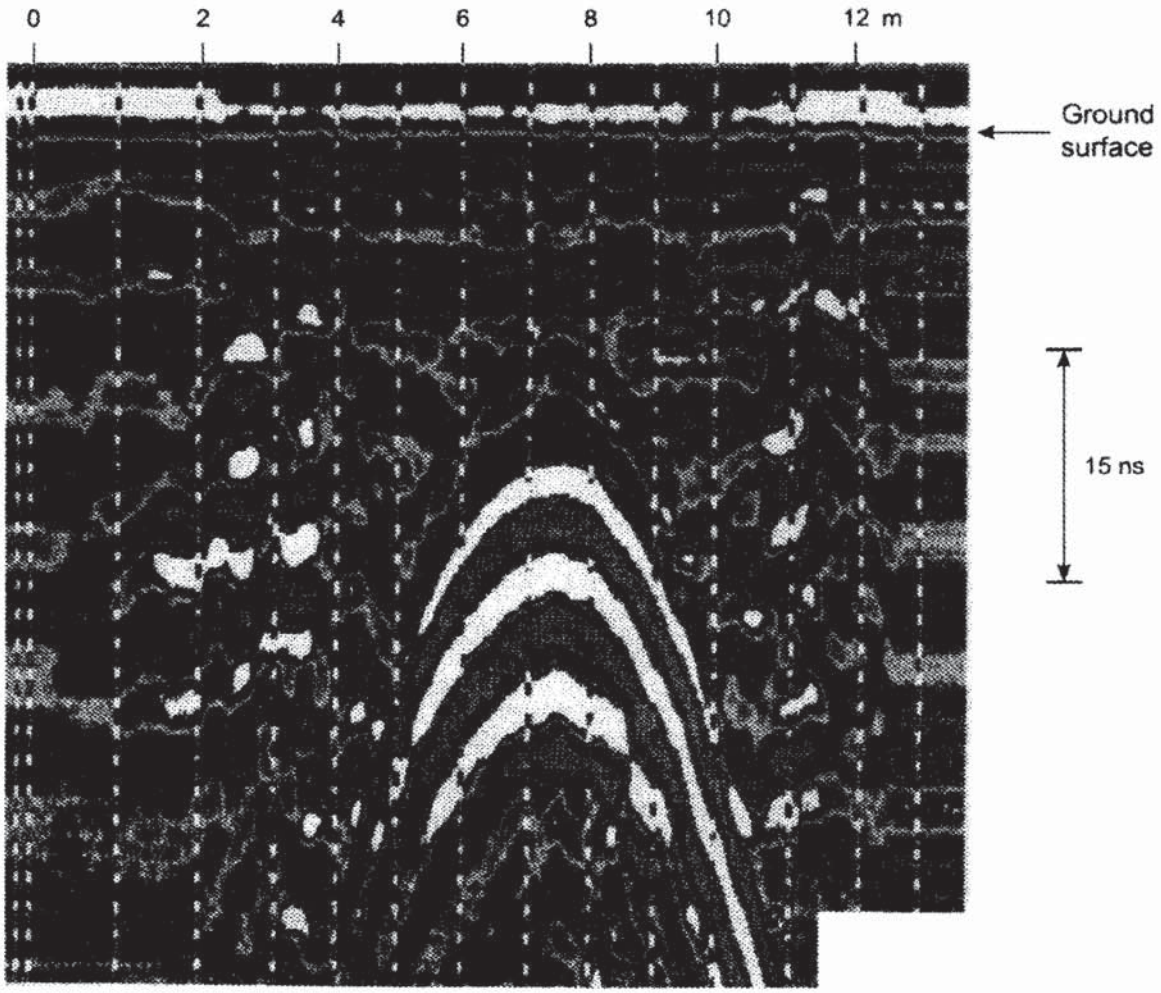

floor (air–stone interface) has the form positive then negative white. The polarity change is attributable to the passage of radiowaves from (a) a slow to fast medium (stone to air) and then (b) from a fast to slow medium (air to stone). Consequently, the phase of the reflection changes as does the sign of the reflection coefficient (see Section 12.3.1).

In some ancient buildings, additional complications can arise from the dimensions of the stone used in the construction of the building in relation to the wavelength of the incident radiowaves. Using a 500 MHz antenna over stone blocks ($V \approx 0.1$ m/ns), the wavelength is 0.2 m which is comparable to the dimensions of the blocks. Consequently, adverse phase interference can arise from internal reflections from the faces of individual blocks, making the overall radargram much more chaotic than it would otherwise have been. Similarly, building materials used to fill-in behind stone walls can be of a wide variety of materials, ranging from stone rubble to soil which may compact to leave air-filled voids.

Figure 12.35 Worcester cathedral: radargram over a buried vault. The top of the vault is clearly identified as being at the apex of the strong white anomally which dominates the section. Courtesy of Stratascan Ltd

12.8.6 Archaeological investigations

Radar has many applications in archaeological no-dig investigations, especially as the depth of penetration required is usually small (commonly less than 3 m). Radar can be used as a first-look technique or as a fill-in method between areas of excavation. One example of the successful use of radar in imaging an archaeological feature is given in Figure 12.36. The radargram was obtained using a 300 MHz antenna (range setting = 40 ns) with a GSSI SIR-3 system over flat ground made up of alluvial silts, gravels and boulder clay at a site at Caersws, Powys, Wales. The radargram shows very clearly the reflections arising from the surface of a Roman road with ditches on each side. The swathe of the carriageway appears as a slightly depressed central zone.

The location of graves can be important for at least two reasons. As consecrated ground, there has to be considerable care exercised if the site is wanted for development. Also, there may be important archaeological information associated with the buried remains. It is doubly important, therefore, that the locations of graves can be determined non-destructively. One such survey of graves using GPR among other techniques has been described by Bevan (1991). Radargrams obtained in two orthogonal directions across a postulated grave are shown in Figure 12.37. To aid the interpretation of the radar results, an electromagnetic ground conductivity meter (an EM31) and a magnetometer were used for corroboration. As can be seen from Figure 12.37C and D, these other tools produced geophysical anomalies which are closed (form concentric contours) around the locations of the graves. It should be emphasised that it is the disturbed ground associated with the graves that tends to show up on radargrams, not the bodies themselves.

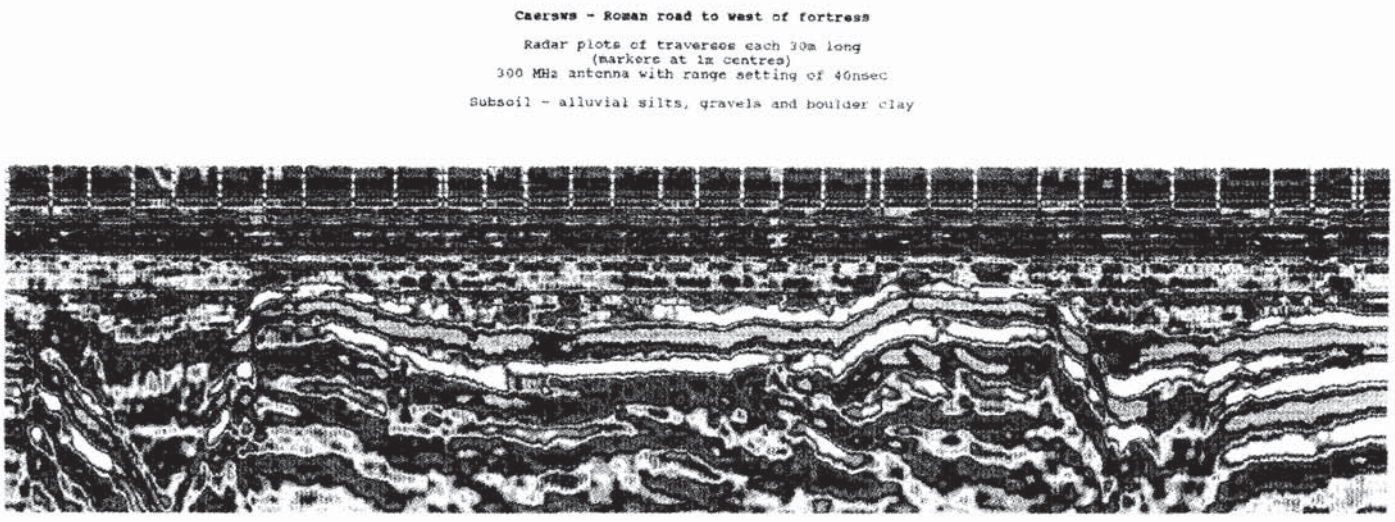

Figure 12.36 Example of a radargram over a buried Roman road. Courtesy of Stratascan Ltd

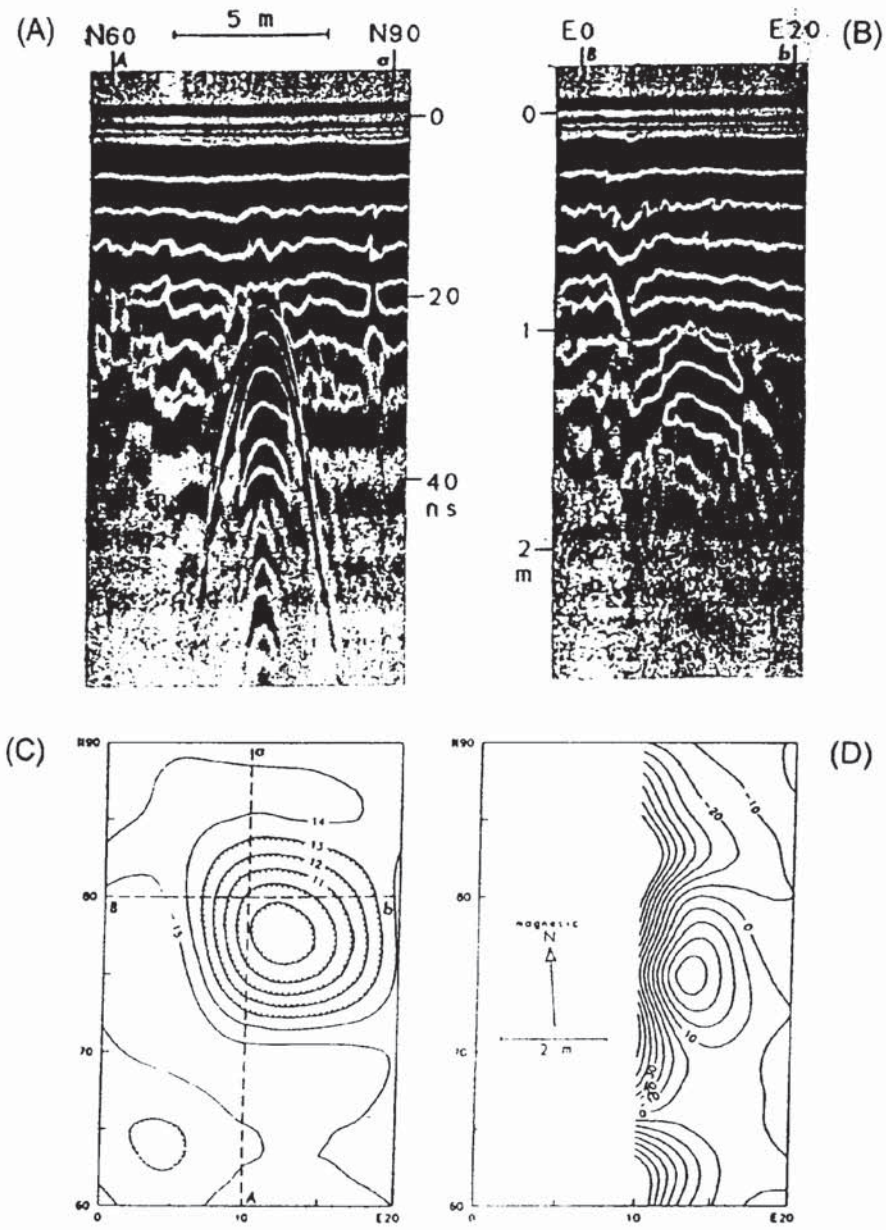

Figure 12.37 (A) North–south radar profile over a possible grave. (B) An east–west profile shows that the object is wider in this direction. (C) Apparent conductivity map with a contour interval of 1 mS/m; dashed lines indicate the orientations of the two radar profiles. (D) There is also buried iron or fired brick; the contour interval of this magnetic anomaly map is 10 nT. From Bevan (1991), by permission

Where human remains are thought to be located in specially protected sites – for example, those which may have been scheduled as 'Ancient Monuments' – radar can be particularly useful. The National Trust of Scotland has used radar in an attempt to locate the remains of the Duke of Northumberland's redcoats who died at the Battle of Culloden in 1746 after the historic routing of Bonnie Prince Charlie and his army. The investigation of the site is important as it is hoped that new information will be forthcoming about one of Scotland's greatest defeats at the hands of the English. It is thought that the remains of some of the English soldiers are buried inside a turf dyke.

12.8.7 Forensic uses of GPR

Radar has been used very successfully in the search not only for ancient graves but also for more recently buried bodies. It has been especially helpful where bodies have been concealed so as to avoid detection. Since the late 1980s, radar has been used increasingly by police in the search for disturbed ground which might indicate where a corpse has been hidden. For example, the States of Jersey, Channel Islands, employed radar to look for the bodies of a married couple which it was thought had been concealed in the back garden of their bungalow. Nothing was found. Radar also played an instrumental role in locating the remains of 12 corpses concealed at three locations in and around Gloucester, UK. A multiple murderer and his accomplice buried the bodies within the concrete foundations and inside newly plastered walls of their own house. The radar was able to identify anomalous targets within the concrete, thereby providing particular locations for excavation. Several more bodies buried in a nearby field were found with the help of radar.

In the USA, at Denton, Maryland, a high-school student Jamie Griffin was murdered, but neither his parents nor local police could locate his body for over seven years. Consequently, the person who had admitted perpetrating the crime could not be tried for murder. The body was thought to have been concealed somewhere within the 20 acres of Gunpowder Falls State Park, north of Baltimore. Previous searches using dogs, scuba divers and earth-moving equipment had been unsuccessful. It was only when a radar system was used that an anomaly was found which turned out to be due to Jamie Griffin's body. Not only was it then possible to convict the suspect of first-degree murder but the victim's family was able to hold a proper funeral for their son.

In addition to aiding the location of concealed corpses, radar has been used in the search for buried bullion following a major robbery in London in the late 1980s. With increasing publicity to such cases, so the forensic applications of radar increase. It is likely that, with the increasing reliability of radar, the applications for forensic investigations will become much more numerous.

12.8.8 Wide-aperture radar mapping and migration processing

Radar surveys are normally executed using one or two antennae in a profiling mode as a single-channel acquisition system. Fisher *et al.* (1992a) carried out a 40-channel GPR survey in a complicated fluvial/aeolian environment in the Ottawa River valley approximately 300 km north-northeast of Toronto, Canada. The receiver antenna was placed at each of 441 survey points at 1 m intervals along the profile line. For each of these receiver locations, data were recorded with the transmitting antenna at each of 40 separate

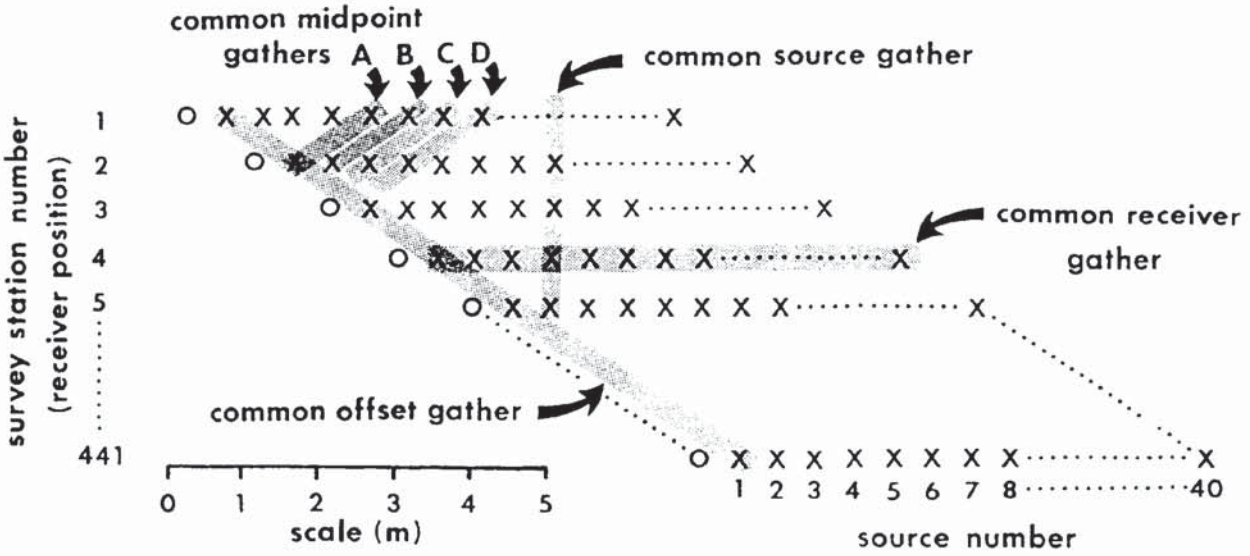

positions along the line, at 0.5 m intervals between 0.5 m and 20 m from the receiver (Figure 12.38). The antennae were orientated parallel to each other with the *E*-plane of the dipoles perpendicular to the survey line. Instead of the usual seismic analogue with a single source recording into a collection of receivers ('common-source gathers'), the common-receiver gathers were acquired. Traces could be sorted into common-source, common-receiver, common-offset or common-midpoint gathers irrespective of the method by which the data were acquired in the field. By obtaining the radar data in this way, traditional seismic processing could be undertaken on the common-midpoint (CMP) gathers.

A PulseEKKO radar system (Sensors & Software Inc.) with 100 MHz antennae was used, producing usable energy within the 50–150 MHz bandwidth. For each recording, 64 source excitations of the 400 V pulser were stacked to improve the signal-to-noise ratio. A total of 1280 samples were recorded with a time sample interval of 800 ps for a total time record of 1024 ns. Given a typical radiowave velocity in soil of 0.065 m/ns, this time range provided a possible depth of penetration of up to 33 m.

The radar data were input into a standard seismic processing sequence (filtering, statics corrections, common-midpoint gathering, velocity analysis, normal- and dip-moveout corrections, stacking and depth migration). More details of the data processing are given in Fisher *et al.* (1992a), and of the migration procedures in Fisher *et al.* (1992b). While the common-receiver and common-midpoint gathers for the radar data look very much like their seismic analogues, the derived RMS velocity estimates from three representative CMP gathers are shown in Figure 12.39. Whereas seismic velocities tend to increase with depth, these velocity panels show that the reverse is true for radar waves.

Figure 12.38 Survey geometry and data-gather definitions. A common-receiver gather contains all the traces recorded at one receiver position. A common-source gather contains all the traces generated at one source position. A common-offset gather contains all the traces with a fixed source-receiver separation. A common-midpoint gather contains all the traces with the same centre point between source and receiver. For the geometry used, there are four common-midpoint positions (cf. A, B, C, D) per receiver position. There are 40 traces in each common-receiver gather and 40 in each common-source gather. Except at the end of the survey, there are 10 traces in each common-midpoint gather. From Fisher *et al.* (1992a), by permission

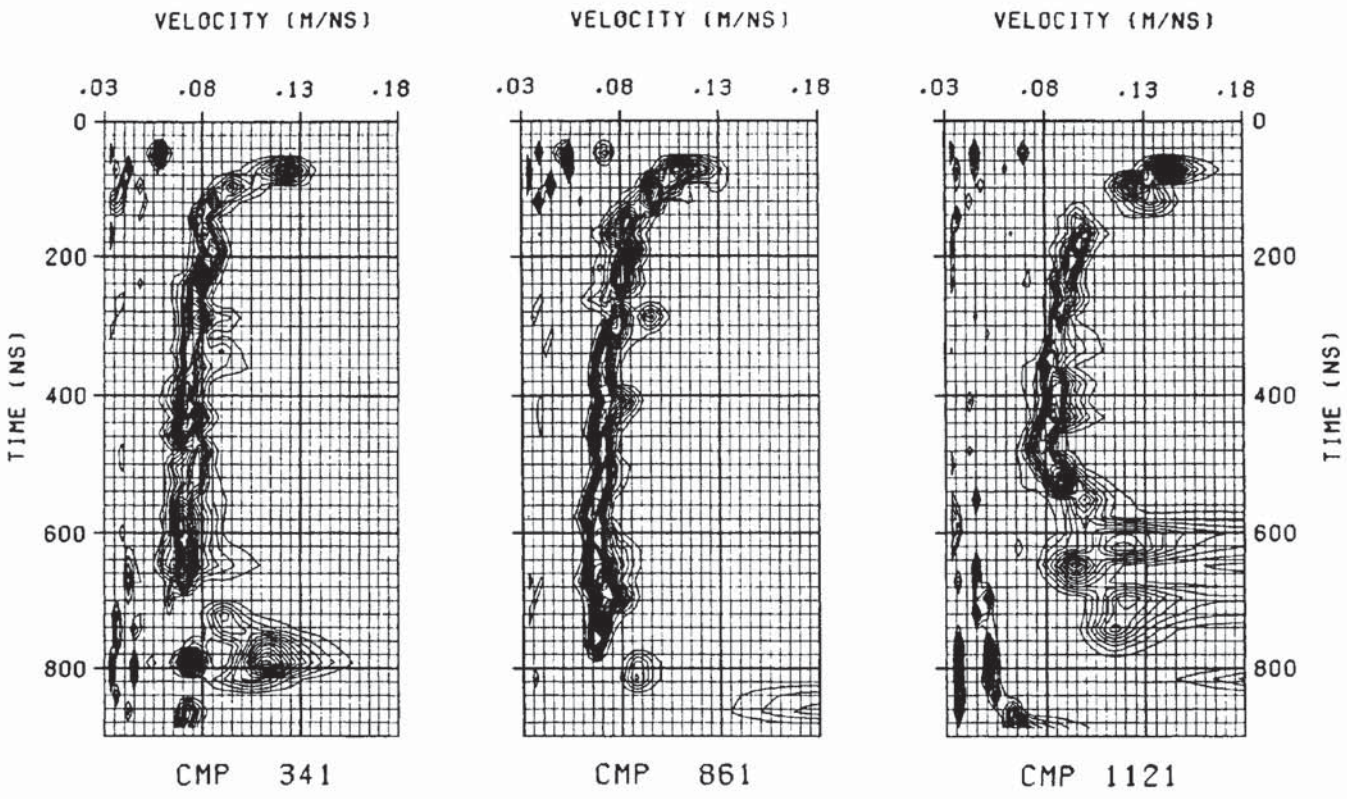

Figure 12.39 RMS velocity estimates from three representative CMP gathers. Velocity generally decreases with increasing depth (i.e. with increasing travel time). Velocity estimates are not reliable at times greater than that at which the last coherent reflection occures. From Fisher *et al.* (1992a), by permission

The results of the data processing are shown in Figures 12.40 and 12.41. Figure 12.40A shows a near-offset section; at each location the trace plotted is that recorded with the smallest (0.5 m) source–receiver separation. Figure 12.40B shows every fourth trace in the stacked time section; at each location, the trace plotted is the stack over the traces at the midpoint.

Note that the two panels in Figure 12.40 are shown as time sections. Compare those with the upper panel in Figure 12.41 which is a migrated depth image; the corresponding interpretation is provided in the lower panel. It is evident that significant detail has been obtained to a depth of over 25 m, as correlated with adjacent boreholes. The final migrated data are quite spectacular and show sub-metre vertical resolution even with a 100 MHz antenna to depths in excess of 20 m. Such success has to be tempered by the fact that, in the UK for example, sites where similar records could be obtained are rare, and comparable depths of penetration and similar resolution would be very difficult to achieve owing to the conductive nature of the soils. However, this example does demonstrate that, given the appropriate field conditions, equipment and processing facilities, exceptionally good results are possible with the method. Comparable results would not be possible using even high-resolution seismic reflection surveying.

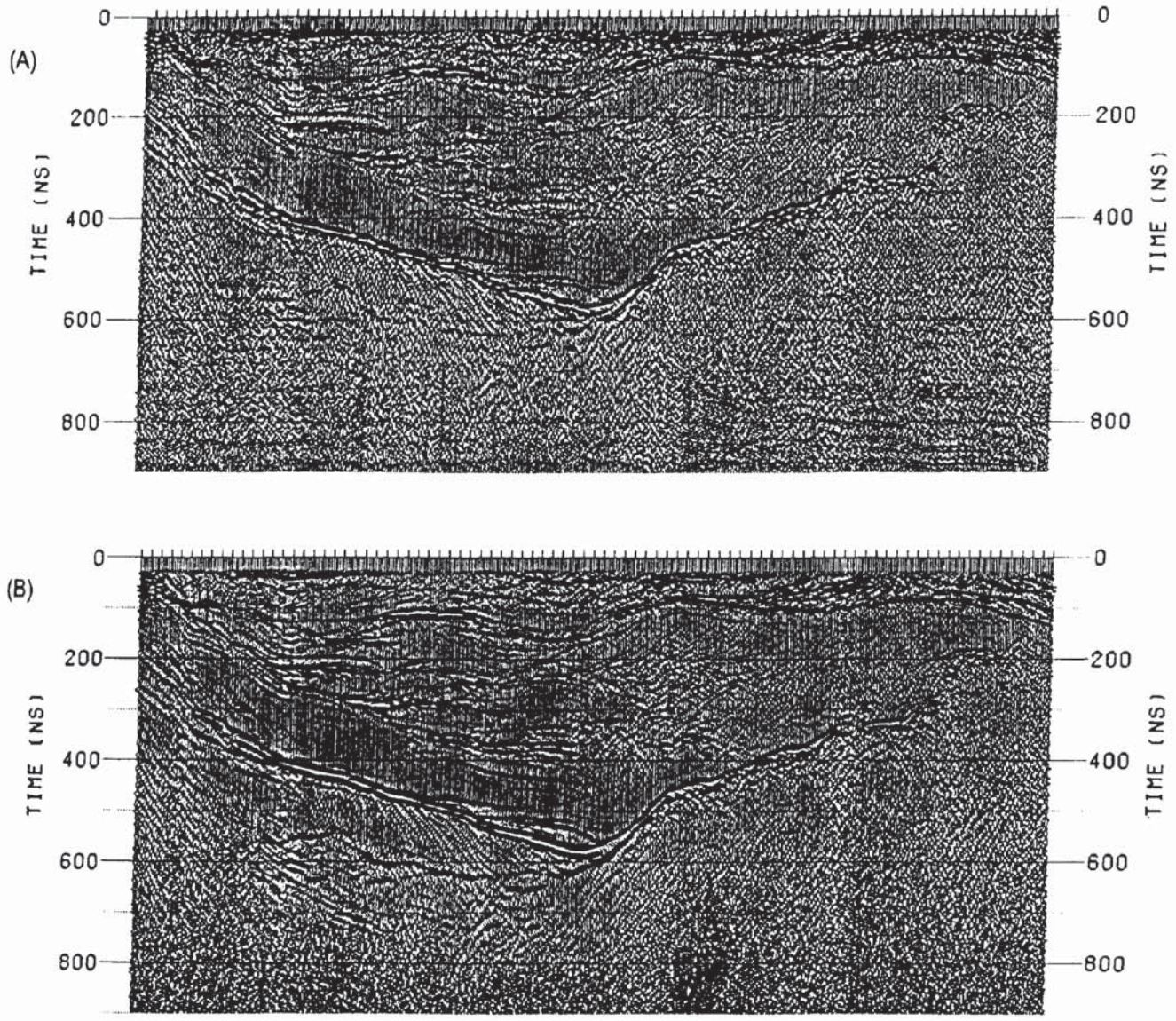

Figure 12.40 Radar sections from a 40-channel radar survey in the Ottawa River valley, Canada. (A) Near-offset section; at each location, the trace plotted is that recorded with the smallest (0.5m) source–receiver separation. (B) Section displayed with every fourth trace of the stacked time section; at each location the trace plotted is the stack over the traces at that midpoint. Both (A) and (B) are plotted with AGC with a 200ns window. From Fisher *et al.* (1992a), by permission

12.8.9 Borehole radar

In parallel with developments in surface ground penetrating radar, borehole systems have been in use since the early 1980s. One system called RAMAC was developed as part of the International Stripa Project in Sweden and is manufactured by Malå Geoscience AB and marketed by ABEM. The Stripa Project was undertaken in order to develop techniques suitable for use in underground nuclear fuel waste repositories. The short-pulse borehole radar was used primarily to obtain information about the structure and integrity of crystalline rock masses at a distance from tunnels and boreholes without affecting the rock in any way. In 1987, a RAMAC survey in Switzerland revealed fractures in granite 160 m away from the surveyed borehole.

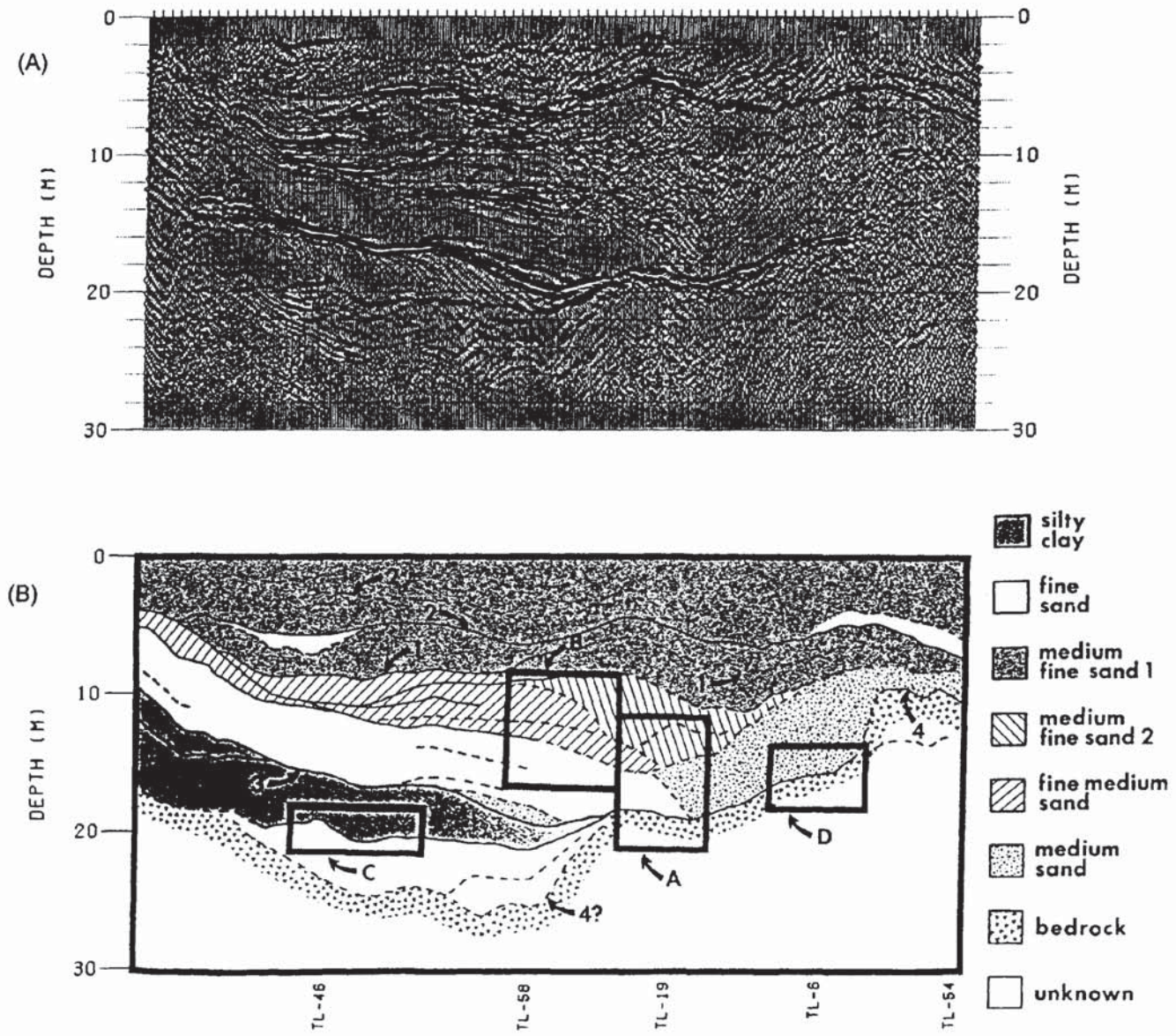

Figure 12.41 (A) Migrated depth image and (B) its interpretation. The image is plotted with AGC and only every fourth trace is shown. Approximate locations of available drill cores are labelled at the bottom of (B). Reflector 1 is a garnet sand; 2 = silt layers; 3 = fine sand gravel; 4 = bedrock. From Fisher *et al.* (1992a), by permission

Since then, RAMAC has been used to record reflections arising from structures at distances greater than 300 m within rocksalt. The system is now well proven and has been used internationally in mining, hydrogeological and rock mechanical investigations. It is also being used to investigate sites for tunnels, dams and other construction type projects.

The basic system is illustrated schematically in Figure 12.42 with a simple radargram. A transmitter is used to generate the radiowaves with a pulse frequency of 43 kHz. A separate receiver is located a short distance further down the hole: typically 2–6 m when surveying in sedimentary rocks, and 5–15 m when in crystalline rocks. The receiver operates with a bandwidth of 10–200 MHz. Different frequency

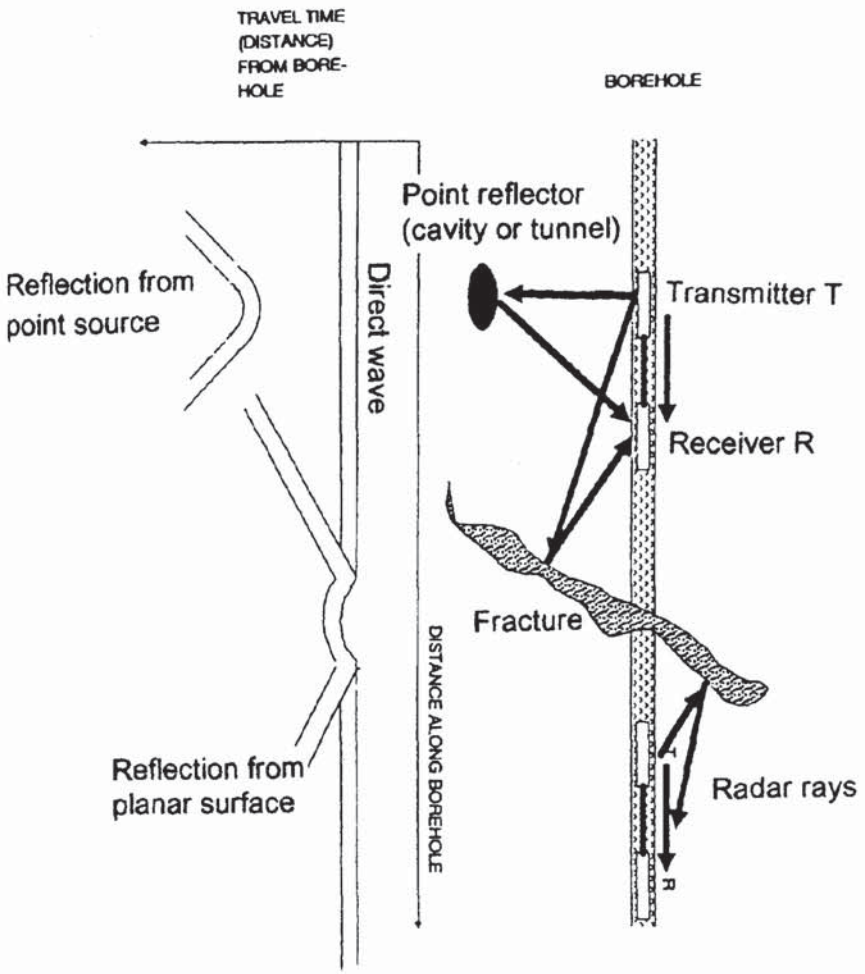

Figure 12.42 Basic arrangement for a borehole radar system with typical radar section images of plane and point reflectors. The cylindrical symmetry of dipole antennae creates V-shaped responses from planar reflectors. Hyperbolae arise from point sources. Courtesy of ABEM

antennae can be used, either 20 MHz or 60 MHz using the standard RAMAC system, or 50, 100, 200 or 400 MHz with a newer version released in 1994. Measurements are made at fixed intervals of 0.5 m or 1 m. It takes at most about 30 seconds at each location to make the required measurements.

Two modes of operation are possible. One uses an omnidirectional dipole antenna, and the other uses directional antennae so that reflections from discretely identified quadrants surrounding the borehole can be identified. The RAMAC system can also be used in cross-hole tomographic configurations with the transmitter antenna in one borehole and the receiver down another. Additionally a receiver can be placed down a borehole while the transmitter is located either in a mine tunnel or on the ground surface, as illustrated in Figure 12.43. Processing of radargrams can be accomplished using on-screen interpretational software.

A simple example of the types of radargrams generated using the RAMAC system is shown in Figure 12.44. The radargram was

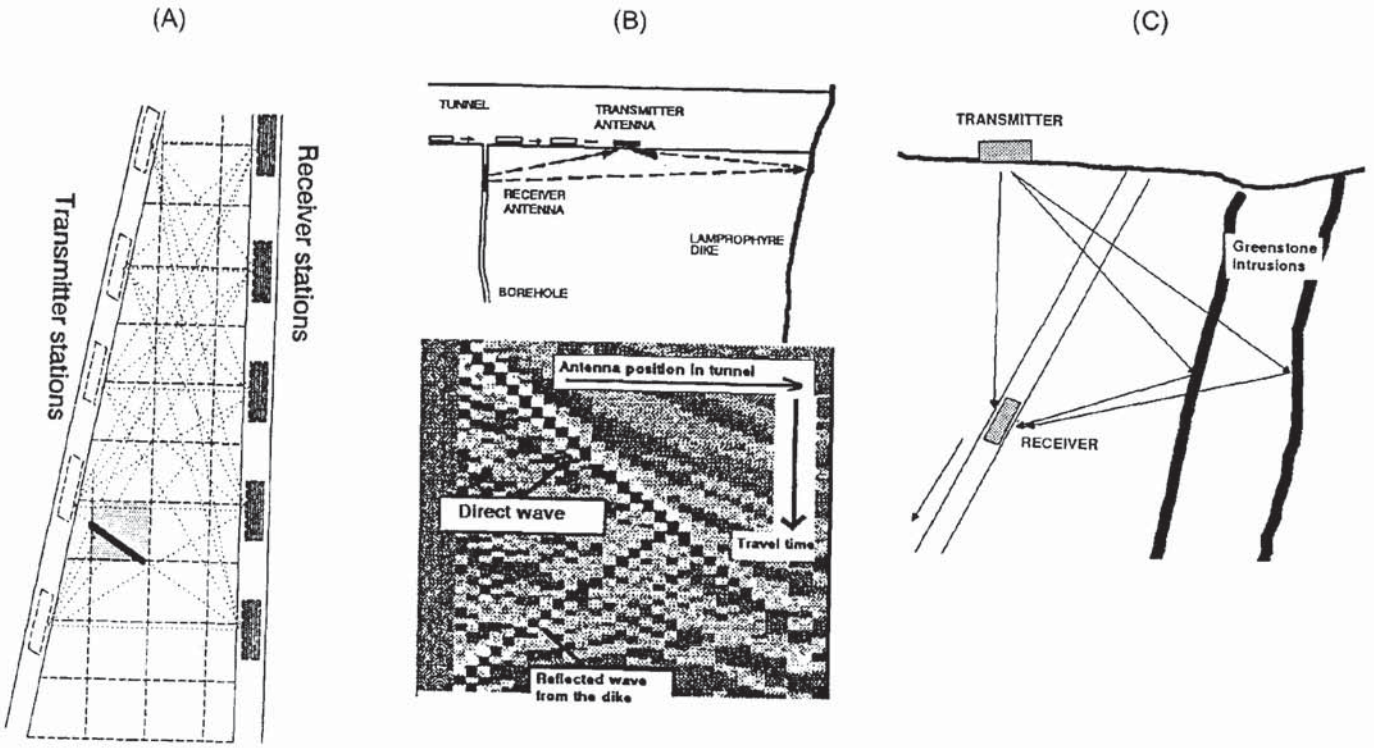

Figure 12.43 (*top*) Three configurations for borehole radar systems: (A) cross-hole tomography; (B) tunnel-to-borehole imaging, and (C) vertical radar profiling where the transmitter is on the ground surface and the receiver is down the borehole. Courtesy of ABEM

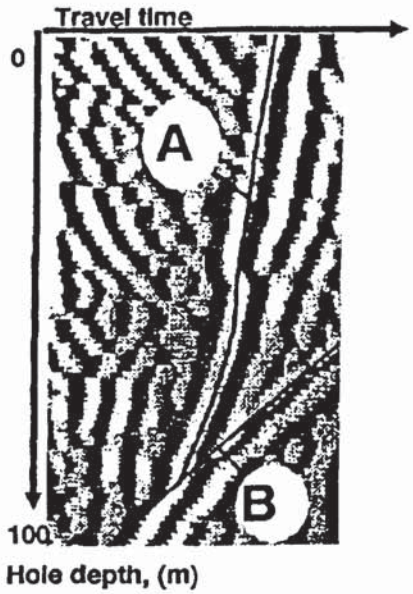

Figure 12.44 (*left*) Borehole radargram showing the location of an abandoned drill string (A) and a major fault zone (B) in which the drillbit was stuck. Courtesy of ABEM

obtained from one of three radar surveys made in three different boreholes to locate an abandoned drill string. Strong reflections from the drill string were observed on radargrams from all three boreholes. The radargrams also revealed the reason why the drill string became stuck – it had intersected an oblique major fault zone.

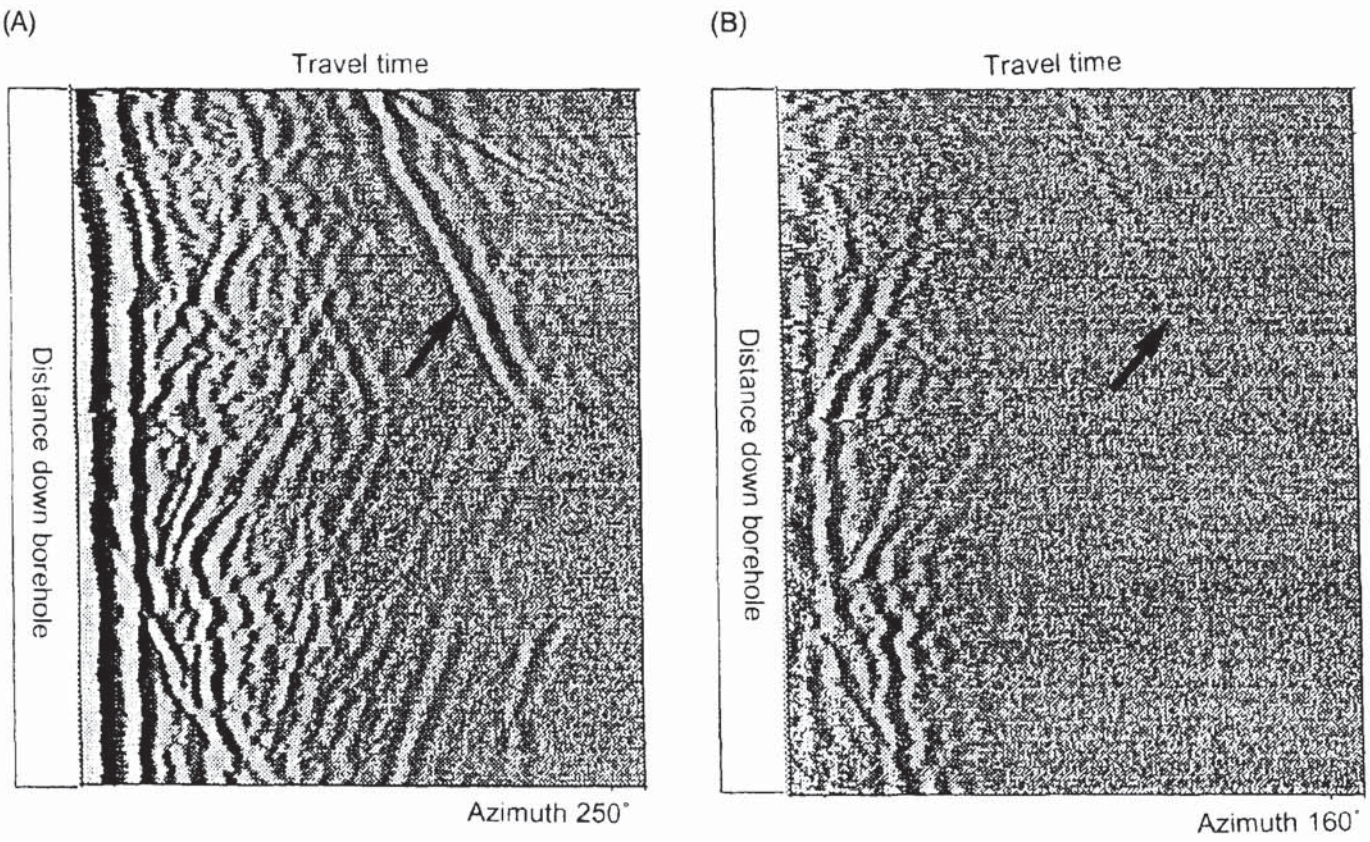

A second example presented in Figure 12.45 shows the effect of azimuth. In Figure 12.45A, the antennae are directed at 250° magnetic bearing and a plane reflection is evident (arrowed). The azimuth is rotated by 90° to 160° magnetic and the reflection is at a minimum (Figure 12.45B). Using such information, the dip and strike of planar features can be determined.

Figure 12.45 Borehole radargrams from the same location showing the effect of azimuth using directional antennae. (A) Azimuth is 250° magnetic with a major strong planar reflection (arrowed). (B) Azimuth is 160° magnetic and the planar reflection strength has decreased to its minimum value. Courtesy of ABEM